Development of a Double Molding Technique for the Microfabrication of Diamond Scanning Probe Tips

A dissertation
submitted to the Faculty of Sciences of the University of Neuchâtel,
in fulfillment of the requirements for the degree of "Docteur ès Sciences"

by

Cynthia Beuret
Diplomée en électronique-physique de l'Université de Neuchâtel

Institute of Microtechnology
University of Neuchâtel
Rue Jaquet-Droz 1, CH-2007 Neuchâtel
Switzerland

1999

IMPRIMATUR POUR LA THÈSE

Development of a double molding technique for the microfabrication of diamond scanning probe tips

de Mme Cynthia Beuret

UNIVERSITÉ DE NEUCHÂTEL

FACULTÉ DES SCIENCES

La Faculté des sciences de l'Université de Neuchâtel sur le rapport des membres du jury,

Mme M. Koudelka-Hep, N. de Rooij (directeur de thèse), U. Staufer, P. Niedermann (CSEM, Neuchâtel) et O. Ohlsson (Wetzlar-Blankenfeld, D)

autorise l'impression de la présente thèse.

Neuchâtel, le 25 mai 1999

Le doyen:

F. Stoeckli

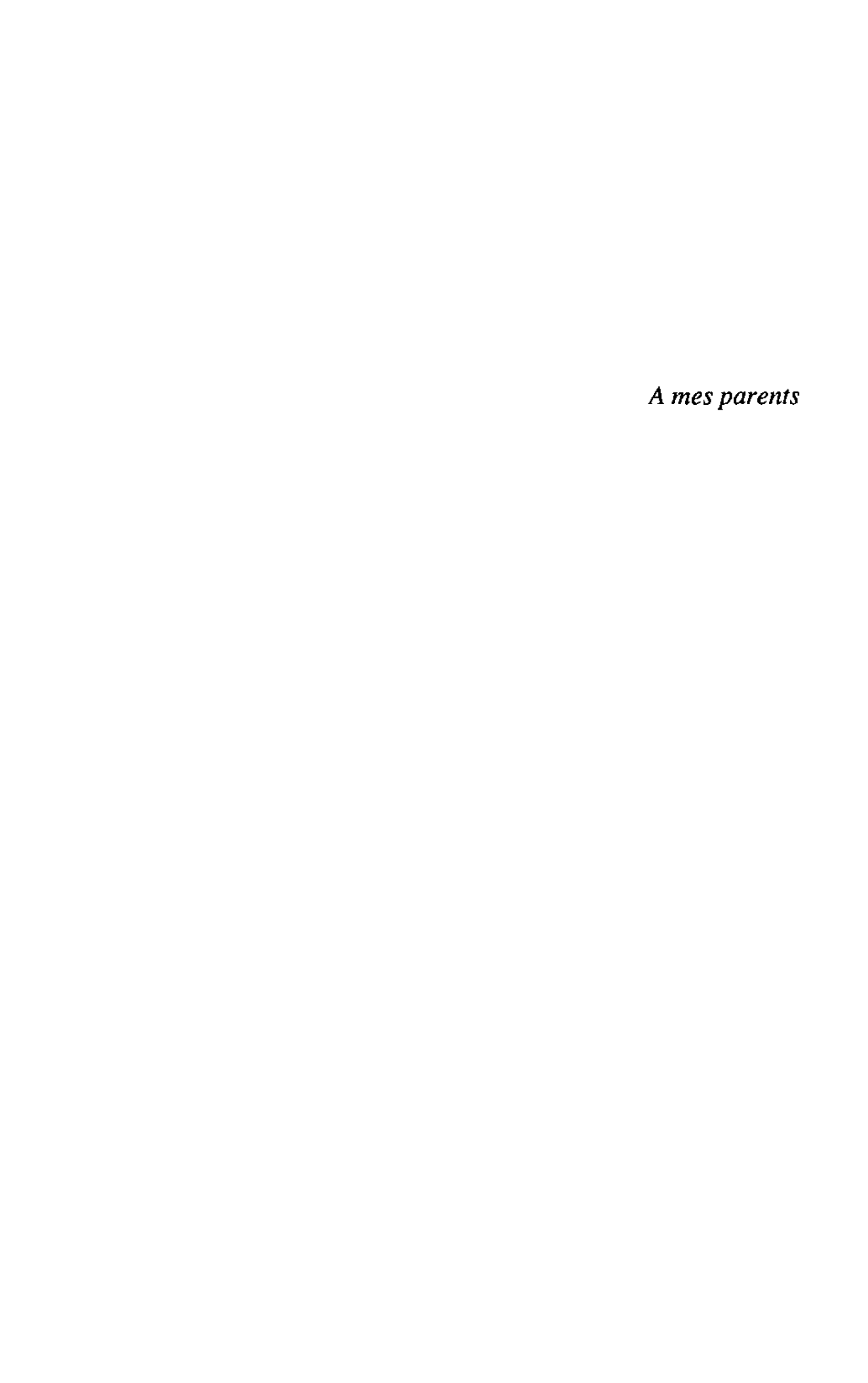

A mes parents

Abstract

In recent years, the decreasing limit of device dimensions obtainable with microfabrication technologies has led to a growing interest in the development of instrumentation able to characterize nanometer scale features. At the same time, a variety of other scientific research fields such as biology, chemistry, metallurgy or physics have expressed a comparable need for such advanced tools. The advent of various scanning probe microscopes in the 80's, of which the atomic force microscope is probably the most widely known, opened a door to the nanoworld by making it possible to image and to manipulate molecules and even atoms.
AFM probes are composed of a tiny cantilever, at the end of which a sharp tip is integrated. Such devices are usually realized in silicon or in silicon nitride with microfabrication techniques. Due to its dimensions, the silicon tip apex can suffer from wear or can be damaged after several topographical investigations. On the other hand, a high resolution profilometer has recently been developed, allowing macroscopic scale investigations of a sample, as well as high resolution imaging to be performed with the same tool. This profiler has a working principle similar to that of an atomic force microscope, but the load applied on the measuring tip is about 500x higher. So, the fabrication of sharp scanning probes in harder materials, like diamond, became crucial. Addressing this need, this thesis deals with the development of a microfabrication technology based on two successive molding steps, allowing the realization of diamond scanning probe tips having a high aspect ratio and a very sharp apex.
In this dissertation, the fabrication of the silicon tips acting as first mold is studied in a first step. Then, a technology to realize silicon tips integrated on thin cantilevers in a reproducible way is presented. Thicker cantilevers provided with sharp tips have also been produced. Once coated with a thin diamond layer, these devices can be used to perform nanoscratching experiments on hard material samples, and to immediately image the nanomodifications induced with a high resolution.

In the next chapters, the double molding technique is described for the realization of platinum as well as diamond tips. Finally, these diamond tips are analyzed by means of Raman spectroscopy or transmission electron microscopy, and are mounted on stubs or on cantilevers to be investigated as probes for high resolution profilometry and atomic force microscopy, respectively.

Table of Contents

Abstract i
Table of Contents iii
Abbreviations vii

Chapter 1 **Introduction**

1.1 Applications of Microtips 1
1.1.1 Scanning Probe Microscopies 1
1.1.2 High Resolution Profilometry 5
1.1.3 Other Applications 6
1.2 Fabrication Techniques for Microtips 8
1.2.1 Silicon Tips 8
1.2.2 Tips in Other Materials 11
1.3 Diamond Deposition 14
1.3.1 Hot-Filament-CVD Technique 14
1.3.2 CVD Diamond Tips 17
References 19

Chapter 2 **Silicon Tips: Fabrication and Study**

2.1 Introduction 25
2.2 Fabrication of KOH-Etched Silicon Tips 27
2.3 Results and Observations 30
2.3.1 Influence of the KOH Bath Set-Up 30
2.3.2 Silicon Dioxide Mask Design 34
2.3.3 Influence of Overetching 36
2.3.4 Tip Height Distribution 37
2.3.5 Tip Apex Shape 38
2.3.6 Crystallographic Planes 39
2.4 Conclusions 45
References 46

Chapter 3 **Silicon/Diamond Tips on Cantilevers**

3.1 Introduction 49
3.2 Cantilever Design 52
3.3 Fabrication 55
3.4 Results of the Fabrication 62
3.4.1 Determination of the Cantilever Thickness 64
3.4.2 Tip Height and Radius of Curvature 65
3.5 Measurements 68
3.5.1 AFM Measurements 68
3.5.2 Nanomechanical Modifications 69
3.6 Conclusions 71
References 72

Chapter 4 **Double Molding Process I: Fabrication of Platinum Tips**

4.1 Introduction 75
4.2 Description of the Double Molding Process 77
4.3 Evaluation of the Double Molding Process: Fabrication of Platinum Tips and Results 79
4.3.1 First Mold Definition 79
4.3.2 Second Mold Fabrication 79
4.3.3 Filling and Removal of the Second Mold 82
4.4 Conclusions 85
References 86

Chapter 5 **Double Molding Process II: Fabrication of Diamond Tips**

5.1 Introduction 89
5.2 Fabrication of Diamond Tips: Modifications of the Double Molding Process I and Results 91
5.2.1 Second Mold Filling: Diamond Deposition 91
5.2.2 Removal of the Silicon Nitride Mold 94
5.2.3 Diamond Evaluation 97

5.3 Mounting of the Diamond Tips 111
5.3.1 Mounting on Stubs for Profilometry Applications 111
5.3.2 Mounting on Cantilevers for AFM Applications 114
5.4 Conclusions 116
References 117

Chapter 6 Diamond Tips: Probes for High Resolution Profilometry

6.1 Introduction 121
6.2 The HRP 100: A High Resolution Profiler 124
6.3 Measurements 126
6.3.1 HRP Diamond Probes 126
6.3.2 Comparison on Different Samples 130
6.4 Conclusions 139
References 140

Chapter 7 Diamond Tips: Probes for AFM

7.1 Introduction 141
7.2 Measurements 142
7.3 Conclusions 144
References 145

Conclusions 147

Acknowledgments 151
List of Publications 155
Biography 157

Abbreviations

AFM	Atomic force microscope / microscopy
BHF	Buffered hydrofluoric acid
C_D	Diamond carbon
CH_3*	Methyl radical
CH_4	Methane
CVD	Chemical vapor phase deposition
DLC	Diamond-like carbon
DNA	Deoxyribonucleic acid
EDP	Ethylene diamine pyrocatechol
EDS	Energy dispersive spectroscopy
FIB	Focused ion beam
H*	Hydrogen radical
H_2O_2	Hydrogen peroxide
HRP	High resolution profiler
HSG	Hemispherically grained silicon
H_2SO_4	Sulfuric acid
H_3PO_4	Phosphoric acid
HF	Hydrofluoric acid
HF-CVD	Hot-filament chemical vapor phase deposition
HMDS	Hexamethyldisilazane
HNA	Hydrofluoric/nitric/acetic acid mixture

HNO_3	Nitric acid
IPA	Isopropanol
KOH	Potassium hydroxide
KOH/IPA	Isopropanol-saturated potassium hydroxide
LPCVD	Low pressure chemical vapor deposition
MFM	Magnetic force microscope / microscopy
NH_4F	Ammonium fluoride
O_3	Ozone
PECVD	Plasma enhanced chemical vapor deposition
RIE	Reactive ion etching
SEM	Scanning electron microscope / micrograph
SiO_2	Silicon dioxide
Si_3N_4	Standard stoichiometric LPCVD silicon nitride
Si_xN_y	Low stress, silicon rich, LPCVD silicon nitride
SNOM	Scanning near-field optical microscope / microscopy
SOI	Silicon-on-insulator
SPM	Scanning probe microscope / microscopy
STI	Shallow trenches isolation
STM	Scanning tunneling microscope / microscopy
TEM	Transmission electron microscope
TF-CVD	Thermal filament chemical vapor phase deposition
TMAH	Tetramethyl ammonium hydroxide
TMB	Trimethylboron
VLS	Vapor-liquid-solid

Introduction 1

With the number of applications for microtips increasing, a high demand has arisen for durable, hard and sharp microtips. Therefore, a new technology called double molding has been developed in this work, for the realization of diamond microtips having a high aspect ratio, regular shape and small radius of curvature.
In this introduction, some of the main applications of microtips are presented. Various fabrication processes for silicon tips are then described, as well as some of the existing technologies used to produce microtips in other materials. Finally, the principle of chemical vapor deposition of diamond is explained and its use for diamond tips formation is presented.

1.1 Applications of Microtips

Nowadays, the most widespread applications of microtips are probably the various kinds of scanning probe microscopes (SPM), where the tip is used as a probe to scan the surface and to study it with a very small contact or interaction area. Continued improvements in the resolution that profilometers can achieve has resulted in a need for extremely hard probes with ever smaller radii of curvature. Microtips have also been used for a long time as field emitters, and have recently emerged as key components in biological and medical applications. Some of these applications are briefly presented below.

1.1.1 Scanning Probe Microscopies

Scanning Tunneling Microscopy

In 1982, Gerd Binnig and Heinrich Rohrer presented for the first time a revolutionary microscope, which allowed images of the topography of a

conducting sample to be obtained on an atomic scale: the Scanning Tunneling Microscope (STM) [1] was born. The principle of the STM is based on scanning a sharp *conducting* tip very close over the surface of a *conducting* sample so that, when a bias voltage is applied between the tip and the sample, a tunneling current occurs. This tunneling current is measured as a function of the tip-sample distance and yields an image of the topography, and/or of the electronic properties of the uppermost atoms at the sample surface, with a very high spatial resolution.
STM was the first step to the development of various other SPM, among them the widely used Atomic Force Microscope (AFM) [2], the Magnetic Force Microscope (MFM) [3] and the Scanning Near-field Optical Microscope (SNOM) [4].

Atomic Force Microscopy

In 1986, Gerd Binnig, Calvin Quate and Christoph Gerber developed the atomic force microscope [2]. In this now well-known microscopy, the image is obtained by detecting the small interatomic forces acting between the apex of a sharp tip and the surface of the sample, thus allowing the imaging of even *insulating* surfaces.
The atomic force microscope consists essentially of a sharp tip located at the free end of a single-side clamped cantilever (probe), a deflection sensor, a signal amplification unit, a feedback loop controller and a xyz-piezo scanner (Fig. 1.1). The sample is mounted on the piezo scanner and conveyed towards the tip until forces are detected. The sample is then scanned relative to the probe in the xy direction. The forces between the sample and the tip cause the cantilever to deflect (Hook's law). The cantilever deflection (z) is detected by the deflection sensor, usually a laser beam focused on the back-side of the cantilever and reflected onto a position sensitive photodiode. The signal is then amplified and sent to the feedback loop controller. There, a feedback loop signal is generated to control the xyz-piezo scanner in order to keep a constant distance between the tip and the sample, whereas the same signal is recorded as a function of the xy position.
In atomic force microscopy, two regimes of working distances can be distinguished: the contact and non-contact modes. In contact mode, at a separation between the tip and the sample on the order of Å, the repulsive

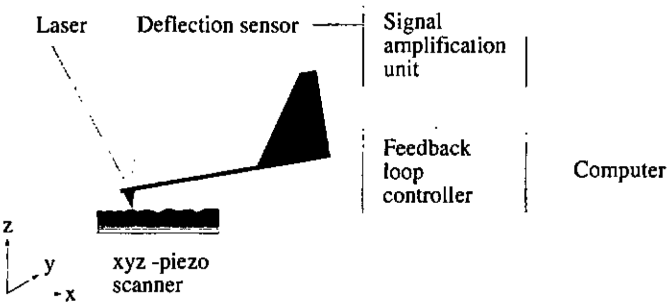

FIG. 1.1: Schematic of an atomic force microscope.

ionic forces are measured. This allows the topography of the sample to be determined with very high resolution, and even with atomic resolution under optimum conditions. In non-contact mode, at a separation between the tip and the sample of 10 to 100nm, the repulsive forces (van der Waals, electrostatic,...) are detected.
The AFM can be operated in either static or dynamic modes (Fig 1.2). In *static mode* (also called dc-mode), the cantilever is deflected due to the force acting on the tip until a static equilibrium is reached. At this point, a second distinction can be made between the equiforce mode and the variable deflection mode. In the equiforce mode, the deflection of the cantilever is kept constant by regulating the height of the sample with respect to the tip by means of the piezo scanner. This is the most commonly used mode. In the variable deflection mode, the height of the sample is kept constant and the variations of the cantilever deflections are recorded. This mode allows high scan rates but is essentially used with very flat surfaces for atomic scale imaging.
In *dynamic mode* (also called ac-mode), the cantilever is vibrated very close to its resonance frequency. The force F acting on the tip has a derivative in the z direction, F', the force gradient. A repulsive force increases the resonance frequency, while an attractive force lowers the resonance frequency. Again, a distinction can be made between the constant gradient mode and the variable gradient mode. In the constant gradient mode, the feedback loop ensures either a constant amplitude or a constant resonance frequency, both resulting in a map of a constant value of the force

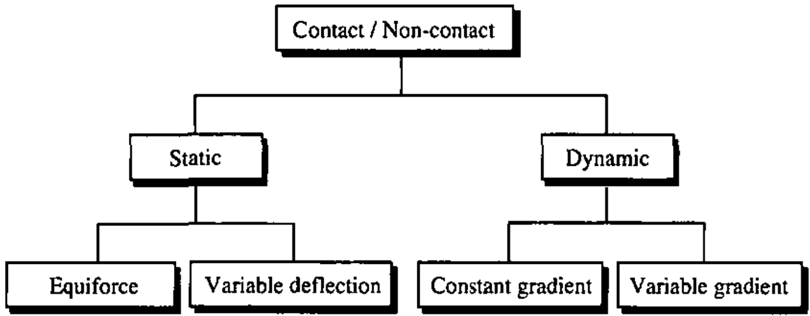

FIG. 1.2: Possible modes of operation in the AFM.

derivative. In the variable gradient mode, the feedback loop is disconnected and images with variable gradients are obtained, which are difficult to interpret. In the dynamic mode, the tip never or only occasionally touches the sample, reducing the wear of the tip and damage to soft samples.
AFM probes are usually realized using micromachining techniques. Indeed, the cantilever has to fulfill two essential conditions. It must have a typical spring constant ranging between 0.01N/m and 100N/m, usually 1N/m, as well as a resonance frequency higher than 10kHz. The value of the spring constant has to be small enough compared to the atomic spring constant (~10N/m) to allow bending of the cantilever rather than destruction of the sample or tip. On the other hand, a high resonance frequency reduces the effect of environmental vibration noises and allows short response times while scanning. To achieve a low spring constant and a high resonance frequency, the mass and the dimensions of the cantilevers should be small, motivating the use of microfabrication technologies. Typical dimensions for a silicon cantilever are a length of 300μm, a width of 60μm and a thickness of 3μm, resulting in a spring constant of 2.5N/m and a resonance frequency of 46kHz.
The tip also has geometric conditions to fulfill. It must be high enough to ensure that the tip and not the end of the cantilever touches the sample, but not so heavy that its mass reduces the resonance frequency of the lever. Therefore, the tip must have a high aspect ratio (height divided by the diameter at the base), which also allows a reduction in tip/sample convolution effects when scanning samples with protruding structures or

deep holes. Moreover, the resolution in atomic force microscopy is directly related to the sharpness of the tip. The tip therefore must have a very small radius of curvature, usually smaller than 50nm.
In most cases, AFM probes are realized either in silicon or in silicon nitride. However, for other SPM, microtips can be realized in various other materials such as metals for STM, magnetic material for MFM, or quartz for SNOM. Moreover, diamond probes can be used in AFM to reduce the wear of the tip in contact mode or the risk of breaking the tip apex when approaching the sample. If mounted in a modified AFM, diamond probes can also be used for nanomechanical modifications of materials. In this case, a high load is applied to the diamond tip to scratch the surface of the sample, and the induced modifications can be imaged directly afterwards with the same tip in a regular AFM mode [5].

1.1.2 High Resolution Profilometry

A high resolution profiler (HRP-100, KLA-Tencor, Milpitas, CA, USA) is a surface profiling system which combines the macroscopic scale topography analysis of a standard profilometer with the microscopic scale analysis of an AFM. The same instrument is therefore able to realize long scans (up to 200mm) for homogeneity analysis of an etched surface, for example, or locate a defined position and there image a small area with very high resolution.
The principle of operation of the HRP-100 is very similar to that of an AFM operated in variable deflection contact mode. However, the minimal force which can be applied to the measuring tip of this high resolution profiler is either 0.1μN or, more often, 0.5μN, which is two to three orders of magnitude higher than the force applied to an AFM tip. The profiler tip must therefore be diamond or at least of a sufficiently hard material.
The probe of the profiler consists of a cantilever, or stylus holder, with one end connected to a capacitive detection as well as to a magnetic stylus force control system, and with the other end tipped with a sharp stylus. The stylus generally consists of a mechanically shaped stainless steel shank whose diamond measuring end has been milled to produce a conical tip having a radius of curvature of about 2μm. For high resolution imaging, these styli can be sharpened by focused ion beam (FIB) to produce a 500nm high

diamond tip having a radius of curvature of 30-50nm with a total cone angle of ~40°. Since FIB sharpening is a serial process, there is a growing interest for diamond microtips realized by micromachining batch processes.
A more complete description of the high resolution profiler, as well as of the various diamond tips generally used or experimented with on this instrument, are given in chapter 6.

1.1.3 Other Applications

Field Emitters

The first applications of microtips were probably as field emitters in vacuum microelectronics. Indeed, without heating the emitter, electron emission in vacuum can be induced by applying a sufficiently high electric field between the emitter and the gate, with a counter-electrode placed close to the emitter. In order to reach these high fields at reasonable voltages, field emitters have been micromachined into protruding objects, such as whiskers or tips, to take advantage of field enhancement of regions of high curvature.
Field emitters can be produced in various materials such as molybdenum [6], monocrystalline silicon [7], polycrystalline silicon [8], diamond [9] and others. Their principal applications are probably flat panel displays, but they can also be used as electron sources in miniature electron microscopes [10], or even as pressure sensors [11].

Applications in Biology

Recently, arrays of silicon microtips have also been produced for biological purposes. In 1995, William Trimmer et al. [12] realized microtip arrays for injecting deoxyribonucleic acid (DNA) into plants and animal tissues. The principle is the following: a solution containing the DNA to be injected is placed onto the plants cells. The microtip array is then pressed onto the culture of cells, with the tip apexes penetrating the cells walls to allow the new genetic material to enter the cells. In a similar way, S. Henry et al. [13] proposed in 1998 to use an array of silicon microtips to perforate the upper layer of the skin in order to enhance the efficiency of transdermal drug delivery.

More challenging has been the realization of arrays of platinum tip-shaped microelectrodes on a porous substrate, used for monitoring the activity of brain slices in vitro [14]. In this case, the silicon tips were passivated, coated with platinum, and passivated again. Then, the Pt layer on the tip apexes was re-exposed. High aspect ratio holes were realized through the whole thickness of the wafer, in order to allow a nutrient solution to contact the brain slice lying on the microtip array. The microelectrodes were high and sharp enough to perforate the external layer of the slice, allowing the unpassivated tip apexes to reach the neurons and measure their activity at the heart of the brain slice exclusively.

The use of diamond tips could also be interesting for these applications. Their hardness would avoid breaking of the tips when perforating cell tissues or skin, increasing tip lifetime. Moreover, diamond is known as a biocompatible material, and, if chemically vapor deposited, it can be doped to be used as a microelectrode material.

1.2 Fabrication Techniques for Microtips

1.2.1 Silicon Tips

Silicon tips are most often used as AFM probes. In this work, however, they also serve as templates for the first molding of the double molding process, determining the exact geometry of the final diamond tips.
Silicon tips can be realized by various techniques resulting in tips of different shapes. They can either be etched from the bulk material using a protection mask (usually silicon dioxide or silicon nitride) or grown as whiskers. The etching techniques can be either isotropic or anisotropic, and can be realized either in a solution (wet etching) or in a plasma reactor (dry etching). Some of these processes and the resulting tip characteristics are presented below.

Dry Etching Techniques

Dry etching of silicon tips can be performed either by an isotropic Reactive Ion Etching (RIE) process using SF_6/O_2 [15, 16, 17], or by an anisotropic RIE with a C_2ClF_5/SF_6 gas mixture [18]. Other gas mixtures resulting in etches of variable anisotropy have been presented in [19]. Isotropic dry etching techniques lead to the formation of tips having a low global aspect ratio (<1) (Fig. 1.3a), while anisotropic etches form high aspect ratio shafts with a flat apex (Fig. 1.3b). Therefore, dry etched silicon tips are sometimes realized with a combination of isotropic and anisotropic RIE techniques resulting in stylus-like or rocket-shaped tips (Fig. 1.3c) [15, 17, 20, 21].

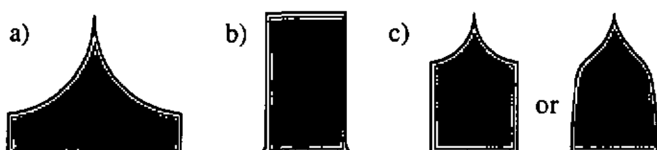

FIG. 1.3: Schematic of silicon tips realized by dry etching techniques: a) Isotropic etching only; b) Anisotropic etching only; c) Combination of isotropic and anisotropic etching: Stylus-like tip (left) [17] and rocket-shaped tip (right) [15] depending on the sequence of the isotropic and anisotropic etching.

Unfortunately, dry etching is not very uniform over the whole surface of a wafer, resulting in overetching and blunting of some tips while others are still covered with their protective masks. Therefore, dry etching is usually stopped before the masks collapse. If the diameter of the interface silicon/protection mask is wider than half a micrometer, the formation of the tips can be completed either by wet isotropic etching in a hydrofluoric/nitric/acetic acid mixture (HNA) [16, 18] or wet anisotropic etching in a potassium hydroxide (KOH) solution [22]. If one wants to sharpen already completed tips, or if the interface diameter is small enough after the dry etching steps, an oxidation sharpening procedure can be performed, leaving uniform tips with a very small radius of curvature.

Oxidation Sharpening

Oxidation sharpening is a well-known procedure to decrease the radii of curvature of silicon tips. It is based on an oxidation inhibition of silicon which occurs at regions of high curvature. This anomaly is due to a stress created at the Si/SiO_2 interface on a non-planar surface due to the increase in molar volume when silicon is oxidized. This stress builds up in thermally grown oxide only at temperatures less than 1050-1100°C, usually 900°C for wet (H_2O) oxidation and 950°C for dry (O_2) oxidation. So, when silicon tips are oxidized under these conditions, the silicon consumption at the tip apex is smaller than at the tip sidewalls. After oxidation, the silicon dioxide is removed in a concentrated hydrofluoric acid (HF), which is preferred to buffered hydrofluoric acid (BHF) due to its higher selectivity with regard to silicon. This two-step procedure uniformly sharpens silicon tips ideally down to radii of curvature as small as 1nm [23].

Wet Etching Techniques

Isotropic as well as anisotropic wet etching of silicon can also be used to form silicon tips. Isotropic etching is generally realized in a HNA solution [23, 24, 25, 26], but can also be performed in modified solutions such as a hydrofluoric/nitric acid mixture (without acetic acid) [27] or in a hydrofluoric acid/nitric acid/ammonium fluoride/water mixture [28]. The resulting tips all have a low global aspect ratio (<1) (Fig. 1.4 a). Moreover, all these solutions exhibit diffusion controlled etch rates, resulting in a lack

of uniformity in the tip etching and therefore tip blunting. This problem can be overcome by rotating the wafer in the solution at an optimal rotation speed [24] or by oxidation sharpening [23, 26, 27, 28]. Finally, differences have been observed in the final tip shapes depending on the crystal orientation of the {111} or {110} wafers [24], as well as on the orientation of the square protective masks relative to the crystal orientation of the {100} silicon wafers [25].

Because of its higher uniformity, anisotropic wet etching has been more extensively studied. Anisotropic etching can be realized with various solutions, like ethylene diamine pyrocatechol (EDP), tetra methyl ammonium hydroxide (TMAH), KOH and KOH-based solutions in which either isopropanol (IPA) or butanol are added. Silicon tips realized with EDP are limited by {111} planes and have therefore a low aspect ratio and a wide opening angle (70°) at the tip apex [29, 30]. Tips realized with KOH-based solutions with either IPA or butanol added exhibit similar characteristics (Fig. 1.4b) [15, 25, 26].

On the other hand, TMAH [31] and KOH [32, 33, 34, 35, 36] make possible silicon tips defined by high index crystallographic planes (Fig. 1.4c). These tips have a regular shape, a high aspect ratio and a small radius of curvature. KOH-etched silicon tips are also self sharpening, which means that no blunting of the tip apex occurs in case of overetching. These tips are therefore easy to produce and can be realized with a single etching step. For these reasons, they have been chosen to act as templates for the double molding process. The detailed fabrication as well as an evaluation of KOH-etched silicon tips will be presented in Chapter 2.

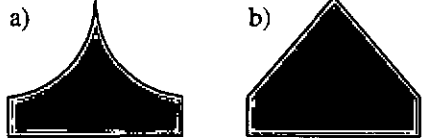

FIG. 1.4: Schematic of wet etched silicon tips: a) Isotropic etching in HF:HNO_3-based solutions; b) Anisotropic etching with EDP, or KOH-based solutions saturated with IPA or butanol; c) Anisotropic etching with TMAH or KOH solutions.

Whisker Growth

The silicon tips having among the highest aspect ratios possible are produced by sharpening a grown silicon whisker. Silicon whisker growth has been studied in [37] and is based on a Vapor-Liquid-Solid (VLS) mechanism. The process starts by depositing small particles of gold (Pt, Ag, Pd, Cu or Ni have also been successfully used) on the surface of a {111} silicon wafer. These particles, heated at 950°C, form small droplets of liquid Au-Si alloy having a relatively low freezing temperature. A gas mixture of hydrogen and $SiCl_4$ is introduced and the liquid droplet, acting as a preferred site for Si deposition from the vapor, becomes saturated with Si. Most of the Si contained in the droplet freezes out at the interface between solid Si and the liquid alloy, displacing vertically the droplet and resulting in whisker growth (Fig. 1.5a). The whisker grows in length by this mechanism until the Au is consumed or until the growth conditions are changed.
Ultrasharp silicon tips having a very high aspect ratio (>5) have been realized by sharpening silicon whiskers with a two-step procedure (Fig. 1.5b) [38]. The whiskers, on top of which the small Au/Si alloy droplets were still present, were first isotropically etched in a HNA solution until the alloy cap was dislodged and then sharpened by the oxidation-dissolution technique presented above.

1.2.2 Tips in Other Materials

Microtips in various materials, such as silicon dioxide, silicon nitride, metals or diamond, can also be realized. Various technologies have been developed to do this, some of which are presented below.

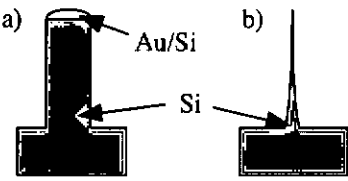

FIG. 1.5: Schematic of silicon whiskers: a) As grown and b) After the sharpening procedure.

Evaporation Through a Small Aperture

A well-known process to realize metallic tips involves evaporating a metal through a closely spaced aperture, producing a self aligned metal cone underneath the hole as the hole diameter is reduced (Fig. 1.6a) [6]. Various materials can be evaporated, such as molybdenum, niobium, iridium, tantalum, aluminum or even silicon dioxide and amorphous silicon [6, 8, 20]. These techniques produce sharp tips the height of which is unfortunately limited by the separation between the hole in the mask and the substrate. Moreover, there is a high risk of breaking the tip when removing the mask. Therefore, other fabrication processes have been developed to produce higher tips and to limit the risks of breakage.

Thin Film Deposition on a Silicon Tip

The easiest process to realize microtips in materials other than silicon consists of evaporating or depositing a thin layer of the desired material on a silicon tip (Fig. 1.6b). This process allows a wide selection of materials to be used to cover the tip. For example, tungsten [30], platinum [14], or diamond [39] tips have been produced in this way. However, while the global aspect ratio of the original silicon tip is preserved, the radius of curvature is considerably increased, depending on the thickness of the deposited film. Moreover, thin metallic films may easily rupture upon contact, leaving a poorly or even non-conductive apex.

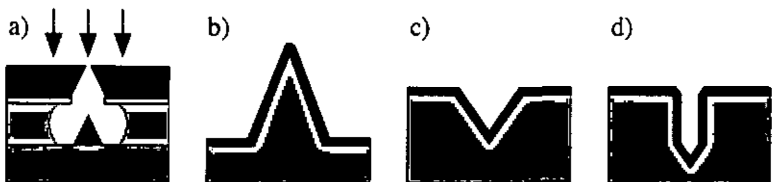

FIG. 1.6: Schematic of various processes for non-silicon tip formation: a) Evaporation through a small aperture; b) Deposition of a thin film on a silicon tip; c) Simple molding process; d) Modified simple molding process.

Molding Processes

To produce sharp microtips, a simple molding process has been developed [20]. In this process, pyramidal pits are etched in {100} silicon using anisotropic wet etching in KOH. The geometry of these holes is defined by four {111} Si planes. The desired tip material is then deposited on the wafer surface and in the pyramidal holes (Fig. 1.6c). This material can be patterned if necessary before being bonded onto another substrate like glass. Finally, the silicon mold is completely etched away. Well-defined microtips in Si_3N_4, W, Ni or diamond have been realized with this process [9, 20, 39, 40, 41]. To increase the aspect ratio at the tip apex, as well as to decrease the radius of curvature and the aperture angle, the silicon mold can be sharpened by low temperature thermal oxidation [40]. Though very sharp tips can be realized with the simple molding process, the global aspect ratio of the tips is still quite low (~0.7). To address this problem, a modified simple molding process has been developed for higher aspect ratio metallic tips [41]. The steps are identical to the process described above, but an anisotropic RIE of Si is performed before the pyramidal pit formation (Fig. 1.6d). This process results in a tip having a high aspect ratio shaft with a pyramidal apex. Unfortunately, this process is difficult to control, since the cross-section of the RIE hole must be perfectly symmetrical. Otherwise, a "knife edge" tip instead of a sharp regular pyramid will be formed at the apex during the wet etching step.

In this work, a double molding process has been developed and successfully applied for the realization of sharp Pt and diamond tips having a regular shape and a high aspect ratio. This process will be presented in chapters 4 and 5.

1.3 Diamond Deposition

Various techniques for chemical vapor phase deposition (CVD) of diamond are used nowadays. This section will focus on the hot-filament CVD (HF-CVD) technique, also known as thermal filament CVD (TF-CVD), which was exclusively used for all the diamond depositions in this study.

1.3.1 Hot-Filament-CVD Technique

The deposition of polycrystalline diamond films by the HF-CVD technique on silicon or silicon nitride substrate is generally composed of three main steps: the preparation of the sample, the seeding process, and finally the diamond deposition itself [42, 43].

Preparation or Pretreatment of the Sample

The purpose of the preparation of the sample is to rid preprocessed silicon wafers of various contaminations, and particularly to etch away possible silicon dioxide residues which can seriously compromise the diamond deposition. Indeed, the seeding process, as well as the diamond deposition step, require a perfectly clean and well defined sample surface.
A typical pretreatment begins by immersing the wafer in a wetting agent, immediately followed by a short silicon dioxide etch in a 5% HF solution. The wafer is then reoxidized (10-20Å) in fuming nitric acid (100% HNO_3), in which organic and metallic contaminations are also removed. After rinsing, the wafer is subjected to a thermal treatment to evaporate remaining surface contaminations. These steps generally result in a clean and well-defined surface.

Seeding Process

In the first step of the seeding process, the native silicon dioxide layer is removed from the silicon surface. This can be done in an activation solution such as HF, BHF, ammonium fluoride (NH_4F) or in alkaline media. After an intense rinse in DI water, the wafer is immersed in the seeding solution, an aqueous- or alcohol-based suspension containing very small commercially available particles (<100nm) of diamond. Generally, ultrasonic agitation is

performed during this step to increase the seeding efficiency. Ideally, one can obtain a *high density seeding (10^{12}-10^{13} crystallites/cm^2)* of *individual* crystallites at the surface of the silicon or of the silicon nitride layer.
In some cases, the seeding process can also be realized by just scratching the substrate with a diamond paste. This procedure is difficult to control and, of course, can damage the substrate.

HF-CVD of Diamond

The mechanism of the hot-filament chemical vapor phase deposition of diamond is depicted in Fig. 1.7. It takes place in a CVD reactor, where the silicon substrate is fixed on a graphite chuck and heated to a temperature of 830°C. Opposite to the chuck, a tantalum filament is heated to a temperature of about 2500°C. During the diamond deposition, the surface of this Ta-filament reacts with the methane (CH_4) and is transformed into TaC. Tungsten filaments can also be used but are more fragile.
The reactive gases hydrogen and methane are introduced into the reactor with the ratio H_2:CH_4=99:1 (Fig. 1.7a). The hydrogen molecules are adsorbed in the TaC surface of the filament, and dissociate to yield highly reactive atomic hydrogen (H*) as shown in Fig. 1.7b (Eq. 1.1).

$$H_2 + Energy \text{ -----> } 2H^* \qquad (1.1)$$

These hydrogen radicals strip hydrogen atoms from methane to form methyl radicals (CH_3*) (Eq. 1.2 and Fig. 1.7c).

$$CH_4 + H^* \text{ -----> } CH_3^* + H_2 \qquad (1.2)$$

Hydrogen atoms can also be removed from diamond carbons (C_D) at the surface of the crystallite, to form highly reactive dangling bonds (Eq. 1.3 and Fig. 1.7d).

$$C_DH + H^* \text{ -----> } C_D^* + H_2 \qquad (1.3)$$

Dangling bonds at the surface of the diamond crystallite are then occupied by methyl radicals, in this way adding diamond carbon atoms to the crystallite (Eq. 1.4 and Fig. 1.7e).

$$C_D^* + CH_3^* \text{ -----> } C_D\text{-}C_DH_3 \qquad (1.4)$$

Under these reaction conditions, sp^3 diamond films can be grown with a very low content of sp^2 graphite (10-1000ppm), found mainly in the grain boundaries of the polycrystalline diamond deposit.

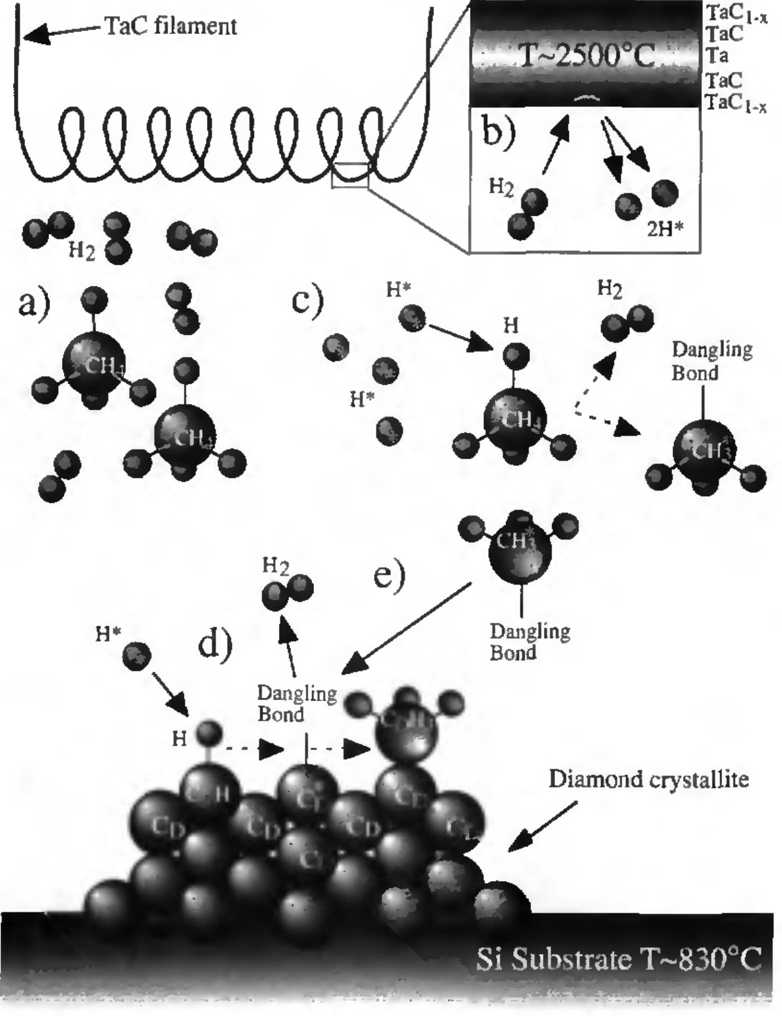

FIG. 1.7: Schematic of the hot-filament CVD diamond deposition process.

These diamond layers can be p-doped in situ by adding boron, in the form of trimethylboron (TMB), during the deposition. Typical film thicknesses range from 100nm to 2μm. and, under these conditions, are grown at a rate of about 0.25μm/h.

1.3.2 CVD Diamond Tips

Hot-filament CVD diamond has been used in the fabrication of different types of diamond tips. The easiest way to fabricate diamond tips is to deposit a thin (~100nm) diamond layer on etched tungsten wires [44] or on an already processed silicon tip [45, 46]. The radius of curvature of such tips is strongly influenced by the thickness of the diamond layer (Fig. 1.8). Nevertheless, it is possible in some cases to sharpen such diamond tips with an ion beam [46].
Another technology used to realize diamond tips uses the simple molding process described in section 1.2.2. In this case, HF-CVD diamond films are deposited in pyramidal holes defined by the {111} planes of silicon. The diamond tips are then released by completely removing the silicon which

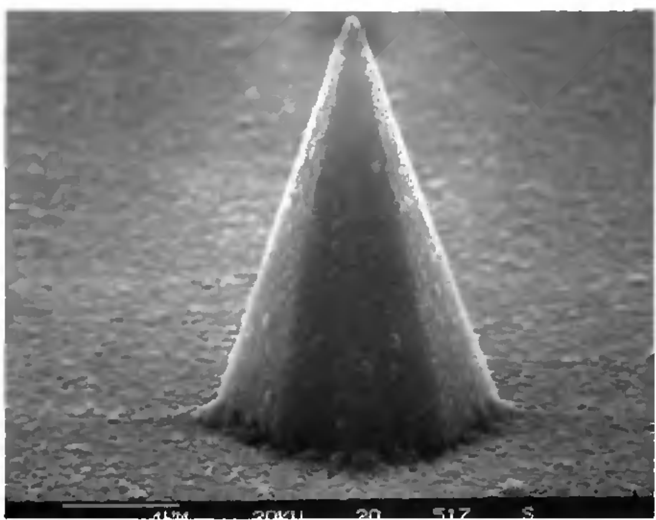

FIG. 1.8: Scanning electron microscope (SEM) picture of a HF-CVD diamond coated silicon tip, having a radius of curvature of about 200nm.

served as the mold [45, 47]. This technique allows the realization of diamond tips having radii of curvature as small as 20nm without further sharpening. Unfortunately, the aspect ratio of such tips is strictly limited by the {111} planes of silicon.

Finally, high aspect ratio, sharp HF-CVD diamond tips realized with the double molding process developed during this work are presented in chapter 5.

References

1 G. Binnig, H. Rohrer, Ch. Gerber and E. Weibel, "Surface Studies by Scanning Tunneling Microscopy", Physical Review Letters 49 (1982) 57-61.

2 G. Binnig, C.F. Quate and Ch. Gerber, "Atomic Force Microscope", Physical Review Letters 56 (1986) 930-933.

3 U. Hartmann, "Magnetic Force Microscopy: Some Remarks from the Micromagnetic Point of View", Journal of Applied Physics 64 (1988) 1561-1564.

4 D.W. Pohl, W. Denk and M. Lanz, "Optical Stethoscopy: Image Recording with Resolution λ/20", Applied Physics Letters 44 (1984) 651-653.

5 N.X. Randall, "Development and Application of a Multifunctional Nanotribological Tool", PhD Dissertation, University of Neuchâtel, Switzerland (1997).

6 C.A. Spindt, I. Brodie, L. Humphrey and E.R. Westerberg, "Physical Properties of Thin-Film Field Emission Cathodes with Molybdenum Cones", Journal of Applied Physics 47 (1976) 5248-5263.

7 R.N. Thomas, R.A. Wickstrom, D.K. Schroder and H.C. Nathanson, "Fabrication and Some Applications of Large-Area Silicon Field Emission Arrays", Solid-State Electronics 17 (1974) 155-163.

8 G.P. Myers, M. Aslam, P. Klimecky, L.W Cathey, R.E. Ider and B.E. Artz, " Fabrication and Characterization of Electron Beam Evaporated Silicon Field Emitter Arrays", Journal of Vacuum Science and Technology B 11 (1993) 642-646.

9 K. Okano, K. Hoshina, M. Iida, S. Koizumi and T. Inuzuka, "Fabrication of a Diamond Field Emitter Array", Applied Physics Letters 64 (1994) 2742-2744.

10 L.P. Muray, U. Staufer, E. Bassous, D.P. Kern and T.H.P. Chang, "Experimental Evaluation of a Scanning Tunneling Microscope-Microlens System", Journal of Vacuum Science and Technology B 9 (1991) 2955-2961.

11 H.H. Busta, "Vacuum Microelectronics-1992", Journal of Micromechanics and Microengineering 2 (1992) 43-74.

12 W. Trimmer, P. Ling, C.-K. Chin, P. Orton, R. Gaugler, S. Hashmi, G. Hashmi, B. Brunett and M. Reed, "Injection of DNA into Plant and Animal Tissues with Micromechanical Piercing Structures", Proceedings of MEMS'95, International Workshop on Micro Electro Mechanical Systems, Amsterdam, the Netherlands (1995) 111-115.

13 S. Henry, D.V. McAllister, M.G. Allen and M.R. Prausnitz, "Micromachined Needles for the Transdermal Delivery of Drugs", Proceedings of MEMS'98, International Workshop on Micro Electro Mechanical Systems, Heidelberg, Germany (1998) 494-498.

14 P. Thiébaud, C. Beuret, M. Koudelka-Hep, M. Bove, S. Martinoia, M. Grattarola, H. Jahnsen, R. Rebaudo, M. Balestrino, J. Zimmer and Y. Dupont, "An Array of Pt-Tip Microelectrodes for Extracellular Monitoring of Activity of Brain Slices", Biosensors & Bioelectronics 14 (1999) 61-65.

15 A. Boisen, O. Hansen and S. Bouwstra, "AFM Probes with Directly Fabricated Tips", Journal of Micromechanics and Microengineering 6 (1996) 58-62.

16 M.M. Farooqui, A.G.R. Evans, M. Stedman and J. Haycocks, "Micromachined Silicon Sensors for Atomic Force Microscopy", Nanotechnology 3 (1992) 91-97.

17 P.-F. Indermühle, "Microfabricated Probes with Integrated Functions for Scanning Probe Microscopy", PhD Dissertation, University of Neuchâtel, Switzerland, 1998.

18 J. Brugger, R.A. Buser and N.F. de Rooij, "Silicon Cantilevers and Tips for Scanning Force Microscopy", Sensors and Actuators A 34 (1992) 193-200.

19 I.W. Rangelow, "Sharp Silicon Tips for AFM and Field Emission", Microelectronic Engineering 23 (1994) 369-372.

20 T.R. Albrecht, S. Akamine, T.E. Carver and C.F. Quate, "Microfabrication of Cantilever Styli for the Atomic Force Microscope", Journal of Vacuum Science and Technology A 8 (1990) 3386-3396.

21 D.W. Kim, S.H. Lym, M.Y. Jung and S.S. Choi, "Fabrication of Field Emission Si-tip Array Using Reduced Submicron Masks Generated by Isotropic Etching of Mask Patterns", Proceedings of MNE'98, the International Conference on Micro- and Nanofabrication, Leuven, Belgium (1998) 177-178.

22 J. Itoh, Y. Tohma, S. Kanemaru and K. Shimizu, "Fabrication of an Ultrasharp and High-Aspect-Ratio Microprobe with a Silicon-On-Insulator Wafer for Scanning Force Microscopy", Journal of Vacuum Science and Technology B 13 (1995) 331-334.

23 R.B. Marcus, T.S. Ravi, T. Gmitter, K. Chin, D. Liu, W.J. Orvis, D.R. Ciarlo, C.E. Hunt and J. Trujillo, "Formation of Silicon Tips with <1nm Radius", Applied Physics Letters 56 (1990) 236-238.

24 R.N. Thomas, R.A. Wickstrom, D.K. Schroder and H.C. Nathanson, "Fabrication and Some Applications of Large-Area Silicon Field Emission Arrays", Solid-State Electronics 17 (1974) 155-163.

25 N.A. Cade, R.A. Lee and C. Patel, "Wet Etching of Cusp Structures for Field-Emission Devices", IEEE Transactions on Electron Devices 36 (1989) 2709-2714.

26 J.T. Trujillo and C.E. Hunt, "Fabrication of Silicon Field Emission Points for Vacuum Microelectronics by Wet Chemical Etching", Semiconductors Science Technology 6 (1991) 223-225.

27 A. Folch, M.S. Wrighton and M.A. Schmidt, "Microfabrication of Oxidation-Sharpened Silicon Tips on Silicon Nitride Cantilevers for Atomic Force Microscopy", Journal of Microelectromechanical Systems 6 (1997) 303-306.

28 R.C. Davis, C.C. Williams and P. Neuzil, "Micromachined Submicrometer Photodiode for Scanning Probe Microscopy", Applied Physics Letters 66 (1995) 2309-2311.

29 K.E. Bean, "Anisotropic Etching of Silicon", IEEE Transactions on Electron Devices ED-25 (1978) 1185-1193.

30 H.H. Busta, R.R. Shadduck and W.J. Orvis, "Field Emission from Tungsten-Clad Silicon Pyramids", IEEE Transactions on Electron Devices 36 (1989) 2679-2685.

31 P.B. Grabiec, F. Shi, P. Hudek, T. Gotszalk, M. Zaborowski, P. Dumania and I.W. Rangelow, "Scanning Probe Sharp Tip Formation for IC Integration Using Mesa Technique", Microelectronic Engineering 35 (1997) 329-332.

32 O. Wolter, Th. Bayer and J. Greschner, "Micromachined Silicon Sensors for Scanning Force Microscopy", Journal of Vacuum Science Technology B 9 (1990) 1353-1357.

33 H.L. Offereins, K. Kühl and H. Sandmaier, "Methods for the Fabrication of Convex Corners in Anisotropic Etching of (100) Silicon in Aqueous KOH", Sensors and Actuators A 25-27 (1991) 9-13.

34 J.-H. Liu, T.M. Betzner and H. Thurman Henderson, "Etching of Self-Sharpening {338} Tips in (100) Silicon", Journal of Micromechanics and Microenginering 5 (1995) 18-24.

35 P.-F. Indermühle and N.F. de Rooij, "Integration of a Large Tip with High Aspect Ratio on an XY-Micro Stage for AFM Imaging", Proceedings of Transducers'95 & Eurosensors IX, Stockholm, Sweden (1995) 652-655.

36 I.J. Chung, D.B. Murfett, A. Hariz and M.R. Haskard, "Fabrication of High Aspect Ratio Silicon Micro-Tips for Field Emission Devices", Journal of Materials Science 32 (1997) 4999-5003.

37 R.S. Wagner and W.C. Ellis, "Vapor-Liquid-Solid Mechanism of Single Crystal Growth", Applied Physics Letters 4 (1964) 89-90.

38 E.I. Givargizov, "Ultrasharp Tips for Field Emission Applications Prepared by the Vapor-Liquid-Solid Growth Technique", Journal of Vacuum Science Technology B 11 (1993) 449-453.

39 Ph. Niedermann, W. Hänni, N. Blanc, R. Christoph and J. Burger, "Chemical Vapor Deposition Diamond for Tips in Nanoprobe Experiments", Journal of Vacuum Science Technology A 14 (1996) 1233-1236.

40 S. Akamine and C.F. Quate "Low Temperature Thermal Oxidation Sharpening of Microcast Tips", Journal of Vacuum Science Technology B 10 (1992) 2307-2310.

41 A. Boisen, J.P. Rasmussen, O. Hansen and S. Bouwstra, "Indirect Tip Fabrication for Scanning Probe Microscopy", Microelectronic Engineering 30 (1996) 579-582.

42 Private communication with W. Hänni, CSEM, Neuchâtel.

43 H.E. Hintermann and A.K. Chattopadhyay, "Low Pressure Synthesis of Diamond Coatings", Annals of the CIRP 42 (1993) 769-783.

44 G.J. Germann, G.M. McClelland, Y. Matsuda, M. Buck and H. Seiki, "Diamond Force Microscope Tips Fabricated by Chemical Vapour Deposition", Review of Scientific Instrument 63 (1992) 4053-4055.

45 Ph. Niedermann, W. Hänni, N. Blanc, R. Christoph and J. Burger, "Chemical Vapor Deposition Diamond for Tips in Nanoprobe Experiments", Journal of Vacuum Science Technology A 14 (1996) 1233-1236.

46 E.I. Givargizov, A.N. Stepanova, E.S. Mashkova, V.A. Molchanov, F. Shi, P. Hudek and I.W. Rangelow, "Ultrasharp Diamond-Coated Silicon Tips for Scanning Probe Devices", Microelectronic Engineering 41/42 (1998) 499-502.

47 H. Björkman, P. Rangsten, U. Simu, J. Karlsson, P. Hollman and K. Hjort, "Diamond Microstructure Replicas from Silicon Masters". Proceedings of MEMS'98, International Workshop on Micro Electro Mechanical Systems, Heidelberg, Germany (1998) 34-39.

Silicon Tips: Fabrication and Study 2

Among various microfabrication techniques for the realization of silicon tips, previously reported studies showed that tips obtained by anisotropic wet etching in KOH have well-defined sidewalls, a high aspect ratio, and a small radius of curvature [1, 2, 3, 4, 5]. Moreover, such tips are uniformly etched over the whole surface of a wafer, and self-sharpening occurs in case of overetching.
The objective of this work was to study the fabrication of silicon tips by anisotropic wet etching in KOH and to analyze the characteristics of the tips obtained with this process. The use of this technology to fabricate integrated silicon tips on cantilevers is foreseen. These silicon tips can also act as a first mold in the double molding process to be described in a later chapter. Parts of this study have been published in [6].

2.1 Introduction

In recent years, a multitude of fabrication processes for silicon tips have been developed. Indeed, if silicon tips were originally used as field emitters in vacuum microelectronics applications [7, 8, 9, 10], the advent of the atomic force microscope in 1986 [11] has aroused a new interest in further investigations for silicon tip fabrication technologies.
As both applications require batch-processed tips having a high aspect ratio and a very small radius of curvature at the tip apex, new fabrication technologies tend to combine two or more etching steps to fulfill these conditions, especially when using dry etching techniques [12, 13]. However, as mentioned in section 1.2.1, anisotropic wet etching in KOH produces tips having such characteristics in a single technological step and in a reproducible way. This is essentially due to the good uniformity of KOH

etching over the whole surface of the wafer, as well as to the self-sharpening property of the KOH-etched tips. Moreover, overetching does not lead to blunting or changes in the general shape of the tips. Finally, their well-defined geometry seems to be a good compromise (high aspect ratio/rigidity) for probes used in various applications, such as AFM, nanomechanical modification for thin layer characterization, or contact profilometry.

This chapter describes the fabrication and characterization of silicon tips made by etching with KOH. This study forms the basis for the realization of the more complex devices presented in following chapters.

2.2 Fabrication of KOH-Etched Silicon Tips

In this section, the basic microfabrication process used to realize KOH-etched silicon tips is presented in detail. Following sections and chapters will refer back to this section as necessary, since these standard procedures also form the basis of several new techniques presented later.

Standard Cleaning and Oxidation

The first step involved preparing the {100} silicon wafer for oxidation by means of a three-step procedure called "standard cleaning". This procedure started with the removal of organic compounds on the silicon surface by immersing the wafer in a 100% nitric acid bath for 10 minutes. The native silicon dioxide was then removed in a BHF solution for one minute, and finally a clean, very thin silicon dioxide layer was grown in a 70% boiling nitric acid bath for 10 minutes. As soon as possible after the standard cleaning, a layer of wet thermal silicon dioxide (SiO_2), typically 3000Å thick, was grown on both sides of the wafer (Fig. 2.1a).

Patterning of the Silicon Dioxide: Photolithography and Wet Etching

Photolithography began with a dehydration step in a convection oven at 200°C for 30 minutes, in order to remove the adsorbed water molecules from the wafer surface. To prevent further adsorption of water and to improve the adhesion of the photoresist to the substrate, a priming procedure was then immediately carried out in a vapor phase of hexamethyldisilazane (HMDS) at room temperature for 15 minutes. A positive photoresist layer (AZ 1518, Hoechst), typically 1.8μm thick, was then spun onto the back-side of the wafer at 4000 rpm for 40 seconds, and hard-baked at 120°C in a convection oven for 30 minutes. This first photoresist layer protected the back-side silicon dioxide layer during patterning of the top-side by wet etching.

A second, identical photoresist layer was spun onto the top-side and prebaked (pre-exposure baked) at 85°C for 35 minutes in a convection oven. The wafer was then inserted in a commercial double-side mask aligner (AL6-2, Electronic Vision). As the tips are anisotropically etched, the

crystalline character of silicon determines their geometry. Therefore, square patterns on the mask had to be very carefully aligned to less than ±1°, with their sides parallel to the {110} planes as indicated by the <110> oriented flat of the wafer. The top-side of the wafer was then exposed in contact with the mask to an energy of $45mJ/cm^2$. Finally, the exposed photoresist was dissolved in an alkaline developer bath (AZ351:DI water 1:4) for 60 seconds, and the remaining photoresist was hard-baked (Fig. 2.1b).
The bare silicon dioxide was etched in a buffered hydrofluoric acid bath containing 7 parts of 40% NH_4F to 1 part of concentrated HF (BHF 7:1) at a typical rate of 600Å/min. Silicon dioxide being hydrophilic and silicon hydrophobic, it was very easy to check that the silicon dioxide was completely removed. Finally, both photoresist layers were stripped in acetone for 5 minutes, and the wafer rinsed in isopropanol and DI water (Fig. 2.1c).

Tip Anisotropic Etching

Tip anisotropic etching was performed in a 40% KOH solution at 60°C. The silicon wafer was immersed in an inclined position in order to facilitate the removal, from the surface of the etched silicon, of the hydrogen bubbles generated by the etching reaction. In these experiments, the solution temperature was controlled through a "bain-marie" set-up, that is, by immersion of the etch bath in a controlled temperature water bath. Another

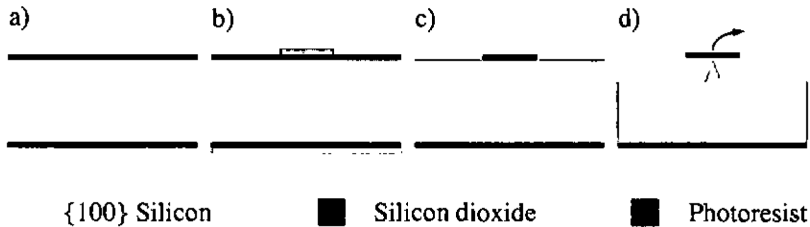

FIG. 2.1: Process sequence for the realization of KOH-etched silicon tips: a) Cleaning and oxidation of a {100} silicon wafer. b) Back-side: Protection of the silicon dioxide with a photoresist layer. Top-side: photolithography for silicon dioxide masks patterning. c) Silicon dioxide wet etching and photoresist stripping. d) KOH underetching of the silicon dioxide mask and tip formation.

bath with direct temperature control was also initially used, as described in section 2.3.1. Silicon was anisotropically etched under the silicon dioxide masks, whose shapes will be discussed in section 2.3.2, until the different slow etching high slope planes intersected each other. At this point, the silicon dioxide masks fell away, leaving well-defined silicon tips having an aspect ratio of approximately 1.5 (Fig. 2.1d). Under these conditions, the etching time depended essentially on the mask dimensions and geometry.
Finally, depending on the following steps of the process, the remaining silicon dioxide could be etched away on both sides of the wafer in a BHF bath. Alternatively, if the back-side oxide was required for further processing, it could be protected with a hard-baked photoresist layer.

2.3 Results and Observations

While the fabrication of KOH-etched silicon tips seems to be straight forward when reading the previous section, it should be noted that the etching mechanism is not completely understood and some observations are difficult to explain. Also, the few reports published to date on this subject are contradictory [2, 3, 4].

The work presented here consists of the preliminary studies and observations that were necessary for the development of the devices described in the next chapters. It is on no account a complete study of the formation and characteristics of KOH-etched silicon tips. In some cases, specific further investigations are proposed for a more complete study.

2.3.1 Influence of the KOH Bath Set-Up

Usually, two parameters are used to characterize a KOH etching bath: the KOH concentration and the temperature. Variations in these parameters are known to change the relative etch rates of secondary silicon planes in comparison to the etch rate of {100} planes [3, 14]. The overall etch rate of silicon is also strongly dependent on the temperature. For example, experiments showed that a 40% KOH heated at 60°C etches the {100} planes at a rate of ~16μm/h, and if maintained at room temperature (~24°C), the etch rate decreases to ~1μm/h.

In this work, a 40% KOH solution heated at 60°C was used. The tips were realized either in a so-called "standard KOH set-up" or in a "bain-marie KOH set-up". The standard KOH set-up consisted of a tank heated by a temperature-controlled immersion heater placed at the bottom. To ensure a constant temperature in the whole bath, circulation of the solution was performed by means of a pump. The absence of water in the vicinity of the KOH bath prevented water vapor from condensing in the bath. On the other hand, the "bain-marie KOH set-up" consisted of a temperature-controlled water bath heated by a temperature-controlled immersion heater. The water temperature homogeneity was assured by agitation. The KOH solution, contained in a tightly covered tank, was placed in this water bath and heated. Even if small plastic balls were distributed on the water surface to

limit evaporation, the atmosphere was very humid, making it difficult to maintain the initial KOH concentration. In this set-up, the KOH solution was not stirred.

The first tips were realized in the standard KOH set-up, and the following observations made. These tips are defined by two types of crystal planes: low slope planes form the base of the tip, and higher slope planes the apex of the tip (Fig. 2.2). The presence of the low slope planes considerably reduces the general aspect ratio of the tips and must therefore be avoided. On the same wafer, it was noted that the portion of the tip height formed by low slope planes varies with the density of tips in an array. Indeed, the higher the density of tips, the smaller is the base. Figure 2.3 shows a scanning electron micrograph (SEM) of a 48μm-pitch array of silicon tips directly neighboring the 72μm-pitch tip array shown in Fig. 2.2. The reduction of the tip base is obvious.

Further experiments in the standard KOH set-up showed some variations in the height of the tip base, depending on the age of the KOH solution. Surprisingly, the older, and hence more contaminated, the solution was, the smaller was the base. Unfortunately, the degree of contamination of the KOH bath was difficult to control, as the bath was used by multiple users. The sources of contamination could be photoresist, stainless steel originating from a metallic chuck occasionally used for top-side protection of preprocessed wafers, or other materials that could be released from a wafer if it was accidentally broken during an attack.

It was therefore decided to set up a special KOH bath, used exclusively for making tips: the "bain-marie" KOH set-up. In a first attempt, the relatively old KOH solution from the standard KOH set-up was transferred to the bain-marie set-up. The tips obtained in the same KOH solution, but in the bain-marie instead of the standard set-up, appeared to have nearly no base at all (Fig. 2.4). Some families of low slope planes remained only at four of the eight corners of the octagonal base of the tips. Moreover, no difference was observed either for tips belonging to an array or to more widely spaced tips.

To completely exclude the degree of contamination of the KOH bath as a factor for the appearance of the low slope planes, some more tips were realized in a brand new KOH bath mounted in the bain-marie set-up. Once more, the tips had almost no base, and no changes in the ratio of low-to-high

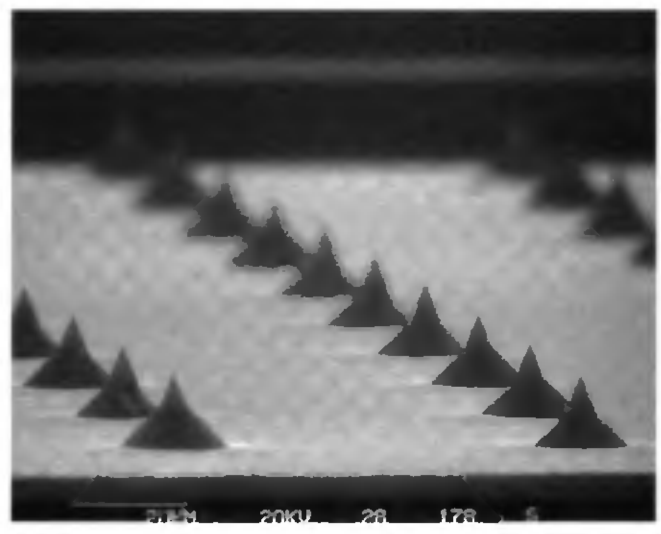

FIG. 2.2: SEM of a 72μm-pitch array of KOH-etched silicon tips. The base of the tips, defined by low slope planes, constitutes a significant portion of the total tip height.

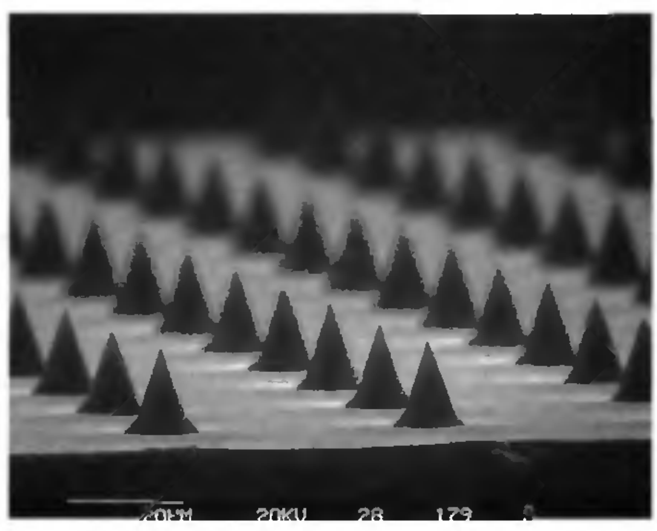

FIG. 2.3: SEM of a 48μm-pitch array of KOH-etched silicon tips. The base of the tips is considerably reduced compared to the tips of Fig. 2.2.

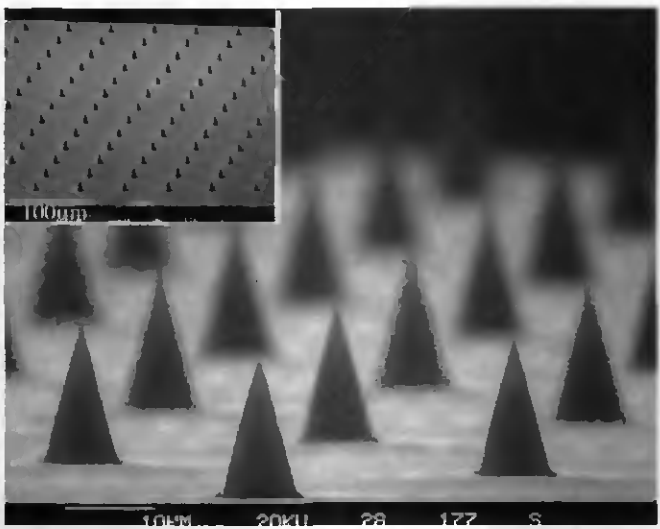

FIG. 2.4: SEM of a tip array realized in the old KOH solution mounted in the bain-marie set-up. These tips have almost no base at all.

slope planes could be observed between these tips and those made in the old KOH bath. From this, it can be concluded that the degree of contamination of the KOH bath does not seem to have an influence on relative etch rates of the low and high slope planes of silicon.

Circulation of solution in the standard KOH set-up was also considered as a possible cause for the etched tips with high bases shown in Figs. 2.2 and 2.3. This circulation could perhaps induce a faster renewal of the KOH solution at the tip etching location. Tips were therefore etched in the standard KOH set-up without turning on the pumping mechanism. Once more, the obtained tips had significantly high bases. To date, it has not been possible to get high aspect ratio tips with the standard KOH set-up.

The reason why nice tips were obtained only when using the bain-marie KOH set-up is still unknown. It is proposed to carry out further etching experiments in the bain-marie set-up, precisely controlling the temperature of the KOH bath itself rather than the water bath, and perhaps verifying the KOH concentration after etching. Since it was observed that nice tips could always be produced when using the bain-marie set-up, this method was used for etching all tips realized in this work.

2.3.2 Silicon Dioxide Mask Design

The goal of these experiments was essentially to define the geometrical shape and size of the silicon dioxide mask necessary to obtain silicon tips having a height of 12-15μm. Tips in this height range were required for several different projects presented in the next chapters. Other tip heights were necessary for a project not described in this thesis, where KOH silicon tips were the base structure for innovative microelectrode arrays, made to record the activity in brain slices in vitro [15]. Different shapes and sizes of silicon dioxide masks were therefore investigated in order to obtain silicon tips having heights of 15μm, 25μm and 50μm.
In this work, essentially four different geometrical shapes of various dimensions were used to define the silicon dioxide masks. The shapes were squares, circles, and two differently oriented octagons. The squares were oriented with their edges parallel to the <110> flat of the wafer, while the octagons either had their edges parallel to the flat (octagons I) or one of their corners pointing in the direction of the flat (octagons II = octagons I after a rotation of 22.5°). The octagons II were chosen because their edges are nearly parallel to the edges of the octagon resulting from the intersection of the (001) plane with the eight high slope planes forming the tip. In our case, the dimensions of the squares ranged from 10μm to 100μm in 10μm steps, and the other shapes ranged from 10μm to 200μm with the same size interval.
These experiments were realized in the following manner: after silicon dioxide patterning, the wafers were immersed in the KOH solution for a time corresponding to the desired etch depth of the (001) planes. After rinsing and drying, the etch depth was controlled with a standard profilometer [16] and the wafer was examined using an optical microscope. The heights of the tips corresponding to the most recently fallen silicon dioxide masks of each shape were estimated with the optical microscope, by successively focusing at the base and apex of the tip and reading the vertical displacement of the table from the micrometric screw. The precision of the measurement was estimated to be ±1μm. It is important to note that in some cases the tips were overetched, because the wafer stood too long in the KOH after the silicon dioxide mask had fallen away. The results are summarized in Table 2.1.

TABLE 2.1: Summary of the silicon dioxide mask shapes and dimensions used to realize KOH-etched silicon tips of specific heights. The tips marked with a "" are overetched.*

Mask shape	Mask size	Etch depth	Tip height	Remarks
Square	30μm	12.5μm	11μm	Standard KOH set-up
Square	40μm	15.4μm	15μm	Standard KOH set-up
Octagon I	60μm	17.7μm	14.5μm	Standard KOH set-up
Octagon II	60μm	15.2μm	13.5μm	Standard KOH set-up
Square	40μm	16μm	15μm	Bain-marie KOH set-up
Square	80μm	35μm	25μm *	Bain-marie KOH set-up
Circle	110μm	35μm	17μm *	Bain-marie KOH set-up
Octagon I	120μm	35μm	33μm	Bain-marie KOH set-up
Octagon II	120μm	35μm	34μm	Bain-marie KOH set-up
Circle	190μm	60μm	52μm	Bain-marie KOH set-up
Octagon I	190μm	60μm	49μm	Bain-marie KOH set-up
Octagon II	190μm	60μm	49μm	Bain-marie KOH set-up

SEM observations did not reveal differences in the quality of the tips obtained with the different silicon dioxide mask shapes. The general shape of the tips, as well as their apex, seemed to be similar for all the different masks tested during this work. To obtain a specific tip height, the dimensions of the circle and octagons were very similar, but quite reduced for the square masks. It would be interesting to carry out further investigations, increasing the number of different etch depths, in order to represent the achievable tip height as a function of size for the different shapes tested. Moreover, it would be necessary to limit the cases where the tips suffer from overetching, as the tip height quickly decreases as soon as the mask falls away.

For this work, 40μm square silicon dioxide masks were chosen to produce the 12μm to 15μm high silicon tips used in the projects presented in the next chapters. The resulting tips stayed within the desired specifications, even if they were slightly overetched.

2.3.3 Influence of Overetching

Anisotropic KOH etching has a considerable advantage compared to RIE in that, once the silicon dioxide mask is completely underetched, only the height of the tips is reduced. Therefore, an accidental overetching still produces sharp tips. This is demonstrated in Fig. 2.5. The general shape of the tips remained unchanged and no blunting of the tip occurred even after three successive overetching steps.
However, it is important to note that the rate of tip height reduction is approximately six times higher than the etch rate of the silicon {100} planes. For example, an overetching time of 90sec, at a {100} planes etch rate of 16μm/h, resulted in an overetching of the {100} planes of 0.4μm, but a reduction of the tip height of 2.4μm. Considering that the etch time necessary to realize 15μm high tips is approximately 60 minutes, it is clear that one must be very careful while etching the silicon tips.
Nevertheless, this self sharpening characteristic ensures sharp tips over the whole surface of a wafer, even if the height homogeneity of the tips is reduced. The height homogeneity is usually essential for neighboring tips located on a single structure, but is less important if considering the wafer as a whole.

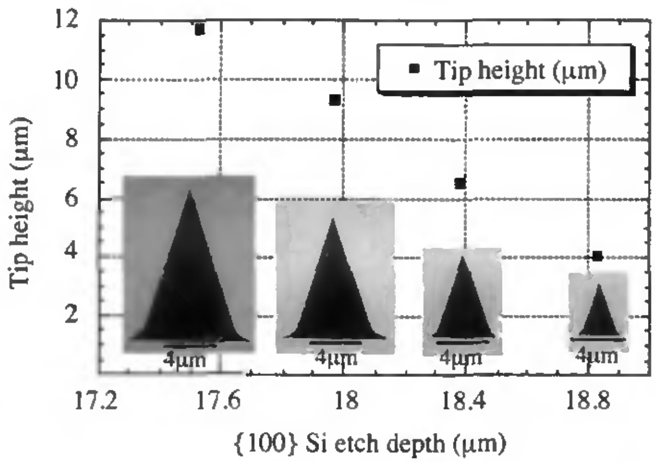

FIG. 2.5: Influence of overetching in KOH on the silicon tip shape and height.

2.3.4 Tip Height Distribution

Tip height measurements were made over a quarter of a wafer, by taking chips at different radial distance from the center of the wafer. These chips were mounted at ~90° in a SEM to measure the height of 88 tips. The results are presented in Fig. 2.6.

This graph clearly shows that the tips located at the edge of the wafer are higher than the tips located at the center. The dependence of the tip height on radial distance appears to be linear. However, this data is not conclusive, since the distances from the center were not recorded with the necessary precision.

This tip height distribution could be due to a number of factors, such as inhomogenous etching as a result of a possible temperature gradient in the bath, or a slight variation in the silicon dioxide mask dimensions due to a photolithography realized with soft contact between the mask and the wafer. On the other hand, a loading effect is unlikely since Price did not find any effect of stirring on the etch rate [17]. From that, it can be concluded that the reaction is not diffusion limited, and that the amount of silicon etched in the vicinity of the tips does not influence the etch rate. Therefore, tip height homogeneity should not be affected either.

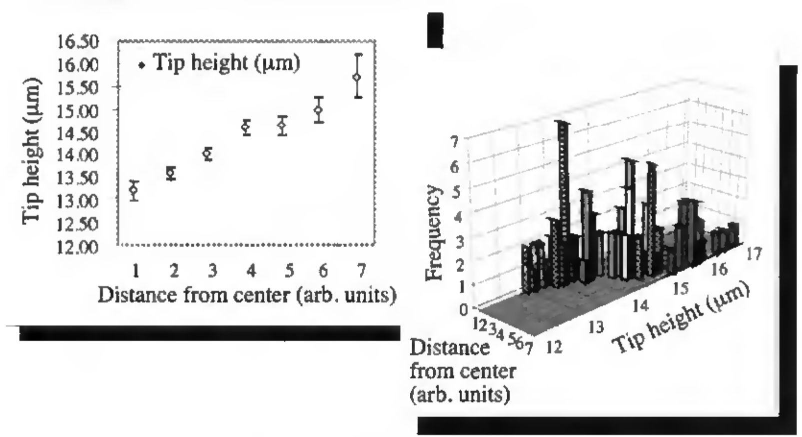

FIG. 2.6: Distribution of the height of silicon tips as a function of their distance from the center. The distance steps are probably not constant.

Since tip height variation was small on a local scale, and the shape and apices of the tips were satisfactory, tip height variation over the wafer was not considered to be a problem for the continuation of the work. Nevertheless, it would be interesting to make further tip height distribution measurements in order to determine if this variation is reproducible, and if so, to explain this phenomenon.

2.3.5 Tip Apex Shape

A sample of more than 500 tips was studied by SEM to determine the fraction of tips having usable apex shape and radius of curvature. Figure 2.7 depicts the occurrence of four apex shape categories. The so-called "ideal shape" and "inclined knife" categories, occurring in 53% and 16%, respectively, of the investigated tips, are considered to be usable. The radius of curvature of the tips classified in both these categories was always smaller than 30nm, and was on average 15.3nm. The 31% remaining tips had either "flat knife" apexes or were dull or broken.
The occurrence of the "flat knife" and "inclined knife" tip apex shapes can be explained as follows. The KOH-etched silicon tips are defined, if the small fraction of the base composed of low slope planes is not taken in consideration, by eight high slope planes ideally intersecting each other in a single point, the tip apex. It was observed by SEM that, in several cases, four of the eight planes vanish before reaching the tip apex, leaving the four remaining planes to form the tip apex. Ideally, these four planes should intersect in a single point and form an "ideal shape" apex. However, a slight asymmetry of the mask or a delay in the etching of one or more planes could perturb the equilibrium, giving rise to the appearance of "flat knife" and even "inclined knife" tip apexes.
Experiments done using slightly rectangular SiO_2 masks demonstrated the formation of essentially "flat knife" tips. Therefore, the occurrence of different tip apex shapes, as can be seen even for neighboring tips in a single array formed with square SiO_2 masks, could be explained by an insufficient precision in the dimensions of the mask used for the photolithography, which are guaranteed at $\pm 0.25\mu m$. So, besides turning to e-beam direct writing for making the SiO_2 masks, the best solution to avoid formation of flat knife tips would be to realize tips whose apexes are defined by the

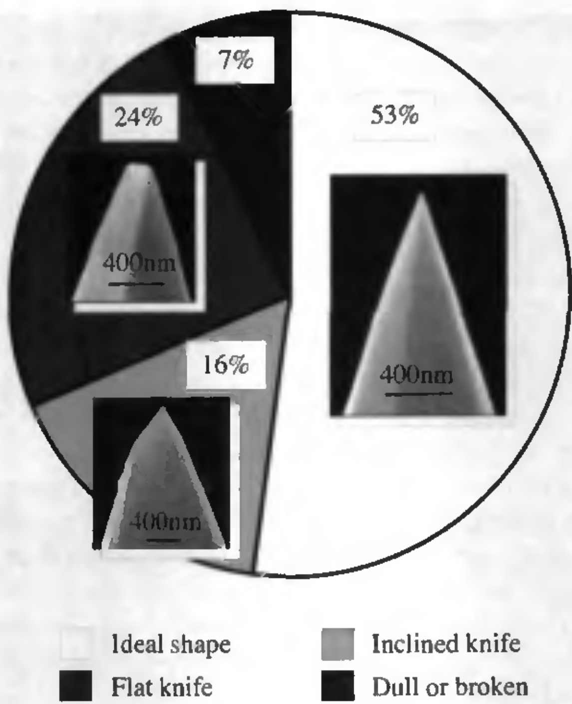

FIG. 2.7: Occurrence of the different silicon tip apex shapes.

intersection of only three planes. This is the strategy used for the realization of the commercially available, Nanosensors tips. The only inconvenience of this tip design lies in the asymmetry of the general tip shape, which can provoke irregular tip artifacts in profilometry applications while scanning samples having high aspect ratio features.

2.3.6 Crystallographic Planes

Among the few reports published on KOH-etched silicon tips, three articles were found, in which the family of high slope silicon planes defining the tip was determined. In 1991, Offereins et al. [2] described silicon tips produced by underetching square silicon dioxide (1000Å) / silicon nitride (4000Å) masks, oriented along the <110> direction and provided with corner compensation beams. They determined that the high slope planes forming

the tip belonged to the family of {411} silicon planes. In 1995, Liu et al. [3] etched silicon tips using circular or square 1.2μm thick silicon dioxide masks parallel to the <100> direction. After repetitive measurements to minimize statistical errors, they reported their tips to be formed by {338} planes. Finally, Chung et al. [4] presented tips etched under 5000Å thick silicon dioxide masks of various shapes (squares, circles, 127°/143° octagons) aligned to various crystal planes, including the [100], [110], [210] and [310] directions. They reported that [100] oriented masks produce tips defined by the {311} planes.

These different results are ambiguous. They are difficult to compare, because the experiments were not done under the same conditions. Nevertheless, it could be interesting to determine which family of planes are responsible for the tips produced in this work.

The high slope silicon planes forming the tips can be determined by measuring the aperture angles at the tip apex and the angles of the octagon formed by the intersection of the eight high slope planes with the (001) plane at the base of the tip (Fig. 2.8). The theoretical values of the octagon and aperture angles can be determined by vectorial analysis, this for each family of planes. In this work, only the three families mentioned above have been considered (Table 2.2).

To make a precise determination, the aperture angle of a silicon tip, measured in a SEM taken perpendicular to the tip axis, must fall between the values of α and β of a particular family of planes. At the same time, the angles of the octagonal intersection of the tip with the (001) plane must coincide with the values δ_1 and δ_2 of the same family of planes.

TABLE 2.2: Theoretical values of the angles defining the octagonal intersection of the different families of planes with the (001) plane (angle δ_1 and δ_2) and the aperture angles of the tip apex (angles α, β and γ) from different view angles.

Planes family	α	β	γ	δ_1	δ_2
{338}	*42.2°*	*38.7°*	*41.1°*	*131.1°*	*138.9°*
{113}	*38.9°*	*35.1°*	*36.9°*	*126.9°*	*143.1°*
{114}	*31.6°*	*27.3°*	*28.1°*	*118.1°*	*151.9°*

In our case, unfortunately, the high slope planes intersect the (001) plane only at four points, with low slope planes remaining at four corners of the tip (Fig. 2.9). As the angles δ_1 and δ_2 vary little from one family of planes to the other, it is impossible to base the plane determination on the characterization of this intersection. The next idea was to stop etching a tip before the silicon dioxide mask fell away, and to use the intersection of the

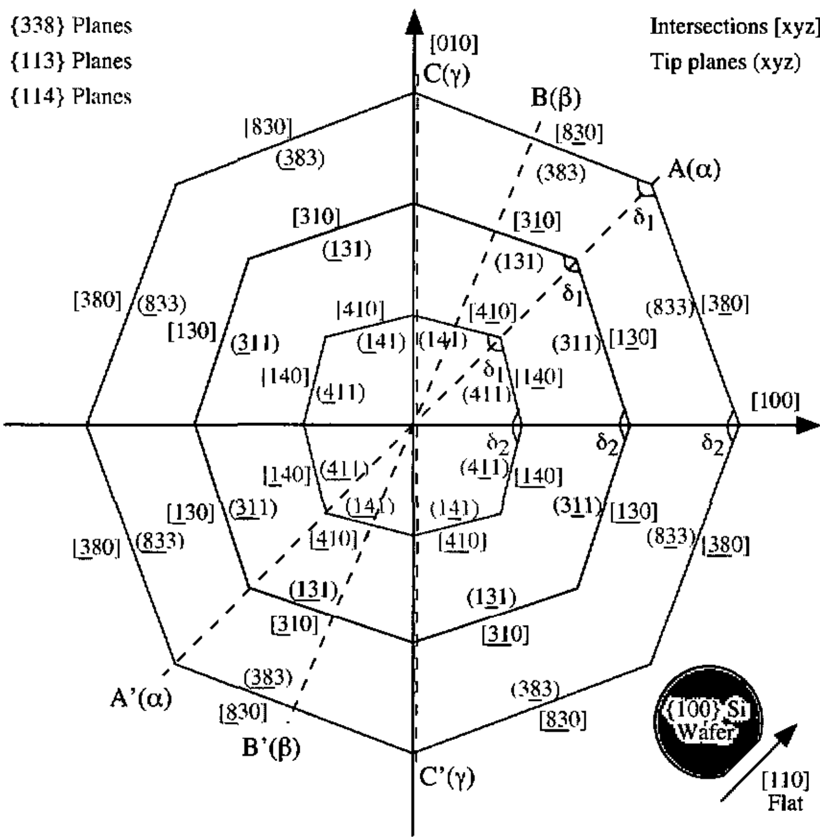

FIG. 2.8: Schematic of the octagonal intersections of the {338}, {113} and {114} families of planes with the (001) plane at the base of the tip. The angles δ_1 and δ_2 define the octagonal intersections, while the lines A-A', B-B' and C-C' present the section of the tip for α, β and γ, the different aperture angles of the tip apex.

high slope planes of the tip with the (001) plane of the silicon dioxide mask. Once more, while the octagonal interface silicon/silicon dioxide is clearly seen in a top view observation, it was realized that when the sample was examined from the side, a change in the etch planes occurs in proximity of the silicon dioxide mask (Fig. 2.10). To date, no solution has been found to precisely determine the angles δ_1 and δ_2 of the KOH-etched tips.
Nevertheless, attempts were made to determine the family of planes forming the tip by measuring the tip apex aperture angle, this on silicon tips at the end of an etch (Fig. 2.11a-c) as well as during underetching (Fig. 2.11d).

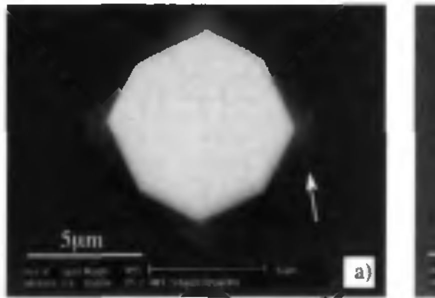

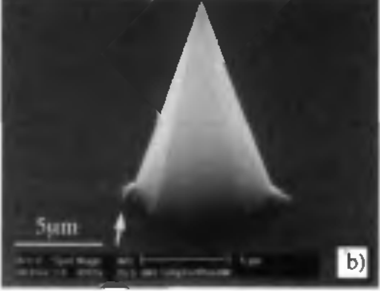

FIG. 2.9: SEMs of a silicon tip taken vertically and horizontally in order to highlight the low slope planes located at the base of the tip, which prevent the high slope planes to intersect the (001) plane.

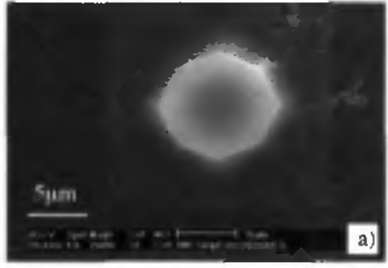

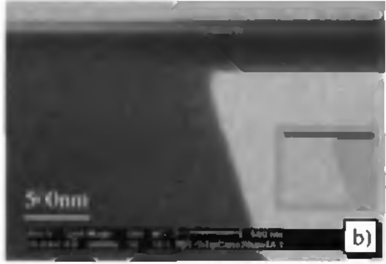

FIG. 2.10: SEMs of the formation of a silicon tip, taken vertically and horizontally in order to highlight the silicon/silicon dioxide interface. This interface is formed by a family of planes probably different from the high slope plane family defining the tip.

The variation of the tip apex aperture angle ranged from 34.5° to 40.7°, thus not allowing the determination of the high slope plane family defining the KOH-etched tips. The only conclusion which can be drawn is that this is certainly not the {114} family.

Due to the variation in measured tip apex aperture angles, the hypothesis was made that the tips are formed not by one family of high slope planes but several. To test this hypothesis, a vectorial analysis was made to represent a tip formed by a combination of {113} and {338} planes, all having a unique common intersection point, namely the tip apex. From these calculations, the theoretical octagonal intersection with the (001) plane was deduced, as well as the different apex aperture angles. The results are presented in Fig. 2.12.

This time, while the calculated aperture angle could nearly match the measured ones, the general shape of the octagonal intersection is quite different from what is experimentally observed.

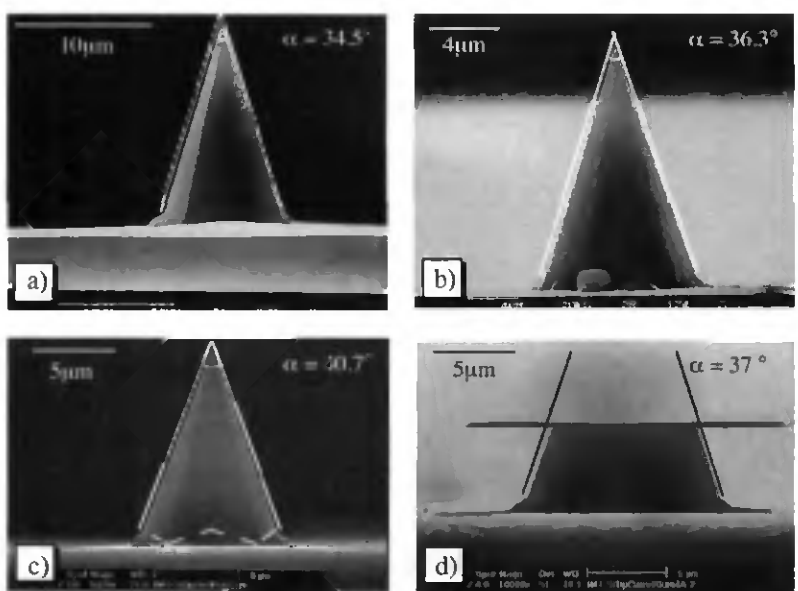

FIG. 2.11: SEMs of different silicon tips, finished (a-c) or not (d), taken for the determination of the tip opex angle of aperture.

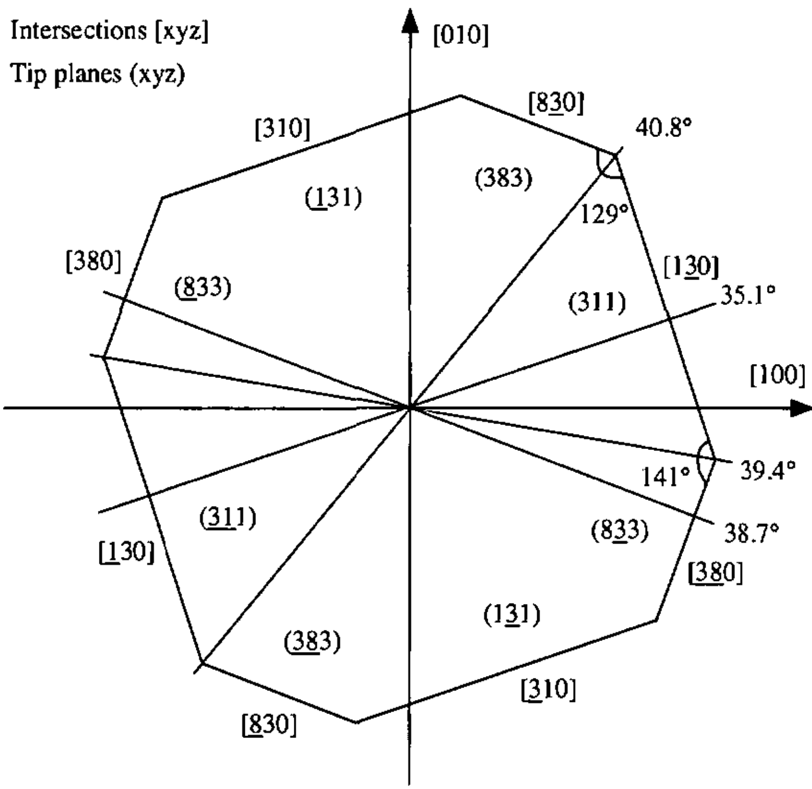

FIG. 2.12: Schematic of the intersection of a tip composed of a mixture of {113} and {338} planes with the (001) plane. The theoretical aperture angles have values between 35.1° and 40.8°, but the general shape of the intersection is far from that experimentally observed.

To conclude, it is very difficult to accurately determine the crystallographic planes defining the KOH-etched silicon tips. This could also explain the ambiguities found in the literature. In our case, the tips are certainly not defined by {114} planes, and it has not been established if these tips are formed from one or more families of planes. It would be of interest to determine if parameters such as KOH concentration and temperature, mask material, thickness, shape and orientation, as well as the amount of etched silicon in the vicinity of the tip or the etch depth, have an influence on the appearance of one or the other family of crystal planes.

2.4 Conclusions

These experiments yielded KOH-etched silicon tips, essentially defined by high slope planes if using a bain-marie set-up for their formation. In a first finding, the circular, octagonal or square shapes of the silicon dioxide masks were found not to influence the quality of the tips, as long as these shapes were not distorted. When using mask shapes different than the usual square masks, their dimensions must be adapted to keep tip height unchanged. An additional finding was that overetching does not affect the aspect ratio of the tip or the radius of curvature. Only the height of the tip decreased rapidly.
Height distribution analysis was carried out on a single quarter of wafer. The results were satisfactory for the applications described in the next chapters. More experiments should be done to verify the reproducibility of this height distribution and determine whether a poor contact photolithography could be the origin of this distribution.
SEM observations of the tip apex highlighted the presence of four different apex shapes, from which two can be used for AFM and profilometry applications. Statistical measurements revealed that 69% of a sample of 500 tips had usable tip apex shapes with radii of curvature smaller than 30nm.
Attempts were also made to determine the family or families of high slope crystal planes defining the KOH-etched silicon tips. After several measurements and calculations, it could be concluded that such tips have angles of aperture ranging from 34.5° to 40.7° and so are not defined by {114} planes. This analysis was quite difficult and perhaps explains the ambiguities found in the literature.
Finally, the characteristics of the KOH-etched silicon tips realized in this work were fully satisfactory for the continuation of the work presented in the next chapters.

References

1 O. Wolter, Th. Bayer and J. Greschner, "Micromachined Silicon Sensors for Scanning Force Microscopy", Journal of Vacuum Science and Technology B 9 (1991) 1353-1357.

2 H.L. Offereins, K. Kühl and H. Sandmaier, "Methods for the Fabrication of Convex Corners in Anisotropic Etching of (100) Silicon in Aqueous KOH", Sensors and Actuators A 25-27 (1991) 9-13.

3 J.-H. Liu, T.M. Betzner and H.T. Henderson, "Etching of Self-Sharpening {338} Tips in (100) Silicon", Journal of Micromechanics and Microengineering 5 (1995) 18-24.

4 I.J. Chung, D. B. Murfett, A. Hariz and M.R. Haskard, "Fabrication of High Aspect Ratio Silicon Micro-Tips for Field Emission Devices", Journal of Materials Science 32 (1997) 4999-5003.

5 P.-F. Indermühle, G. Schürmann, G.-A. Racine and N.F. de Rooij, "Fabrication and Characterization of Cantilevers with Integrated Sharp Tips and Piezoelectric Elements for Actuation and Detection for Parallel AFM Applications", Sensors and Actuators A 60 (1997) 186-190.

6 C. Beuret, Ph. Niedermann, U.Staufer and N.F. de Rooij, "Fabrication of Metallic Probes by a New Technology Based on Double Molding", Microelectronic Engineering 41/42 (1998) 543-546.

7 R.N. Thomas, R.A. Wickstrom, D.K. Schroder and H.C. Nathanson, "Fabrication and Some Applications of Large-Area Silicon Field Emission Arrays", Solid-State Electronics 17 (1974) 155-163.

8 H.H. Busta, R.R. Shadduck and W.J. Orvis, " Field Emission from Tungsten-Clad Silicon Pyramids", IEEE Transactions on Electron Devices 36 (1989) 2679-2685.

9 N.A. Cade, R.A. Lee and C. Patel, "Wet Etching of Cusp Structures for Field-Emission Devices", IEEE Transactions on Electron Devices 36 (1989) 2709-2714.

10 R.B. Marcus, T.S Ravi, T. Gmitter, K. Chin, D. Liu, W.J. Orvis, D.R. Ciarlo, C.E. Hunt and J. Trujillo, "Formation of Silicon Tips with <1nm Radius", Applied Physics Letters 56 (1990) 236-238.

11 G. Binnig, C.F. Quate and Ch. Gerber, "Atomic Force Microscope", Physical Review Letters 56 (1986) 930-933.

12 P.-F. Indermühle, "Microfabricated Probes with Integrated Functions for Scanning Probe Microscopy", Ph.D. Dissertation, University of Neuchâtel, Switzerland 1998.

13 A. Boisen, "Passive & Active AFM Probes: Design, Fabrication & Characterization", Ph.D. Dissertation, Technical University of Denmark, Denmark 1997.

14 H. Seidel, L. Csepregi, A. Heuberger and H. Baumgärtel, "Anisotropic Etching of Crystalline Silicon in Alkaline Solutions", Journal of the Electrochemical Society 137 (1990) 3612-3626.

15 P. Thiébaud, C. Beuret, M. Koudelka-Hep, M. Bove, S. Martinoia, M. Grattarola, H. Jahnsen, R. Rebaudo, M. Balestrino, J. Zimmer and Y. Dupont, "An Array of Pt-Tip Microelectrodes for Extracellular Monitoring of Activity of Brain Slices", Biosensors & Bioelectronics 14 (1999) 61-65.

16 Alpha-step 200 © Tencor Instruments, USA

17 J.B. Price, in "Semiconductor Silicon", edited by H.R. Huff and R.R. Burgess, The Electrochemical Society Softbound Proceedings Series, Princetown, NJ (1973) 339-353.

3 Silicon/Diamond Tips on Cantilevers

The probe of an AFM consists of a sharp tip integrated on a cantilever acting as a spring. The aim of this work was to realize thin silicon cantilevers with tips in a reproducible way over the whole surface of a single wafer. Moreover, devices with thicker cantilevers, and so higher spring constants, were fabricated and coated with diamond to act as scratching tools for nanomechanical surface modifications, as well as probes for immediate AFM imaging of these modifications.

3.1 Introduction

In order to be sensitive to small forces, the spring constant of the cantilever has to be small (0.01-100N/m). At the same time, a high resonance frequency (>10kHz) allows short response times while scanning, and also reduces the influence of acoustic waves and infrastructure vibrations. Since resonance frequency is proportional to (spring constant/mass of the cantilever)$^{1/2}$, it is obvious that the dimensions of the cantilever have to be small to fulfill the conditions mentioned above. Therefore, AFM probes are usually realized by microfabrication techniques, allowing their fabrication in various materials such as silicon [1], silicon nitride [2, 3], silicon dioxide [3], metals [4], diamond [5, 6] or combinations of two or more materials [7]. In this chapter, only silicon or diamond-coated silicon probes will be discussed.

From [8, 9, 10, 11], typical dimensions for a silicon cantilever are a length of 300μm, a width of 60μm and a thickness of 3μm, resulting in a spring constant of 2.5N/m and a resonance frequency of 46kHz. As will be seen in the equations presented in section 3.2, the spring constant and the resonance frequency are particularly dependent on the length of the lever as well as on

its thickness, which must be small in order to permit sufficient vertical bending of the lever. While the length is initially defined by photolithography in a reproducible way over the entire wafer, the thickness homogeneity of silicon cantilevers is more difficult to control. These cantilevers are usually etched from a silicon membrane realized during the back-side anisotropic etch defining the cantilever support structure. The uniformity of membrane thickness depends on the homogeneity of the back-side etching procedure. It also depends on the thickness uniformity of the original wafer, or on the "taper" which is typically guaranteed at ±3μm, and is often not sufficient for reproducible realization of 3μm thick cantilevers. The uniformity of cantilever thickness also depends on the homogeneity of the top-side etching mechanism used to produce the silicon tips.

One way to ensure good thickness uniformity is to create, on the top-side of the wafer, an etch-stop layer for the back-side anisotropic wet etch defining the support structure and the membrane. This etch-stop layer is realized by doping the silicon with boron. Its thickness is controlled by precisely regulating the implantation and annealing parameters used in the doping procedure. The doping process can be performed either after the formation of the tip, in which case the depth of the doped silicon directly corresponds to the thickness of the final cantilever [8, 9], or before tip realization, the tip resulting then from a partial etch of the doped thickness [10]. With this last procedure, the thickness uniformity of the cantilevers is influenced by the tip etching mechanism and is therefore reduced.

Another method to ensure good uniformity of cantilever thickness is to use Silicon On Insulator (SOI) wafers, consisting of a bulk silicon wafer and a well-defined thinner (e.g. 8μm thick) silicon layer, separated by a typically 2μm thick, silicon dioxide layer. Itoh et al. used this kind of wafer in such a way that the tip was defined in the upper silicon layer and the cantilever formed out of the precise silicon dioxide layer [11].

In this work, a process was developed to realize silicon cantilevers and tips, emphasizing good uniformity of cantilever thickness and tip height. To achieve this, the cantilevers and tips were formed out of the upper 20μm thick silicon layer of SOI wafers. Here, only the homogeneity of the etching mechanism used to define the tips could have an influence on cantilever thickness uniformity. Therefore, it was decided to use anisotropic wet etching to define the tips, since the homogeneity of this type of etch is better

than that of isotropic wet etching or dry etching techniques. Moreover, KOH-etched silicon tips proved to have satisfactory characteristics for AFM applications (see chapter 2). Finally, to reduce the risk of breaking the tips during the fabrication procedure, they were realized during the last steps of the process.

Such silicon AFM probes were used directly after fabrication for AFM measurements. Probes with thicker cantilevers and thus higher spring constants were realized with a similar process, but using standard silicon wafers. These last were coated with a CVD diamond film in order to increase their lifetime, avoid breaking the tip during approach of the sample and limit their wear while scanning hard samples. Finally, these diamond-coated probes were used for nanomechanical modification studies of various thin film-deposited materials.

This work represents a first step towards the fabrication of diamond tips with better geometrical characteristics, needed for AFM measurements and high resolution profilometry.

3.2 Cantilever Design

The spring constant of a single-side clamped cantilever having a regular cross-section is given by

$$k = \frac{3EI}{l^3} , \quad (3.1)$$

where E denotes the modulus of elasticity (or Young's modulus) of the material, I the cross-sectional moment of inertia and l the length of the cantilever. For a rectangular cross-section, the moment of inertia is

$$I = \frac{wt^3}{12} , \quad (3.2)$$

where w and t are the width and thickness, respectively, of the cantilever. From the above equations, we obtain

$$k = \frac{Ewt^3}{4l^3} . \quad (3.3)$$

The first resonance frequency, f_0, of a single-side clamped cantilever with a tip at its free end is given by

$$f_0 = \frac{1}{2\pi}\sqrt{\frac{k}{m_{eff}}} , \quad (3.4)$$

where m_{eff} is the effective mass of the lever, which is given by

$$m_{eff} = m_t + 0.24m_c . \quad (3.5)$$

Here, m_c is the distributed mass of the cantilever

$$m_c = lwt\rho , \quad (3.6)$$

with ρ the density of mass. The concentrated mass of the tip, m_t, for a straight cone with circular section, is given by

$$m_t = \frac{1}{3}\pi r^2 h\rho , \quad (3.7)$$

r being the radius of the circular base and h the height of the tip. A rapid calculation, taking a cantilever with typical dimensions and a conical tip

having a height of 10µm and a total angle of aperture of 40°, shows that the mass of the tip represents only ~0.25% of the mass of the cantilever and can therefore be neglected. So, the effective mass of the lever can be set to

$$m_{eff} = 0.24 m_c \quad . \tag{3.8}$$

From the equations (3.3), (3.4), (3.6) and (3.8), the first resonance frequency can be expressed as

$$f_0 = 0.162 \sqrt{\frac{E}{\rho}} \frac{t}{l^2} \quad . \tag{3.9}$$

These equations are valid for cantilevers having a rectangular cross-section. In this work, due to the technology used, the cantilevers have a trapezoidal cross-section, which induces a variation of the moment of inertia. Nevertheless, this variation is sufficiently small to be neglected if, in the calculations, the width of the cantilever is taken as the average of the upper width (w_u) and the lower width (w_l) of the trapezoidal cross-section. The trapezoidal cantilevers are then designed in order to get an average width corresponding to the width of a standard rectangular cantilever.

The following paragraph explains the formation of the trapezoidal cantilevers and the reason why preliminary experiments have to be performed prior to the mask design. The cantilevers are realized in two successive etch steps. The first step, an anisotropic RIE, defines the length and width of the cantilever by vertically etching all the silicon in the neighborhood of the cantilever and of the support. The second step, the anisotropic wet etch in KOH used to realize the tip, defines the thickness of the cantilever. This second step also changes the width of the cantilever defined by RIE as well as the location of its end (Fig. 3.1). Indeed, the cantilever sidewalls are not protected during the KOH etch and some low slope planes on these sidewalls are etched more rapidly than the (001) planes defining the cantilever thickness. This results in a drastic reduction of the original width of the cantilever. Therefore, the mask used to define the cantilever by RIE has to be carefully designed to reach the expected cantilever dimensions and tip location at the end of the process.

For this work, the mask dimensions of the cantilever were determined experimentally. Cantilevers of specific dimensions were etched in silicon to

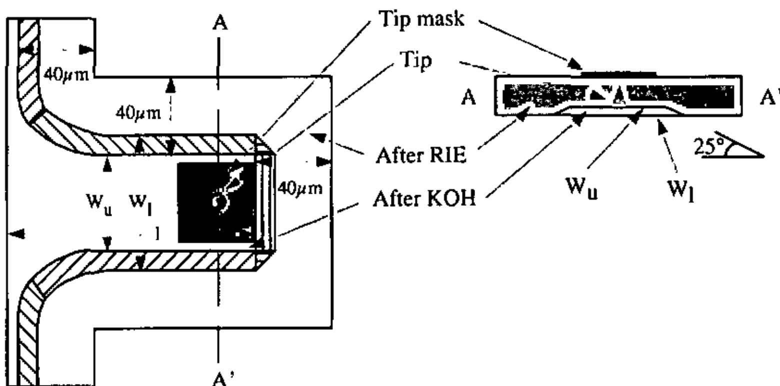

FIG. 3.1: Schematic of the cantilever width reduction and changes in the extremities locotions due to the KOH etching step, compared to the same contilever after only RIE, which dimensions after etching correspond to the initial mask dimensions.

a depth of ~20μm by anisotropic RIE. The wafer was then etched in KOH for a time corresponding to an etch depth of ~16μm for the (001) planes, as for the tip etching step. Finally, the upper width of the cantilever obtained by this procedure was measured and compared to the original width of the cantilevers defined on the mask. It was observed that each sidewall at the surface of the cantilever had been overetched by 40μm.

This experiment also allowed to deduce the angle formed by the (001) plane with the planes defining the final sidewalls of the cantilever. Knowing this angle, the final expected thickness, and the average width of the cantilevers, the final expected upper width of the cantilever could be deduced. In this experiment, the angle was 25°, the expected thickness 4.5μm and the average width 60μm, resulting in an upper width of 50μm. The cantilevers were then defined with a width of 130μm on the mask, 50μm for the final upper width plus twice the overetching value (40μm) corresponding to this precise etch depth.

The length of the cantilever was not affected by the KOH etch step, the support being overetched in the same way as the end of the cantilever. However, the location of the end of the cantilever was changed and this change had to be taken into account for the tip location. The tip mask was therefore positioned so as to avoid a possible influence of cantilever sidewall overetching on the formation of the tip.

3.3 Fabrication

This fabrication process has been developed in order to realize silicon cantilevers and tips having the following specifications:

- The tips must have a height between 10 and 15μm and a radius of curvature smaller than 50nm.
- For AFM applications, the cantilever first resonance frequency must be higher than 10kHz and the spring constant smaller than 1N/m.
- For nanomechanical modifications, the spring constant must be larger than 10N/m, and therefore the cantilevers thicker.

The fabrication process is described hereafter (Fig. 3.2). To summarize, it is based on three etching steps: 1) a KOH etch defining the support structure and the silicon membrane, 2) a RIE defining the length and the initial width of the cantilever and, 3) a second KOH underetch of the tip, which also determines the final cantilever width and thickness. This process has the advantage that the tips are formed only in the last two steps, limiting the risk of breakage during probe fabrication. To ensure a good reproducibility of cantilever thickness over the whole surface of the wafer, it was decided to use SOI wafers (480μm Si, 2μm SiO_2 and 20μm Si) for the fabrication of the thinner cantilevers, thus avoiding possible inhomogeneity due to the first KOH etch (process I). For thicker cantilevers, however, standard, double-side polished, 525μm thick silicon wafers are sufficient to give satisfactory results (process II). Both types of wafers are <100> oriented.
Standard technology steps were already presented in detail in section 2.2, and only new or modified steps will be described in more detail hereafter. Moreover, most of the fabrication steps are identical for both processes, and only the slight differences between them will be highlighted.

Square Mask Definition

The process starts with a standard cleaning, after which a 3000Å thick, wet thermal silicon dioxide layer is grown on both sides of the wafer. A typically 1000Å thick, standard silicon nitride layer is then deposited, also on both sides of the wafer, by low pressure chemical vapor deposition (LPCVD). The back-side is then protected with a hard-baked photoresist

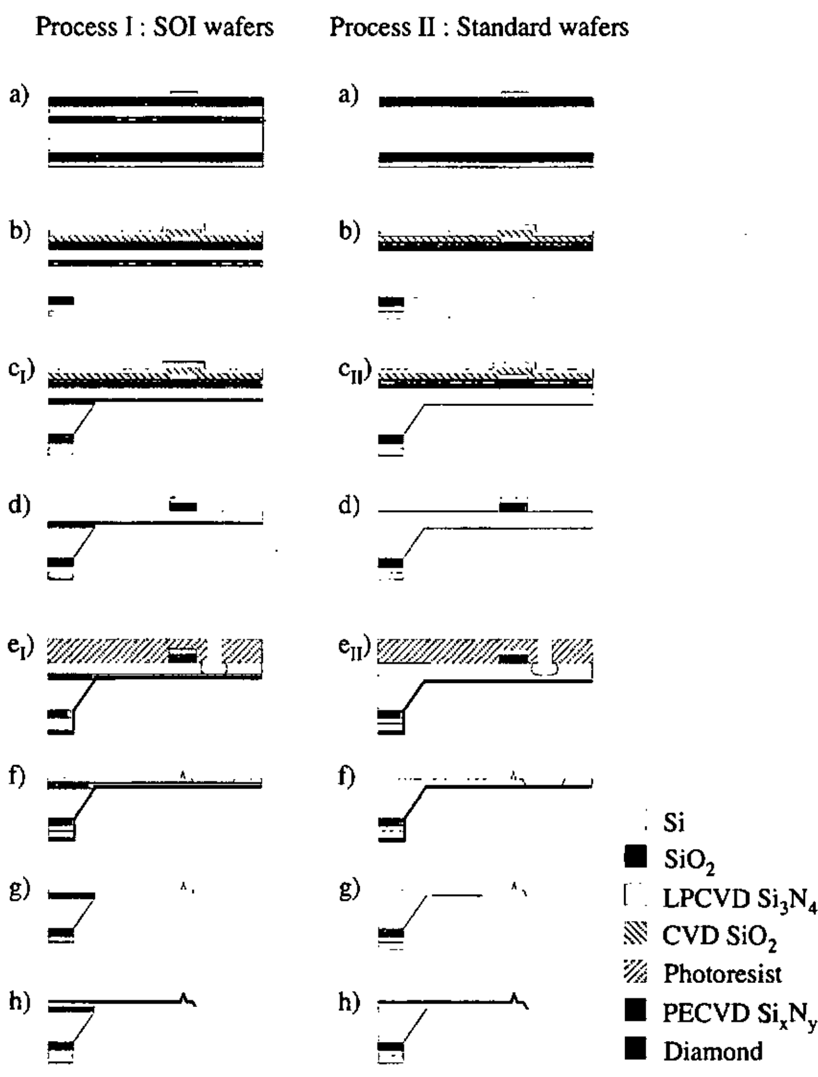

FIG. 3.2: Schematic of the fabrication process for silicon and diamond-coated silicon cantilevers and tips, using SOI wafers for AFM applications (I) and standard wafers for nanomechanical modifications (II).

layer, and the top-side is patterned by photolithography (AZ 1518) to define the 40μm square masks underetched during tip formation at the end of the process.
The top-side, 1000Å thick silicon nitride is then completely removed by etching in SF_6/O_2 plasma, except where it is protected by the photoresist. The silicon dioxide is only slightly etched during this step and thus forms an effective etch-stop layer, allowing the borders of the wafer to be overetched to ensure a complete removal of silicon nitride even at the center. The back-side photoresist layer protects the back-side silicon nitride from possible slight plasma etching due to an improperly sized wafer holding plate (holding plate designed for 3" wafers, but used for 4" wafers).
After silicon nitride etching, both top-side and back-side photoresist layers are stripped by a wet procedure called "piranha" (Fig. 3.2a). This procedure is often used after plasma etching, because the temperature reached during the plasma modifies the photoresist which as a result becomes difficult to strip away using only solvents such as acetone and isopropanol. Indeed, if only solvents are used, the photoresist forms very thin persistent veils which can be redeposited anywhere on the substrate.
The piranha procedure involves immersing the wafer in a 96% sulfuric acid (H_2SO_4) bath for ten minutes. After that, several milliliters of 30% hydrogen peroxide (H_2O_2) are slowly poured on the wafer surface, allowing an exothermic reaction to proceed right above the wafer. After ten more minutes, the wafer can be turned upside-down and some more hydrogen peroxide is poured on it, reactivating the exothermic reaction. Ten minutes after, the wafer is thoroughly rinsed in DI water and blown dry with nitrogen. In case of especially thick photoresist or long plasma etching, wafers can be left several hours in H_2SO_4 before adding the hydrogen peroxide.

Realization of the Support Structure and of the Silicon Membrane

A 2000Å thick, CVD silicon dioxide layer is deposited on the top-side of the wafer before being densified at 625°C for 15 minutes. Next, a standard, 1500Å thick silicon nitride layer is deposited on both sides of the wafers. These two layers will protect the wafer top-side during the long back-side KOH etch used to define the support and the silicon membrane.

Other layers, such as undensified CVD SiO_2/plasma enhanced chemical vapor deposited (PECVD) silicon nitride, or just a thicker standard stoichiometric LPCVD silicon nitride (Si_3N_4) partially etched after the first photolithography, were tried for the same purpose but were not adopted. In the first case, the PECVD Si_xN_y exhibited a poor step coverage and the undensified CVD SiO_2, as well as the thermally grown first SiO_2 layer, were rapidly etched, resulting in an unanticipated underetching of the silicon under the square masks. In the second case, the non-uniformity of the plasma etching between the borders and the center of the wafers resulted in some difficulties to etch reproducible steps in the silicon nitride layer. Moreover, the initial silicon nitride had to be so thick that a high stress and even cracks were observed. A third procedure used a mechanical, hermetic, protection chuck during the KOH etching, but this operation is often dangerous. Some leaks were occasionally observed and, as the etching was nearly accomplished, the breaking of one membrane was sufficient for the infiltration of KOH, damaging parts or even the entire top-side of the wafer. Moreover, if the wafer was not very carefully placed in this chuck, a rupture could be generated, often resulting, if the wafer was sufficiently weak due to etching, in its breaking and the destruction of all the structures. To date, the densified CVD SiO_2/LPCVD Si_3N_4 layers seem to be optimal. With these layers, the top-side of the wafer proved to be unaffected during the long KOH etching step.

The next step consists of patterning the back-side of the wafer for the long KOH etching step. First, the top-side of the wafer is protected by a hard-baked photoresist layer in view of the plasma etching of the back-side silicon nitride. Then the back-side is patterned by photolithography (AZ 1518), aligned to the top-side by means of the double-side mask aligner. The 2500Å (1000Å + 1500Å) thick silicon nitride is then etched in a SF_6/O_2 plasma, and the back-side 3000Å thick SiO_2 is etched in BHF for 6 minutes. Finally, the photoresist is once more removed from both sides of the wafers by a piranha procedure (Fig. 3.2b).

The following step is the lengthy back-side KOH etch of silicon defining the support and the silicon membrane. There, a distinction has to be made between process I (SOI wafers) and process II (standard wafers). For process I, the KOH etching is performed until the entire, 480μm thick silicon layer located under the interstitial silicon dioxide of the SOI wafers

is completely etched, the SiO_2 acting as an etch-stop layer. Then, the 2μm thick, buried silicon dioxide layer is thinned to a thickness of 8000Å in BHF for 20 minutes, in order to reduce stresses in this membrane after cantilever definition (Fig. 3.2c_I). For process II, silicon is etched in KOH from the back-side until the top-side silicon membrane reaches the desired thickness (Fig. 3.2c_{II}). This thickness has to be calculated prior to the etching, depending on the final cantilever thickness one wants to obtain. The membrane thickness (25-31μm) has to be the sum of the final cantilever thickness (8-14μm) and of the KOH etching depth realized during the tip formation (~17μm). This step requires repeated KOH etchings and mechanical membrane thickness measurements with a thickness comparator (Cary-Compar, Le Locle, Switzerland).

Cantilever Formation

The next steps involve removing the layers deposited in order to protect the top-side of the wafer during the long KOH-step. First, the 1500Å thick silicon nitride layer is removed by a SF_6/O_2 plasma etch, the CVD SiO_2 acting as an etch-stop layer. The 2000Å thick densified CVD SiO_2, as well as the 3000Å thick, thermal SiO_2 not protected by the square silicon nitride masks are then etched in BHF for 10 minutes, leaving the final masks for the formation of the tip. During this step, for the SOI wafer, the 8000Å thick SiO_2 located at the back-side of the membrane is reduced to a thickness of 3000Å (Fig. 3.2d). Finally, in order to protect the back-side of the silicon membrane during tip formation, a 3000Å thick PECVD silicon nitride layer is deposited.
After the dehydration and HMDS steps, the wafer is mounted onto an unstructured wafer with a special double-sided tape to realize the thick photoresist (AZ 4562) photolithography needed to pattern the cantilevers by long reactive ion etching. For AZ 4562 photolithography, the photoresist is spun at 3000 rpm for 40 seconds, resulting in a 7μm thick photoresist layer, and prebaked at 85°C for 35 minutes in a convection oven. The wafer is then exposed in contact mode with an energy of $120mJ/cm^2$ and immediately developed in an alkaline developer (AZ351:DI water 1:3) for 90 seconds. The wafer is then separated from the unstructured wafer using a scalpel. Finally, the remaining photoresist is hard-baked at 120°C for 30 minutes.

The cantilevers are then defined by a long RIE. Indeed, to etch 20µm of silicon, a SF_6/C_2ClF_5 RIE has to be performed during approximately 45 minutes, interrupting the etching every ten minutes to let the wafers cool down in order to preserve the photoresist mask (Fig. 3.2e). At this step, it has been observed for the SOI wafer that once the silicon has been completely etched at the border of the wafer, the SiO_2/Si_xN_y membranes are rapidly etched, even underneath the cantilevers. Overetching the borders in order to open the silicon in the center of the wafer appeared to be quite risky, the back-side of the cantilevers being not protected anymore for the last KOH etch. Therefore, it would be useful to stop the etching immediately after the silicon is removed at the borders of the wafers, the remaining silicon at the center being etched away later during the formation of the tips.

Tip Formation

After stripping the photoresist with a long piranha procedure, the wafer is immersed in KOH until total underetching of the 40µm square Si_3N_4/SiO_2 masks is achieved, which corresponds to an etch depth of ~17µm. This step results in the formation of high aspect ratio tips and reduces the cantilevers to their final width and thickness (Fig. 3.2f).
Finally, the SiO_2/Si_xN_y back-side protective layers are completely removed in a 40 minute long BHF etch (Fig. 3.2g). At this step, overetching has no influence. AFM probes are now completed and some of them can already be removed from the wafer by simply breaking the four bridges holding them to the wafer frame.

Diamond Deposition

HF-CVD diamond can be deposited on the AFM probes. This step is realized wafer by wafer. After the pretreatment and the seeding process, the wafer is placed vertically on the graphite chuck in front of the tantalum filament. After heating the wafer to a temperature of 830°C and the filament to a temperature of 2500°C, the reactive gases (H_2 and CH_4) are introduced into the reactor and the growth mechanism begins. After a time corresponding to the expected diamond thickness, the process is stopped and the wafer is unloaded.

The introduction of gasses in the reactor created some problems for the SOI wafers. It was so violent that it created a shock wave which, added to the fact that the bridges holding the probes to the wafer frame were very thin, caused many probes to be dislodged and to fall into the reactor chamber. It is even suspected that some of these structures fell on the filament, perturbing the diamond deposition parameters and resulting in the deposition of an unknown non crystalline material.
More diamond depositions have been performed on the standard wafers provided with thicker cantilevers. The first attempts essentially resulted in isolated diamond grains depositions. The last one, however, benefiting from many pretreatment optimizations, yielded a quasi-continuous diamond layer.
To conclude, silicon AFM probes with thin as well as with thicker cantilevers have been successfully realized. Moreover, probes with thicker cantilevers have been coated with HF-CVD diamond. To obtain satisfactory diamond-coated probes with thin cantilevers, it would be necessary to reinforce the bridges holding the structures to the wafer frame and to slow down the introduction of the gases into the reactor chamber. The pretreatment process carried out prior to seeding would probably also need to be improved.

3.4 Results of the Fabrication

This fabrication process allowed the realization of silicon AFM probes with thin (Fig. 3.3a) or thick (Fig. 3.3b) cantilevers, depending on the type of the starting wafer. Such probes are provided with high aspect ratio tips having radii of curvature as small as 6nm (Fig. 3.4). Moreover, some probes having thick cantilevers were coated with a quasi continuous HF-CVD diamond layer (Fig. 3.5). Such diamond-coated cantilevers and tips were used for the nanomechanical modification studies presented in section 3.5.2.

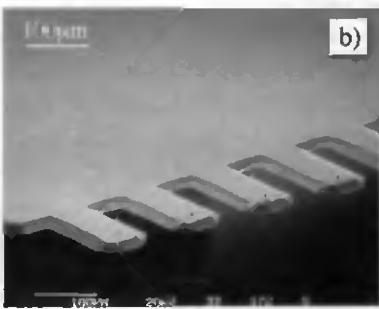

FIG. 3.3: SEMs of completed AFM probes. a) A 2.9μm thick V-shaped cantilever made from a SOI wafer and b) an array of 9μm thick beam cantilevers made from a standard wafer, for applications needing a high spring constant.

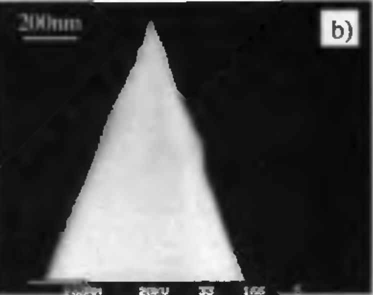

FIG. 3.4: SEMs of a) a high aspect ratio tip resulting from the fabrication process described in the previous section and b) a tip apex having a radius of curvature smaller than 6nm.

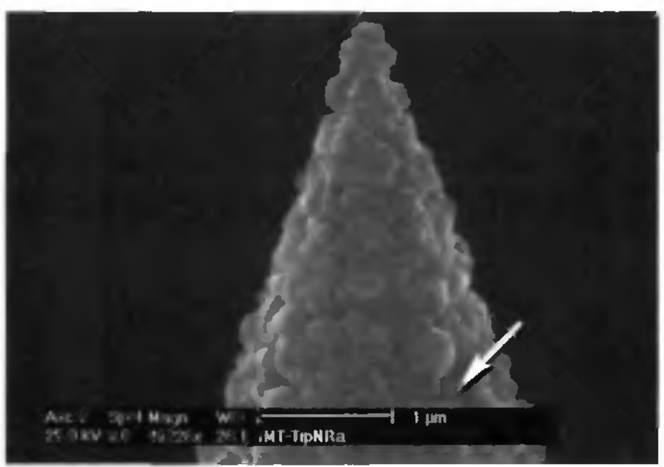

FIG. 3.5: SEM of the tip apex of a diamond-coated AFM probe having a final radius of curvature of approximately 125nm. The diamond layer is quasi continuous, with only a few pin-holes like the one indicated by the arrow.

As this process has been developed in order to realize silicon cantilevers having a high reproducibility in their thickness and high aspect ratio, sharp tips, the analysis discussed below focuses on these particular characteristics. First of all, it should be noted that cantilever thickness was difficult to determine exactly. SEM observations had to be made exactly perpendicular to the tip direction in order to avoid an amplification of the error, due to the trapezoidal cross-section of the cantilever. Therefore, it was decided to determine the reproducibility of cantilever thickness by measuring the first resonance frequency as well as length, and then deducing their thickness from equation (3.9), both for thin cantilevers from a processed SOI wafer and for thicker cantilevers from a standard wafer.
Another interesting observation involved determining the reproducibility of the tip height and radius of curvature. The tip height has to be reproducible, at least for neighboring tips whose levers are attached to a single support, to ensure that only the desired tip will touch the sample while scanning. Moreover, the tip radius has to be small enough to ensure good resolution. These analyses could be done through SEM observations of more than 40 samples extracted from different locations on a single wafer.

3.4.1 Determination of the Cantilever Thickness

The measurement of resonance frequencies was realized in a set-up combining a confocal microscope, a function generator and a lock-in amplifier. The AFM probes were glued onto a piezo disk activated with an alternating voltage produced by the function generator. During the measurements, the frequency of the alternating voltage was swept from a minimum value of 1kHz to a maximum value of 100kHz. To detect the amplitude of the cantilever vibration, the laser beam of the confocal microscope (UBM Messtechnik, Germany) was focused on the cantilever. The detected vibration signal was then plotted as a function of the frequency of the excitation signal through the lock-in amplifier. The first resonance frequency of the cantilever simply corresponds to the frequency of the excitation voltage yielding a maximum vibration amplitude. The lengths of the cantilevers have been measured with an optical microscope by means of a calibrated sliding ruler.
These measurements, summarized in Table 3.1 with their standard deviations, were performed for several cantilevers extracted from different locations on a SOI structured wafer, as well as on a standard processed wafer. After error calculations, the average cantilever thickness could be determined for thin as well as thick cantilevers (Tab. 3.2).

TABLE 3.1: Average first resonance frequencies (f_0) and lengths (l) of thin as well as thick cantilevers.

Wafer	*Average l*	σ_l	*Average f_0*	σ_{f_0}	*Number of samples*
SOI	*204 μm*	*1.5μm*	*51.59 kHz*	*3.53 kHz*	*7*
SOI	*304.2μm*	*1.5μm*	*26.12 kHz*	*0.96 kHz*	*5*
SOI	*402.8μm*	*1.6μm*	*14.97 kHz*	*1 kHz*	*6*
SOI	*502.5μm*	*1.2μm*	*11.73 kHz*	*0.56 kHz*	*4*
SOI	*600.3μm*	*1.4μm*	*6.88 kHz*	*0.31 kHz*	*6*
Standard	*402.1μm*	*0.9μm*	*74.37 kHz*	*2.13 kHz*	*7*
Standard	*500μm*	*0.3μm*	*46.17 kHz*	*1.02 kHz*	*7*
Standard	*601.2μm*	*0.5μm*	*34.21 kHz*	*0.78 kHz*	*7*

TABLE 3.2: Average thickness of thin and thick cantilevers, including standard deviations, resulting from the measurements of their first resonance frequencies and of their lengths.

Wafer	*Average Thickness*	*Standard deviation*	*Number of samples*
SOI	*1.79μm*	*0.04μm (2.2%)*	*28*
Standard	*8.62 μm*	*0.12μm (1.4%)*	*21*

These results demonstrate that the uniformity of the cantilever thickness was satisfactory for both thin and thick cantilevers, proving that this fabrication process may be used to realize silicon AFM probe cantilevers in a reproducible way. The standard deviation of the thickness of the thin cantilevers corresponds to 2.2% of their average thickness, while for the thicker cantilevers it is 1.4%. This result may be surprising, but it can be assumed that the standard deviation of the thickness of the thicker cantilevers probably does not decrease proportionally if their thickness is reduced to that of the thinner cantilevers.
Knowing the thickness, length and width of the cantilevers, their spring constants can be estimated. The average width of the 1.79μm thick cantilevers has been measured to be 55μm, resulting in a spring constant of 1.6N/m for the 204μm long cantilevers, and of 0.06N/m for the 600.3μm long levers. Such spring constants perfectly match the specifications required for AFM measurements. On the other hand, the 8.62μm thick cantilevers have an average width of 84.5μm. From these values, spring constants of 35.4N/m and 10.5N/m could be deduced for 402.1μm and 601.2μm long cantilevers respectively. These values are higher than 10N/m as required for performing nanomechanical modifications.

3.4.2 Tip Height and Radius of Curvature

To analyze the tip height distribution, 48 samples from one wafer were measured, resulting in an average height of 10.38μm with a standard deviation of 0.37μm. In Fig. 3.6, the occurrences of the various measured tip heights are reported.

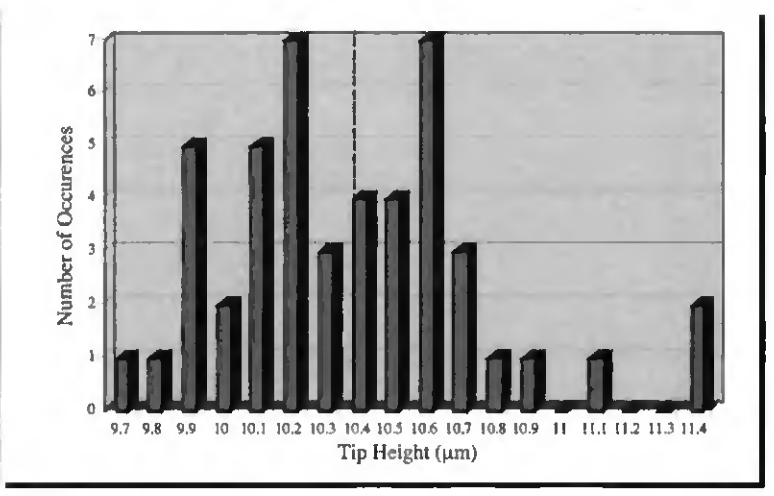

FIG. 3.6: Occurrences of the various measured tip heights. The dashed line corresponds to the average value of 10.38μm.

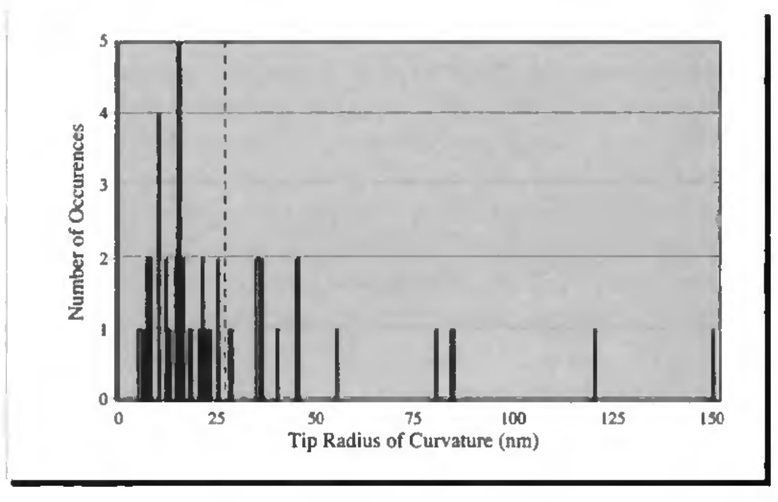

FIG. 3.7: Occurrences of the various measured radii of curvature. Once more, the dashed line represents the average value.

The same procedure was applied to estimate the radius of curvature of 43 tips. The average radius of curvature is 28.3nm with a standard deviation of 29.86nm. This deviation is due to a few tips having a large radius of curvature as can be seen in Fig. 3.7.

These results effectively show that the reproducibility of the tip height is good on one wafer. The value of the radius of curvature of most of the tips is under 50nm, as expected. From this, it can be concluded that this process allows tips to be produced with satisfactory characteristics.

To conclude, it was possible to successfully produce, with good reproducibility, silicon AFM probes, which fulfill the specifications mentioned at the beginning of section 3.3.

3.5 Measurements

In this section, one of the AFM measurements realized with a thin cantilever silicon probe is presented to demonstrate the ability of such probes to perform AFM measurements with good resolution. Moreover, an example of a nanomechanical modification realized with a thick cantilever diamond-coated silicon probe is presented. It was demonstrated that such probes can be employed not only to perform nanomechanical modifications of a defined layer, but also to image the induced modification without changing the probe and so without needing to relocate the modified area.

3.5.1 AFM Measurements

AFM measurements were performed by mounting a silicon probe, realized from a SOI wafer with the process described in this chapter, in a commercial AFM (Nanoscope III, Digital Instrument). The measurements were performed in contact mode on a sample of atomic {111} terraces of gold on mica (terrace height ~1nm). As can be seen in Fig. 3.8, the atomic terraces of gold can clearly be observed, proving that the resolution of these probes is well adapted to such sample geometries.

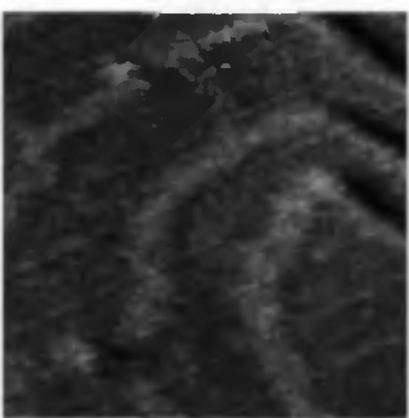

FIG. 3.8: 200nm x 200nm AFM image of atomic {111} terraces of gold on mica measured in contact mode with a silicon cantilever and tip fabricated from a SOI wafer with the process described in section 3.3.

3.5.2 Nanomechanical Modifications

For scratch hardness measurements, a thin film is usually scratched by a sharp stylus made of a hard material, typically diamond, and the load required to scratch the surface is used as a measure of scratch hardness. For very thin films, the influence of the substrate material must be eliminated. Thus, the indentation depth should not exceed a certain percentage of the total coating thickness, so that applied loads in the order of 0.01-50mN are desirable. In such cases, the size of the residual imprint or scratch is less than the resolution limit of a conventional optical microscope, and locating it after the modification is almost impossible, even with an AFM. Therefore, N. Randall combined a highly accurate nanoindentation system with an AFM, in such a way that a specific sample site can be located quickly and easily both before and after an indentation or scratching experiment [12].
In this case, the idea is to use the same probe for the indentation or scratching as for the AFM imaging before and after the modification. For soft materials, such as polymers, commercial silicon nitride cantilevers and tips can be used. For harder coatings, such as Diamond-Like Carbon (DLC) or other hard disk coatings, it is necessary to use harder probes such as diamond-coated silicon. To be able to achieve nanomechanical modifications as well as AFM imaging, such cantilevers must have a spring constant of 10-150N/m. The thickness of a typically 60μm wide, 400μm long silicon cantilever must then be between 6 and 16μm.
AFM probes coated with a quasi continuous diamond layer were used to demonstrate that it is possible to scratch hard films, such as hard disk overcoat materials, and to image the scratching with the same probe (Fig. 3.9). This image shows that the spring constant of the cantilever allows the probe to be used for scratching as well as for imaging. Moreover, its quality demonstrates that AFM imaging with good resolution can still be realized with the same probe, even after many scratching cycles. Finally, SEM observations of the tip apex after these nanomechanical modifications proved that the tip did not suffer significant wear or damage (Fig. 3.10).

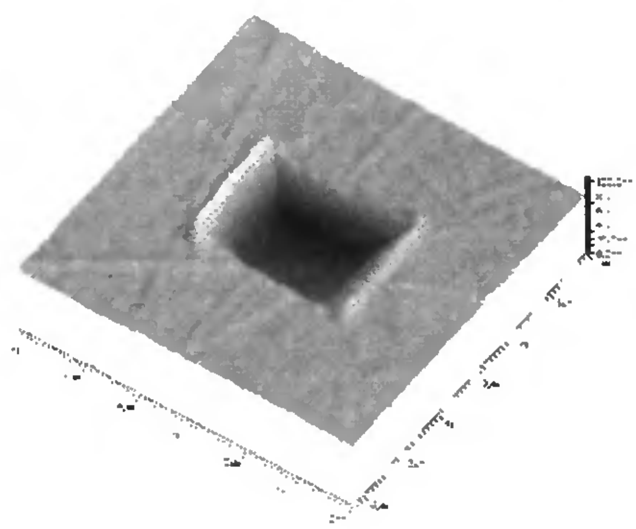

FIG. 3.9: AFM image of the central worn region (2μm x 2μm) of a fluorinated amorphous carbon thin film after 20 cycles of scratching with an applied force of 55μN.

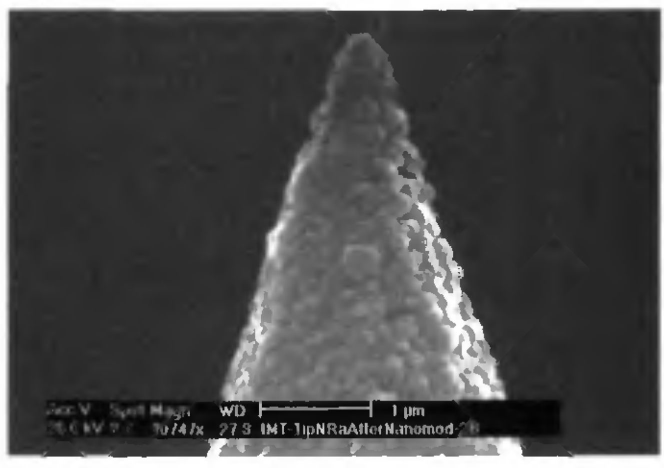

FIG. 3.10: SEM of the apex of the diamond-coated AFM probe tip after performing nanomechanical modifications.

3.6 Conclusions

In this chapter, a fabrication process for the realization of silicon AFM probes with a high reproducibility of the cantilever thickness has been presented. The use of KOH etching allowed these probes to be uniformly provided with high aspect ratio tips having radii of curvature as small as 6nm.

On one hand, using SOI wafers, thin cantilever probes were realized and successfully used for standard AFM imaging. On the other hand, thicker cantilever probes were produced out of standard silicon wafers and coated with a HF-CVD diamond layer. These probes were then mounted in a modified AFM, to successfully perform sequences of nanoscratching experiments and subsequent AFM imaging of the induced nanomodifications with continued high resolution.

Some attempts have been carried out to deposit HF-CVD diamond on the thinner cantilever probes. Unfortunately, the bridges holding the structures to the wafer frame were too thin to stand the shock wave induced by the introduction of gases into the reactor chamber at the beginning of the diamond deposition. As most of the probes fell into the reactor and even onto the filament, the diamond deposition was seriously perturbed and resulted in the formation of an unknown amorphous material.

To successfully deposit HF-CVD diamond on the thinner cantilever probes, the following improvements are suggested. First of all, it would be useful to design stiffer bridges to hold the structures to the wafer frame. Secondly, the entry of the reactive gases in the reactor has to be slowed down and finally, it could be useful to optimize the pretreatment procedure realized before the seeding process of the diamond deposition technology. This last suggestion is meant to improve the reproducibility and the continuity of the deposited diamond layers.

References

1 J. Brugger, R.A. Buser and N.F. de Rooij, "Silicon Cantilevers and Tips for Scanning Force Microscopy", Sensors and Actuators A 34 (1992) 193-200.

2 A.G.T. Ruiter , M.H.P. Moers, N.F. van Hulst and M. de Boer, "Microfabrication of Near-Field Optical Probes", Journal of Vacuum Science and Technology B 14 (1996) 597-601.

3 T.R. Albrecht, S. Akamine, T.E. Carver and C.F. Quate, "Microfabrication of Cantilever Styli for the Atomic Force Microscope", Journal of Vacuum Science and Technology A 8 (1990) 3386-3396.

4 J.P. Rasmussen, P.T. Tang, C. Sander, O. Hansen and P. Moller, "Fabrication of an All-Metal Atomic Force Microscope Probe", Proceedings of Transducers'97, International Conference on Solid-State Sensors and Actuators, Chicago, USA (1997) 463-466.

5 Ph. Niedermann, W. Hänni, D. Morel, A. Perret, N. Skinner, P.-F. Indermühle, N.F. de Rooij and P.-A. Buffat, "CVD Diamond Probes for Nanotechnology", Applied Physics A 66 (1998) S31-S34.

6 W. Kulisch, A. Malave, G. Lippold, W. Scholz, C. Mihalcea and E. Oesterschulze, "Fabrication of Integrated Diamond Cantilevers with Tips for SPM Applications", Diamond and Related Materials 6 (1997) 906-911.

7 S. Akamine, R.C. Barrett and C.F. Quate, "Improved Atomic Force Microscope Images Using Microcantilevers with Sharp Tips", Applied Physics Letters 57 (1990) 316-318.

8 M. Tortonese, "Cantilevers and Tips for Atomic Force Microscopy", IEEE Engineering in Medicine and Biology, March/April (1997), 28-33.

9 A. Boisen, O. Hansen and S. Bouwstra, "AFM Probes with Directly Fabricated Tips", Journal of Micromechanics and Microengineering 6 (1996) 58-62.

10 M.M. Farooqui, A.G.R. Evans, M. Stedman and J. Haycocks, "Micromachined Silicon Sensors for Atomic Force Microscopy", Nanotechnology 3 (1992) 91-97.

11 J. Itoh, Y. Tohma, S. Kanemaru and K. Shimizu, "Fabrication of an Ultrasharp and High-Aspect-Ratio Microprobe with a Silicon-On-Insulator Wafer for Scanning Force Microscopy", Journal of Vacuum Science and Technology B 13 (1995) 331-334.

12 N.X. Randall, "Development and Application of a Multifunctional Nanotribological Tool", PhD Dissertation, University of Neuchâtel, Switzerland (1997).

Double Molding Process I: Fabrication of Platinum Tips

The aim of this work was to investigate a new tip fabrication process based on two successive molding steps. This technology could allow tips to be realized in a wide variety of materials. In this study, platinum was used to achieve tips having the same aspect ratio and, in particular, the same radius of curvature as the anisotropically etched silicon tips described in Chapter 2. After feasibility was demonstrated, this process was used and slightly modified for the diamond tip fabrication to be presented in Chapter 5.
A short introduction explaining the motivation for developing such a fabrication process is given. The principle of the so-called double molding process is then presented. Finally, the fabrication of platinum tips is described and studied step by step, with emphasis on the critical ones. Parts of this chapter have been published in [1].

4.1 Introduction

Well-defined metallic probes having a high aspect ratio and a small radius of curvature are required for many applications, such as scanning tunneling microscopy [2], potentiometry [3] or vacuum microelectronics (electron field emitters) [4].
Before the age of near field probes, metallic tips were already microfabricated e.g. for applications in field emission displays. The tips were created by evaporating metal through a closely spaced aperture, producing a self aligned metal cone underneath the hole [5]. These tips are very sharp but their height is limited by the separation between the mask and the substrate. There is also a high risk of breaking the tip when removing the mask.

Today, with the increasing demand for conductive tips for various applications, other fabrication processes have been developed. The easiest consists of evaporating a metallic layer on a silicon probe. However, while the original aspect ratio is preserved, the radius of curvature is considerably increased, depending on the thickness of the deposited metallic layer. Moreover, such thin metallic films may easily rupture upon contact, leaving a non or poorly conductive apex. This is especially critical for potentiometric applications.
Metallic probes can also be realized by a single molding technique: {100} silicon is etched in KOH through a very accurately patterned mask, resulting in pyramidal holes defined by the intersection of the {111} planes [6]. These molds can be filled by metal sputtering [7], evaporation or electroplating [8, 9]. In the next step, the silicon molds are removed. All-metal tips with very good radii of curvature are obtained, but with an aspect ratio limited by the {111} planes of silicon. Instead of using the pyramidal pit etched into silicon as template, higher aspect ratio molds fabricated by RIE or by a combination of RIE and KOH/IPA anisotropic etching have also been used for electroplating tips [10]. Nevertheless, none of these simple molding techniques achieve tips having at the same time a small radius of curvature and an angle of aperture smaller then the one of the pyramidal tips.
A third method to realize all-metal probes is to use a focused ion or electron beam to crack an organo-metallic gas. The resulting tips have a good aspect ratio and radius of curvature, but this serial process is slow and it is difficult to control the shape of the tips [11].
In this chapter, a new fabrication technology based on two successive molding steps is presented. With this process, all-metal probes having the same aspect ratios and radii of curvature as the best anisotropically etched silicon tips can be formed in a reproducible way [12]. With this technology, sharp platinum tips having a height of up to 47μm, a half cone angle of 19° and a radius of curvature as small as 15nm have been realized. The same technique would also allow the fabrication of other metal tips, such as ferromagnetic probes for magnetic force microscopy.

4.2 Description of the Double Molding Process

This section briefly presents the principle of the double molding process [13]. Each step will be extensively described in the next section, where this technology is applied and studied for the fabrication of platinum tips.
The sequence for the double molding process is depicted in Figure 4.1. The first step consists of defining the first mold, an anisotropically etched silicon tip (Fig. 4.1a). For this purpose, processing starts with the thermal wet oxidation of a standard {100} silicon wafer, followed by photolithographic patterning and wet chemical etching of the mask to form the tips. The silicon wafer is then immersed in KOH and anisotropically etched until the silicon dioxide mask falls off.
In the next step, a low stress, silicon nitride layer is deposited on both sides of the wafer by LPCVD, followed by patterning of the back-side by photolithography, RIE and wet etching (Fig. 4.1b).

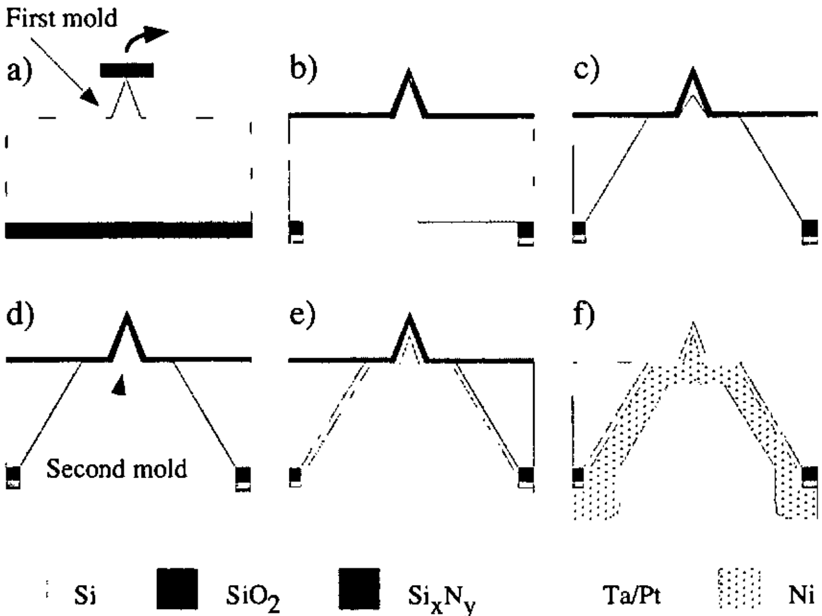

FIG. 4.1: Schematic of the sequence for the double molding process

The wafer is again anisotropically etched in KOH in order to remove the silicon underneath the tip. A silicon nitride membrane and a partially attacked silicon tip are left (Fig. 4.1c). The remaining silicon is then removed by isotropic etching in HNA (Fig. 4.1d).
The resulting silicon nitride film is then coated from the back-side by evaporating a metallic layer (Fig. 4.1e). Nickel can be electroplated to stiffen stressed metallic membranes in order to allow the removal of the silicon nitride on the front side. The second mold is finally attacked by extended wet chemical etching, leaving a metallic tip with the same aspect ratio and radius of curvature as the silicon tip acting as the first mold (Fig. 4.1f).

4.3 Evaluation of the Double Molding Process: Fabrication of Platinum Tips and Results

4.3.1 First Mold Definition

The KOH-etched silicon tips acting as a first mold (Fig. 4.2) were realized with the fabrication process described in detail in section 2.2. In this case, after tip definition, the back-side of the wafer was protected with photoresist during the removal in BHF of the silicon dioxide remaining on the top-side of the wafer. Finally, the photoresist was stripped off.

4.3.2 Second Mold Fabrication

Choice of the Material for the Second Mold

At this point, the first thing to do is to determine the material for the second mold, and deposit this in a layer on the silicon tip acting as a first mold. This layer has to fulfill the following conditions. First of all, it has to endure wet chemical etching in KOH for about 25 hours without itself being

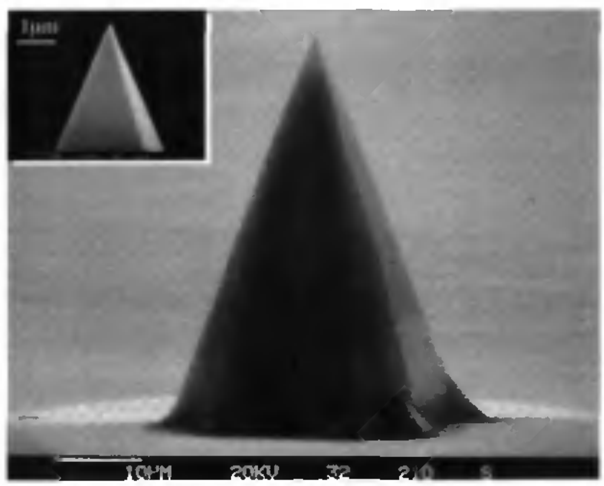

FIG. 4.2: SEM of a 47μm high Si tip having a radius of curvature smaller than 50nm.

significantly etched, as well as 30min in a HNA solution during the isotropic etching of the silicon remaining under the second mold. Moreover, this layer must be low stress in nature, in order to be able to stand by itself when the silicon is completely removed under it. It must also be sufficiently rigid to perfectly retain the original shape of the silicon tip, until it is removed in the final step of the procedure. Finally, this material must be able to withstand the high temperatures, up to 830°C, needed for the hot-filament chemical vapor deposition of diamond, which will be discussed in the next chapter.

Because of the hydrofluoric acid contained in the HNA, CVD and thermal silicon dioxide layers could immediately be excluded as suitable layers for the second mold. Polysilicon is rapidly etched in KOH and was therefore also not chosen. Silicon nitride layers were then the only remaining candidates. Standard stoichiometric LPCVD silicon nitride (Si_3N_4) unfortunately has too many internal stresses to stand by itself, while low-stress PECVD silicon nitride, which is deposited at 400°C, is not stable at temperatures as high as 800°C. Finally, a non-stoichiometric, silicon rich, low stress LPCVD silicon nitride (Si_xN_y) was chosen to serve as the second mold.

Preliminary tests for making Si_xN_y self-standing membranes and depositing HFCVD diamond on them showed that Si_xN_y was able to satisfy the conditions required for the second mold.

Second Mold Fabrication

After another standard cleaning, with a shorter BHF etching to preserve the silicon dioxide remaining at the back-side, a typically 6000Å thick, low stress, LPCVD Si_xN_y layer was deposited on both sides of the wafer. The tips on the top-side were then protected with 80μm of soft-baked photoresist and the back-side was patterned by photolithography (AZ 1518). RIE and BHF etching were used to open a window allowing the removal of the silicon under the tips (Fig. 4.1b). The photoresist was removed after the RIE using the piranha procedure described in section 3.3.

To etch away most of the silicon underneath the tip, the wafer was immersed in a 40% KOH bath at 60°C for about 25 hours, until the etching was drastically slowed down inside the tip by the appearance of the {111} planes (Fig. 4.1c). At this point, 30 to 70 % of the Si_xN_y molds were broken.

It was observed that this breakage of the tip-shaped molds appeared already at the very beginning of the KOH etching, and only when the molds were far away from each other (about 800µm). Indeed, in the case of 15µm high tip arrays with a spacing of 44µm to 72µm between two molds, no breakage was observed. This breakage was probably due to an accumulation of stress in the silicon nitride layer at the base of the tip, and could probably be avoided by integrating a stress barrier (lines of tips for example) at the border of the chip or of the membrane. This idea will be tested in a subsequent design.

The small amount of silicon remaining inside the tip-shaped mold was finally removed by isotropic etching in a HNA solution for 30 minutes (Fig. 4.1d). SEM investigations were necessary to ensure that the silicon nitride mold had been completely emptied (Fig. 4.3). It happened sometimes that a gas bubble prevented the HNA to enter a tip-shaped mold. In these cases, a second HNA etching was generally sufficient to empty it. It is important to note that the second mold did not appear to be etched at all in the HNA. This allowed the mold to reproduce exactly the dimensions of the original silicon tip and particularly of the tip apex, where the nanometer-sized radius of curvature was also preserved.

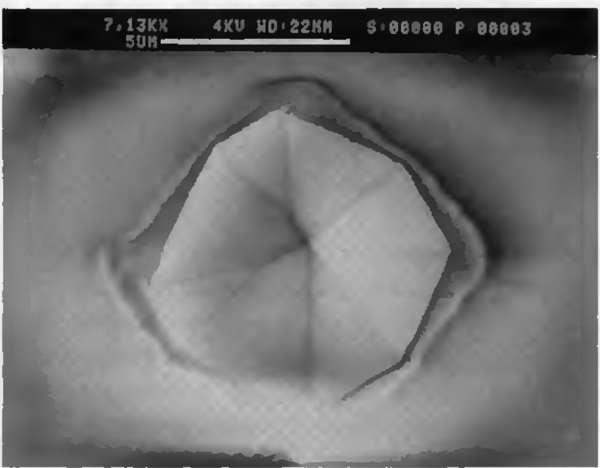

FIG. 4.3: SEM of a silicon nitride tip-shaped mold observed from the back-side of the wafer. In this case the original 15µm high silicon tip has been completely etched away.

4.3.3 Filling and Removal of the Second Mold

The first attempt to fill the Si_xN_y mold with a platinum layer and to remove the mold by RIE revealed two major problems. First, stresses in the platinum membranes were too great for them to stand by themselves, and all of them broke during the RIE. Breakage of these platinum membranes can be avoided by strengthening the platinum layer by electroplating ~50μm of nickel onto the back-side before the removal of the second mold. The second problem is the redeposition of material observed on silicon and especially on platinum after RIE. Many attempts have been made to remove these residues, such as different wet chemical etches, oxygen plasma and platinum electrochemical cleaning. As no solution was found for the removal of the RIE residues, a wet chemical etch of the Si_xN_y was considered. In the next section, several wet etchants for silicon nitride have been studied and evaluated with regard to the rate with which they etch the silicon nitride, the electrodeposited nickel and two different adhesion layers for the Pt evaporation, titanium and tantalum.

Determination of the Adhesion Layer and of the Wet Etchant for Si_xN_y

For this study, two silicon wafers were prepared according to the following process. The goal was to obtain, on each sample, structures which allowed simultaneous contact of the wet etchant with bare Si_xN_y, platinum and nickel. In this way, the etching rate of Si_xN_y and Ni could be determined, as well as the degree of underetching of the adhesion layers, using the platinum layer as a reference for the measurements.
First of all, an 8000Å thick, low stress, LPCVD silicon nitride layer was deposited on both sides of the wafers. In the following step, broad photoresist stripes (several mm) were painted on the top-side of both wafers in order to structure the adhesion and platinum layers by lift-off. 100Å of Ti, immediately followed by 3000Å of Pt, were evaporated onto one of the wafers, while 100Å of Ta and 3000Å of Pt were evaporated onto the second wafer. These metallic layers were patterned by dissolving the photoresist underneath them in acetone. Then, sections of the platinum structures were protected with photoresist during the electrodeposition of 100μm of Ni. Finally, the photoresist was stripped off and the wafers were cut in quarters.

TABLE 4.1: Summary of the etching rate and underetching appreciation of various materials in different wet etchants.

	H_3PO_4	HF	BHF
Etching time	*80min*	*160min*	*38 hours*
Si_xN_y *etch rate*	*90A/min*	*33A/min*	*208A/hour*
Ni etch rate	*4μm/min*	*negligible*	*negligible*
Ti underetching appreciation	*negligible*	*totally etched*	*very significant*
Ta underetching appreciation	*negligible*	*significant*	*negligible*

In this study, three different wet etchants were evaluated: a) 85% phosphoric acid (H_3PO_4) at 180°C, b) 50% HF at room temperature and c) BHF, also at room temperature. The results of this study are summarized in Table 4.1. It should be noted that the HF bath was not new, therefore a variation of the concentration has to be taken in consideration.

Based on Table 4.1, H_3PO_4 can immediately be rejected because of the high etching rate of Ni in this solution. HF is also unsuitable, due to the significant underetching of both Ti and Ta adhesion layers. BHF seems therefore to be the most promising candidate, despite the long etching time needed. As the underetching of Ti in BHF is very significant, Ta will be retained as the adhesion layer for platinum.

As a last verification, the fourth quarter with the Ta adhesion layer was immersed in KOH for 4 hours. It appeared that the nickel was not etched and the Ta not underetched either.

Second Mold Filling and Removal

In accordance with the results of the preceding study, the silicon nitride mold was coated from the back-side by evaporating a 100Å Ta adhesion layer followed by a 3000Å thick Pt layer (Fig. 4.1e). About 50μm of Ni was then electroplated on the back-side.

Finally, the Si_xN_y and the Ta adhesion layer were removed in a 33 hour long BHF etch, leaving a Pt tip having the same shape and radius of curvature as the silicon tip used as a first mold. Figure 4.4 is a general view of the Pt membrane and tip in its frame of silicon. Figure 4.5 shows one of the 47μm high Pt tips obtained at the end of the process, having a radius of curvature smaller than 15nm.

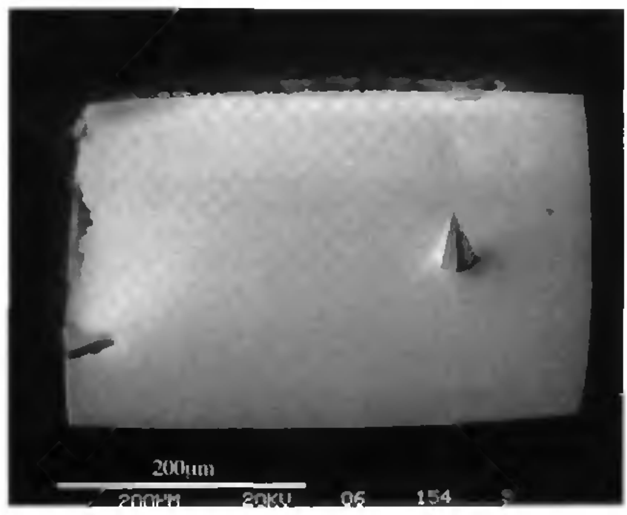

FIG. 4.4: SEM of a Pt membrane and tip in a frame of silicon at the end of the double molding process.

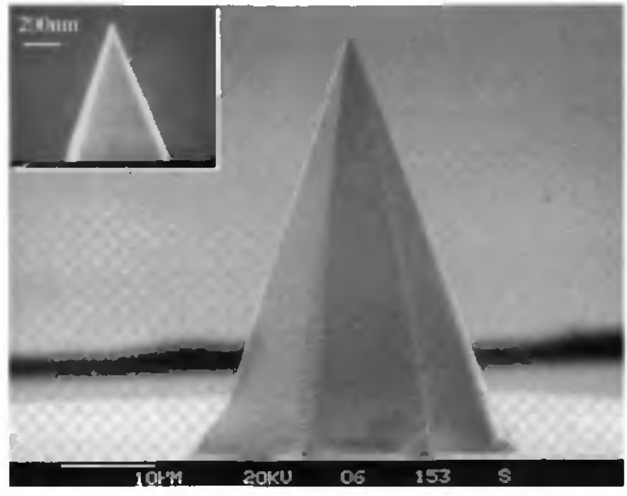

FIG. 4.5: SEM of a Pt tip realized by the double molding technique, which clearly shows the identical shape and radius of curvature as the Si tip of Fig. 4.2. Tip height is 47μm and the radius of curvature is smaller than 15nm. The latter was difficult to measure due to SEM vibrations during the observation.

4.4 Conclusions

It has been demonstrated that this new fabrication process based on a double molding technique is capable of perfectly reproducing the shape and radius of curvature (<15nm) of anisotropically etched silicon template-tips. The different steps of this batch process are not critical, except for the formation of the silicon template-tip, where overetching in KOH causes a rapid decrease of the tip height. However, the required etching times proved not to be critical for the shape and radius of curvature. Concerning the breakage of silicon nitride molds during silicon underetching in KOH, the addition, in a next generation, of stress barriers all around the membrane will certainly be sufficient to eradicate this inconvenience.
Further advantages of this process are its great flexibility in tip material selection and the wide range of achievable tip heights. Indeed, this process has been successfully applied for the realization of platinum tips with heights ranging from 15μm to 50μm and until now, no limitations have been noted.

References

1 C. Beuret, Ph. Niedermann, U. Staufer and N.F. de Rooij, "Fabrication of Metallic Probes by a New Technology Based on Double Molding", Microelectronic Engineering 41/42 (1998) 543-546.

2 G. Binnig, H. Rohrer, Ch. Gerber and E. Weibel, "Surface Studies by Scanning Tunneling Microscopy", Physical Review Letters 49 (1982) 57-60.

3 P. Muralt and D. W. Pohl, " Scanning Tunneling Potentiometry", Applied Physics Letters 48 (1986) 514-516.

4 cf. e.g. Proceedings of First International Vacuum Microelectronics Conference, IEEE Transactions on Electron Devices 36 (1989) 2635ff.

5 C.A. Spindt, I. Brodie, L. Humphrey and E.R. Westerberg, "Physical Properties of Thin-Film Field Emission Cathodes with Molybdenum Cones", Journal of Applied Physics 47 (1976) 5248-5263.

6 T.R. Albrecht, S. Akamine, T.E. Carver and C.F. Quate, "Microfabrication of Cantilever Styli for the Atomic Force Microscope", Journal of Vacuum Science Technology A 8 (1990) 3386-3396.

7 T. Yagi, Y. Shimada, T. Ikeda, O. Takamatsu, H. Matsuda, K. Takimoto and Y. Hirai, "A New Method to Fabricate Metal Tips for Scanning Probe Microscopy", Proceedings of MEMS'97, International Workshop on Micro Electro Mechanical Systems, Nagoya, Japan (1997) 129-134.

8 J.P. Rasmussen, P.T. Tang, C. Sander, O. Hansen and P. Moller, "Fabrication of an All-Metal Atomic Force Microscope Probe", Proceedings of Transducers'97, International Conference on Solid-State Sensors and Actuators, Chicago, USA (1997) 463-466.

9 T. Hantschel, P. De Wolf, T. Trenkler, R. Stephenson and W. Vandervorst, "Fabrication and Use of Metal Tip and Tip-on-Tip Probes for AFM-Based Device Analysis", SPIE Proceedings of Micromachining and Microfabrication '98, Vol. 3512, Santa Clara, CA, USA (1998) 92-103.

10 A. Boisen, J.P. Rasmussen, O. Hansen and S. Bouwstra, "Indirect Tip Fabrication for Scanning Probe Microscopy", Microelectronic Engineering 30 (1996) 579-582.

11 T. Akiyama, A. Tonin, H.R. Hidber, J. Brugger, P. Vettiger, U. Staufer and N.F. de Rooij, "Fabrication and Testing of an Integrated Force Sensor Based on a MOS Transistor for Applications in Scanning Force Microscopy", Proceedings of MEMS'97, International Workshop on Micro Electro Mechanical Systems, Nagoya, Japan (1997) 141-146.

12 O. Wolter, Th. Bayer and J. Greschner, "Micromachined Silicon Sensors for Scanning Force Microscopy", Journal of Vacuum Science and Technology B 9 (1991) 1353-1357.

13 Ph. Niedermann, C. Beuret and S. Jeanneret, "Procédé de fabrication d'un organe palpeur pour capteur micromécanique, notamment pour microscope à force atomique", European Patent Application EP 0 882 944 A1 (December 9, 1998).

Double Molding Process II: Fabrication of Diamond Tips 5

The goal of this work was to modify the double molding process for the fabrication of hot-filament CVD diamond tips. Moreover, transfer processes were developed to mount these diamond tips on stubs to be used as probes in high resolution profilometry, as well as on cantilevers for atomic force microscopy measurements.

5.1 Introduction

The unique properties of diamond, such as its extreme hardness, its very good resistance to wear and its chemical inertness, makes this material an excellent candidate for the fabrication of many devices [1, 2, 3, 4]. The use of diamond tips is of particular interest in many SPM applications, especially in AFM, or in high resolution profilometry, where the imaging is performed in contact mode and, hence, the wear of the tip is a critical factor. The first diamond probes used in AFM were made of a small fragment of a gem [5] whose geometry, however, could not be well controlled. The increasing progress in thin film diamond deposition by various CVD techniques [4] have made it possible to overcome this inconvenience. Moreover, by adding boron or nitrogen during the deposition, diamond can also be doped, opening the opportunity to use this material for conducting probes in STM [2] and for the realization of field emitter devices [3].
In the search for new tip materials for SPM applications, thin diamond films have been deposited on batch processed silicon tips [2] or etched tungsten wires [6], either by microwave plasma assisted-[6] or hot filament-CVD [2, 4] techniques. While the general shape of the tips obtained with these techniques is well controlled, the radius of curvature increases proportionally to the thickness of the deposited film, worsening the

resolution of AFM tips. In order to avoid this dependence, a simple molding process, previously developed for silicon nitride tips [7], has been adapted to realize pyramidal CVD diamond tips with radii of curvature as small as 20nm [2].
The imaging in AFM and profilometry is always a convolution of the topography of the sample and the tip. Unfortunately, the aspect ratio of such pyramidal tips is restricted by the {111} planes of the anisotropically etched silicon holes used as mold. This renders such tips of limited use on highly corrugated surfaces, which have themselves features of high aspect ratio.
In this work, the batch fabrication process based on the double molding technique has been further developed in order to realize high aspect ratio diamond tips having radii of curvature smaller than 20nm. Such diamond tips have been mounted on stubs for high resolution profilometry applications, as well as on cantilevers for AFM measurements.

5.2 Fabrication of Diamond Tips: Modifications of the Double Molding Process I and Results

The first steps of the double molding process described in the preceding chapter (Fig. 4.1a-d) were not modified for the fabrication of diamond tips. Only the steps which involve filling the second mold and its subsequent removal were changed, and are presented in this section (Fig. 5.1). The size of the square silicon dioxide mask used to define the silicon tips has been reduced to 40μm in order to obtain tips having a height of 15μm, which is considered to be sufficient for high resolution profilometry and AFM measurements.

5.2.1 Second Mold Filling: Diamond Deposition

The diamond deposition inside the second mold was realized with the hot-filament CVD technique [2, 4, 8] described in section 1.3.1. In this double molding process, the diamond deposition was performed with the wafer placed upside-down on a graphite chuck (Fig. 5.2). In this way, diamond was deposited on the back-side of the wafer, that is to say on the Si_xN_y frame, on the {111} silicon planes, and on the back-side of the silicon nitride membrane acting as second mold.

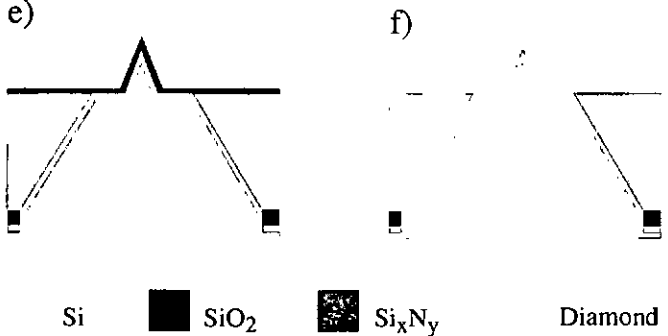

FIG. 5.1: Steps of the double molding process modified for the realization of diamond tips. In this case, diamond can stand by itself and nickel is not necessary anymore to strengthen the membranes.

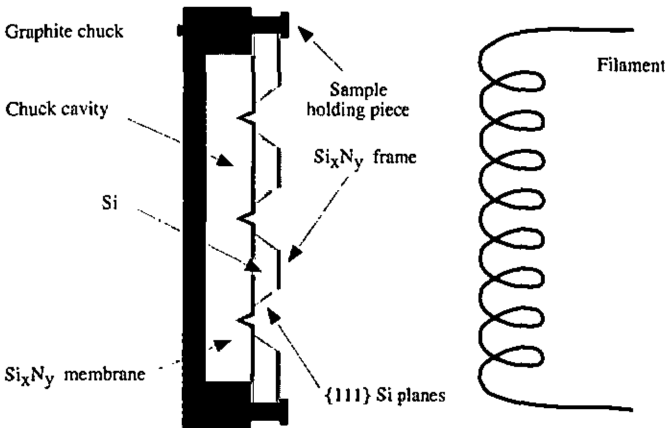

FIG. 5.2: Schematic of the sample mounted on the graphite chuck during diamond deposition.

The first test of diamond deposition, realized without the cleaning steps previously mentioned as preparation of the sample, resulted in only 4% of the Si_xN_y membranes filled with a continuous layer of nanocrystalline, instead of polycrystalline, diamond (Fig. 5.3). The silicon nitride frame, however, was continuously covered with a polycrystalline diamond film. This was interpreted to be the result of a non-uniform seeding process.
To resolve this problem, ultrasonic agitation was used in a first attempt during the seeding process in order to insure better diffusion of the seeding solution into the holes. Unfortunately, all the Si_xN_y membranes broke during the ultrasonic agitation. For subsequent depositions, a preparation of the sample before the seeding process was added (see section 1.3.1). This dramatically increased the seeding efficiency and homogeneity.
Finally, with the improved diamond deposition process, continuous layers of polycrystalline diamond on the Si_xN_y frame, {111} Si planes, Si_xN_y membrane, as well as inside the tip-shaped second mold, could be obtained, at least as deep as could be observed by SEM (Fig. 5.4).
Different types and thicknesses of diamond films were deposited in the Si_xN_y membranes. At this step, SEM observations did not reveal any differences in the quality of the polycrystalline diamond for 1μm or 2μm thicknesses, or for intrinsic, slightly boron-doped (1ppm) or heavily boron-doped (3ppm) layers.

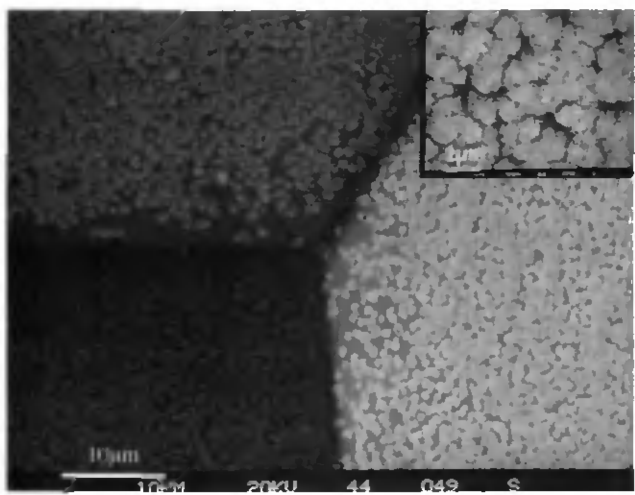

FIG. 5.3: SEM of a discontinuous layer of CVD nanocrystalline diamond deposited on the {111} silicon planes and on the Si_3N_4 membrane. The inset in the upper right corner of the figure shows an enlargement of the nanocrystalline structure of this diamond layer.

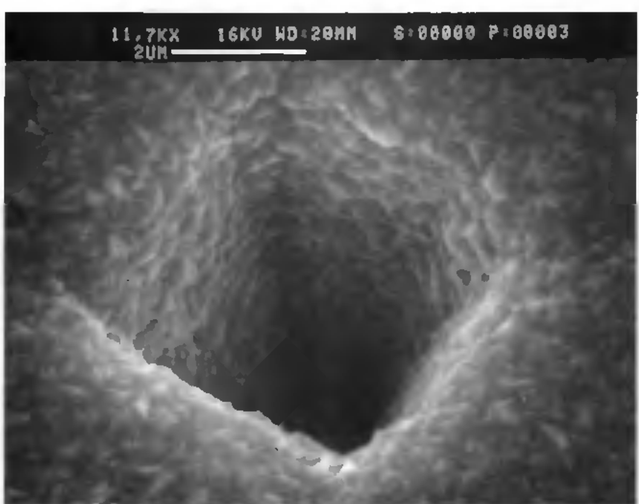

FIG. 5.4: SEM of the back-side of the second mold uniformly filled with a 2μm thick layer of CVD, boron-doped diamond.

5.2.2 Removal of the Silicon Nitride Mold

At this step, the 8000Å thick silicon nitride appeared to be very difficult to remove. In the first trial, this layer was etched in BHF, as in the double molding process used for platinum tips. However, after 66 hours in this solution, the silicon nitride was not etched at all. Many other etching processes have been investigated, such as dry etching with various reactive gases (SF_6/O_2, SF_6/C_2ClF_5, $Cl_2/SiCl_4/N_2$), wet etching in different solutions (BHF, H_3PO_4, $HF:H_2O_2:H_2O$) and combinations of both wet and dry etching. While some of these techniques presented promising results for other applications as mentioned in Fig. 5.5, no efficient and reproducible attack could be developed at this point of the work. The results of these various methods are summarized in Table 5.1.

FIG. 5.5: SEM of a partially released diamond tip pointing out of the silicon nitride layer remaining after a combination of dry etching (SF_6/O_2, 8min) and wet etching (H_3PO_4, 180°C, 45 min). The base diameter of the boron-doped diamond tip apex not passivated by the insulating layer is 220nm, its height about 300nm, while its radius of curvature is estimated to be smaller than 20nm. Such structures could be used as ultra-precise nanoelectrodes or nanoprobes.

TABLE 5.1: Summary of the various etching processes used to investigate the removol of the silicon nitride mold after diamond deposition.

Etchant	Etching time	Observation
BHF	66h00	No etching
SF_6/O_2	8 min	Si_xN_y etched on flat surfaces and tip apex only. In case of overetching, diamond tip apex etched. Plasma residue difficult to remove
SF_6/O_2 H_3PO_4 180°C	8 min 45min	Si_xN_y etched on flat surfaces and tip apex only. Danger of averetching in SF_6/O_2. Tip apex clean but H_3PO_4 etching too slow. See Fig. 5.5
SF_6/O_2 H_3PO_4 180°C SF_6/C_2ClF_5	8 min 45 min 30 min	Si_xN_y etched on flat surfaces and tip apex only. Danger of overetching in SF_6/O_2. Tip apex clean but H_3PO_4 etching too slow. SF_6/C_2ClF_5 etched the tip apex
$Cl_2/SiCl_4/N_2$	40 min	Etching rate too slow: 10A/min
$HF:H_2O_2:H_2O$ 1:1:5	38h00	Redeposition of films on the wafer. Si_xN_y sometimes completely etched depending on the density and thickness of the films covering the Si_xN_y
$HF:H_2O_2:H_2O$ 1:1:5 FC 93 (wetting agent)	36h00 3 drops when taking out	No more redeposition of films on the wafer. Si_xN_y sometimes completely etched depending on the density and thickness of the films covering the Si_xN_y
SF_6/O_2 $HF:H_2O_2:H_2O$ 1:1:5 FC 93 (wetting agent	2-8 min 34-72h00 3 drops	Results not reproducihle. Strong influence of film thickness and density on the attack. Sometimes perfectly clean, sometimes tip apex overetched or films and silicon nitride remain (see Fig. 5.6)

These investigations revealed the presence of a thin film covering the top-side of the silicon nitride layer (Fig. 5.6). This film was deposited during the diamond deposition on the side of the wafer which is located against the surface of the graphite chuck used to hold the wafer. None of the wet etching processes used in this work could etch this film. In the case of dry etching, the silicon nitride was probably underetched, and the film redeposited in small pieces on the surface of the wafer.

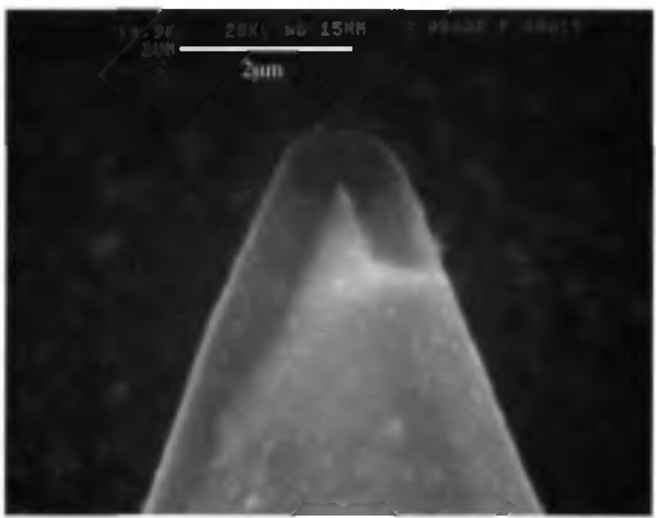

FIG. 5.6: SEM of a diamond tip apex nppearing inside the partially etched silicon nitride second mold. The composition of the transparent film located on the silicon nitride is not known. This film, as well as a small amount of the silicon nitride, has been removed from the apex of the diamond tip by successive SF_6/O_2 dry etching and wet etching in a $HF:H_2O_2:H_2O$ solution.

The composition of this film has not been determined so far, but it could be silicon carbide. It was observed that the density and thickness of this film depends on the number and location of broken molds. Indeed, a high proportion of membranes missing their tip-shaped molds would allow larger quantities of reactive gases to reach the side of the sample placed against the graphite chuck. At this point, an unknown reaction could occur between the gases, the sample, and perhaps the chuck, resulting in the formation of this undesirable film.

A cavity in the chuck was necessary to prevent the silicon nitride molds from being crushed against the chuck. To reduce the supply of gases from the sides of the wafer, a special chuck was manufactured with a cavity whose geometry is identical but with slightly smaller dimensions than the sample dimensions (Fig. 5.2). Samples on which diamond depositions were performed using this new chuck exhibited a sufficient reduction of the thickness and density of the film. Complete removal of the silicon nitride

second mold by wet etching in the hydrofluoric/peroxide/water solution was then possible. Also in this case, the film was underetched and floated on the surface of the etch bath. Adding 2-3 drops of a wetting agent (FC 93) in the bath just before taking out the sample prevented redeposition of this hydrophobic film on the wafer. Trying to etch the film with SF_6/O_2 prior to the wet etching described above leads only to the formation of residues which are very difficult to remove.
In summary, to be able to etch the silicon nitride second mold after diamond deposition, the deposition had to be done using a quasi-hermetic chuck. Etching could only be realized in a hydrofluoric/peroxide/water solution, adding just 2-3 drops of a wetting agent before removing the sample, in order to avoid film redeposition on the wafer.
By this modified double molding technology, it was demonstrated that diamond tips perfectly reproduce the shape and radius of curvature of the initial anisotropically etched silicon tips (Fig. 5.7).

5.2.3 Diamond Evaluation

Up to this point in this work, only SEM studies of diamond layers have been presented. These observations have given an idea of the crystal structure of deposited diamond layers. Indeed, if crystal facets can easily be seen, it suggests that the layer is probably essentially composed of polycrystalline sp^3 diamond. If not, the layer is either nanocrystalline or even amorphous.
To have a better idea of their composition, some diamond layers were investigated by Raman spectroscopy. These qualitative measurements are very sensitive to any sp^2 carbon content. Therefore, as soon as a diamond peak can be detected in the presence of graphitic defects, it can be concluded that the layer is essentially composed of polycrystalline diamond with only a small amount (5-500ppm) of graphitic carbon. Unfortunately, it was not possible to perform Raman measurements on or in the tip itself due to a lack of precision in the laser location.
To complete the evaluation of the diamond layers, then, imaging was performed with a Transmission Electron Microscope (TEM). With this microscope, very high resolution light- or dark-field images of thin samples can be obtained. Moreover, using a small diaphragm, it is also possible to get the diffraction pattern of a selected area of the sample.

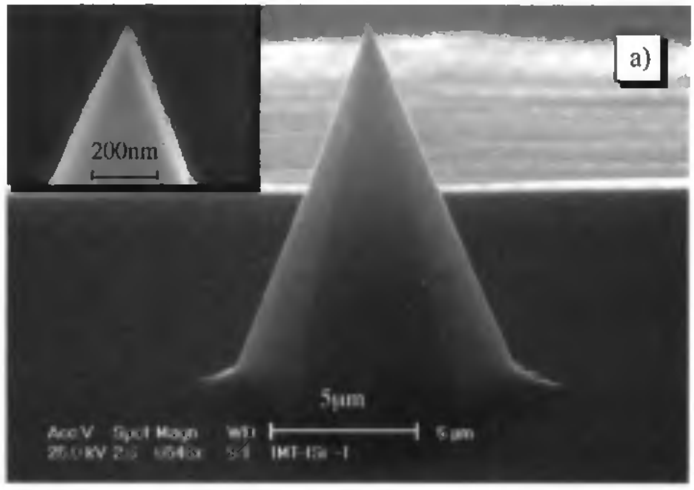

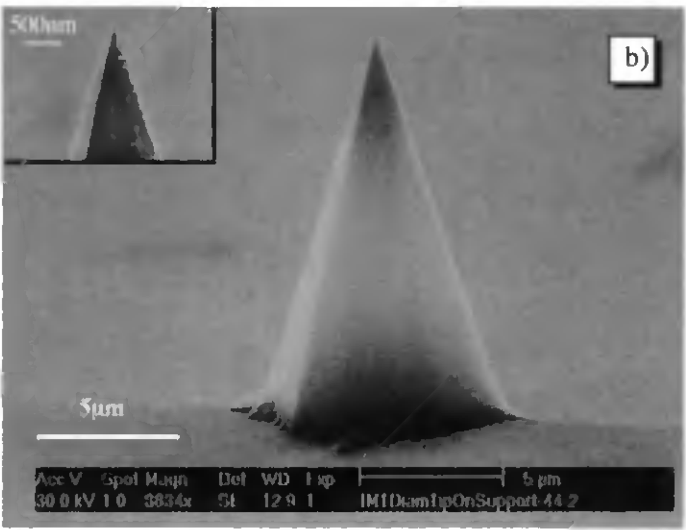

FIG. 5.7: Comparison between: (a) a typical anisotropically etched silicon tip acting as a first mold and (b) a 13µm high, CVD diamond tip obtained with the double molding process after the removal of the silicon nitride second mold. Both tips have an aspect ratio of 1.45 and radii of curvature as small as 20nm.

Raman and TEM investigations were first realized on the wafer from which diamond tips were extracted for mounting on stubs for high resolution profilometry applications (sample A). Based on the results of these investigations, which are presented hereafter, attempts to extend the diamond deposition into the apex of the tip-shaped silicon nitride mold were performed. To this end, cyclic pressure variations were added during diamond deposition in order to improve the gas exchange into the mold. The results of the Raman analysis and of the TEM observations realized on this second sample (sample B) are also presented in this section.

Raman Spectroscopy Investigation of the Diamond Layer

Raman spectroscopy is one of the principal characterization tools for diamond materials. Indeed, the presence of sharp Raman lines allows diamond to be recognized against a background of sp^2 carbon and also to characterize the graphitic carbon [9, 10, 11]. Table 5.2 gives the wavenumber values of the Raman peaks or domains corresponding to the presence of diamond and various types of graphitic carbon in a sample.

TABLE 5.2: Raman peak locations for various materials

Wavenumber (cm^{-1})	*Material*
520	*Silicon (can vary with doping)*
790	*Silicon carbide (disordered cubic)*
970	*Silicon carbide (hexagonal)*
1130-1150	*Micro/Nanocrystalline diamond*
1230-1250	*Nanocrystalline diamond*
1315-1326	*Hexagonal diamond (lonsdaleite)*
1332 (±10)	*Monocrystalline diamond (cubic)*
1340-1360	*Disordered graphite ("D")*
1465-1475	*Micro/Nanocrystalline diamond*
1520-1560	*Diamite or bridged graphite (diamond-like films)*
1580	*Monocrystalline Graphite ("G")*

These measurements are qualitative and not quantitative. Indeed, compared to diamond, graphitic carbons and other sp^2 bonded amorphous carbons are strong Raman scatterers in spite of their intense optical absorption. So, as the Raman intensity of the various sp^2 carbon spectra is much higher than that of the diamond spectrum, Raman spectroscopy is a very effective means of detecting very small amounts of sp^2 carbon in diamond films. However, it is not a sensitive test for diamond in the presence of other types of carbon.
Measured spectra of CVD diamond films usually consist of more than just the narrow diamond Raman line. Non-diamond carbon Raman lines and Raman peaks from the substrate material can add up to rather complex spectral structures which are difficult to interpret. In order to quantify the individual features, a computer peak analysis routine is applied. However, it has to be taken into account that such an analysis can produce results with the peak position being shifted due to unidentified small peaks. Moreover, Raman lines can be shifted due to various factors. For example, adding boron in the diamond layer induces a shift of the diamond Raman line towards the lower wavenumbers (negative shift). Reducing the diamond grain size [12], or heating the diamond layer with the light source, also produces a negative shift. The orientation of the diamond crystal, as well as the angle of incidence of the light source on the crystal, can also have an influence on peak position [13]. Finally, the internal stresses in the diamond layer, brought about during the deposition by a mismatch between the diamond film and the substrate, can also produce small shifts, negative for films in tension and positive for films in compression [9].
In our case, Raman spectroscopy investigations were realized with an Ar-laser monochromatic light source at a wavelength of 514.5nm (Ramascope System 2000 © Renishaw) at different locations, on the top-side as well as on the back-side of the samples. The Raman spectrum realized on the wafer from which boron-doped diamond tips were extracted for the high resolution profilometry measurements (sample A) are presented in Fig. 5.8. The three individual components of the fit are depicted underneath the measured curve. For a better clarity, a schematic of the measurement location is presented for each measurement.
In Fig. 5.8a) and 5.8b), the diamond peak is clearly visible, even if it is a little shifted towards lower wavenumbers (1325-1327cm^{-1} instead of

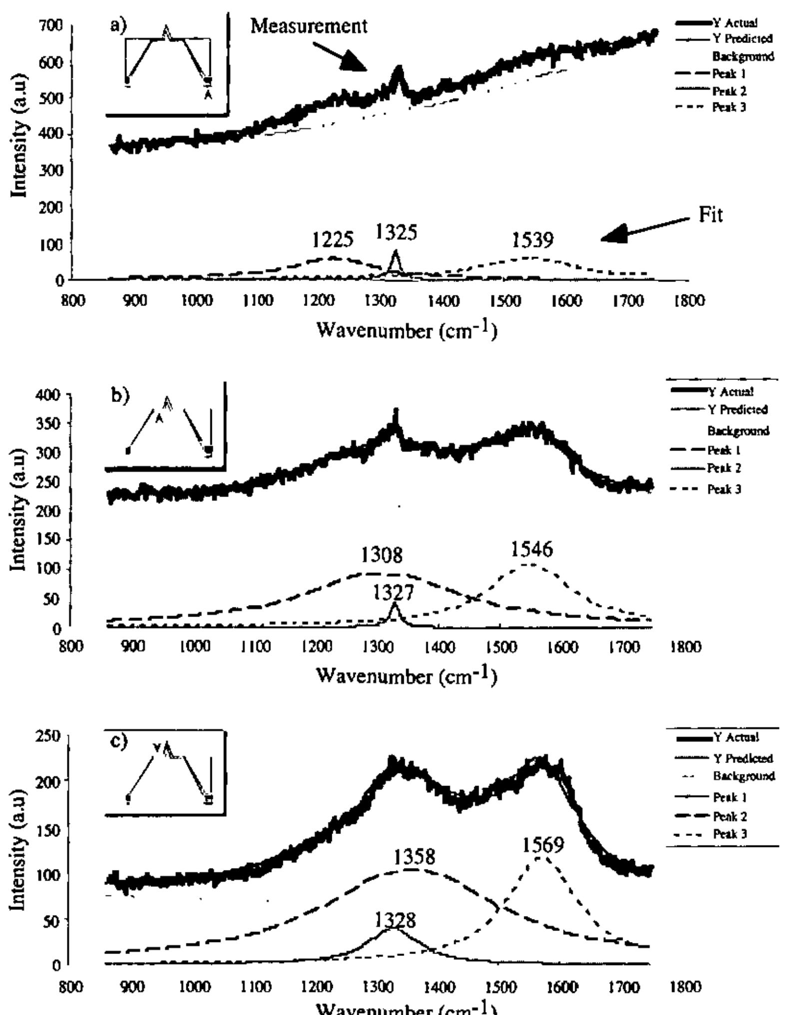

FIG. 5.8: Raman measurements realized at different locations on sample A. o) Bock-side of the wafer, on the surface of the diamond layer deposited on the silicon nitride/silicon frome. b) Diamond membrane from the back-side of the wafer, corresponding to the surface of the diomond layer at the end of the deposition. c) Diamond membrane from the top-side of the wofer, corresponding to the diamond initially deposited at the beginning of the mold filling process.

1332cm^{-1}). In Fig 5.8c), the diamond peak is wider, but still present at 1328cm^{-1}. These shifts can appear when diamond is doped with boron. In all these measurements, other peaks are present. It is difficult to determine exactly to which materials they correspond. Their positions are influenced by the way the fits have been made. In this work, only the number of peaks has been fixed, letting the program determining the peak positions for an optimal fit using Lorentzian functions.

Based on the experience acquired with repeated Raman measurements of diamond layers deposited under the same conditions and in the same reactor chamber as the one presented here, it can be deduced that the peaks located between 1520cm^{-1} and 1580cm^{-1} (a) 1539cm^{-1} b) 1546cm^{-1} and c) 1569 cm^{-1}) are probably due to a certain amount of graphitic defects. From earlier experiments, the peak at 1225cm^{-1} of Fig. 5.8a) is identified to be due to the presence of nanocrystalline diamond, while the peak at 1358cm^{-1} of Fig. 5.8c) corresponds probably to a small amount of disordered graphite "D". Concerning the peak at 1308cm^{-1} of Fig. 5.8b), it could either correspond to some disordered graphite "D", or it could be the result of the combination of two peaks at 1243cm^{-1} and 1441cm^{-1} (these values were obtained by allowing four peaks instead of three as fitting parameters). Both peaks correspond to the presence of nanocrystalline diamond. As some nanocrystalline diamond has also been identified in the Raman spectrum of Fig. 5.8a), this last interpretation seems to be more reasonable.

These measurements prove that this layer, at least the membrane and the coating on the frame, is essentially composed of polycrystalline diamond, with some nanocrystalline diamond on the back-side of the wafer. In all cases, the presence of a certain amount of sp^2 carbon has been demonstrated.

Raman spectroscopy investigations were also performed on sample B and are presented in Fig. 5.9. The diamond layer deposited on this wafer differs from the one of sample A in the following ways. Firstly, during the diamond deposition, the pressure in the reactor chamber was varied at least every ten minutes to improve the gas exchange into the tip-shaped mold. Secondly, no boron was added during the deposition, resulting in an "intrinsic" diamond layer. Finally, after the removal of the second mold, the sample was immersed in a 100% HNO_3 bath for 16 hours in order to remove any graphitic compounds that could still be present. The surface of the tips

appeared to be quite rough after this step, demonstrating that some graphite had certainly been located in the diamond grains junctions. Nevertheless, the general shape of the tips, as well as their apex, had been preserved.

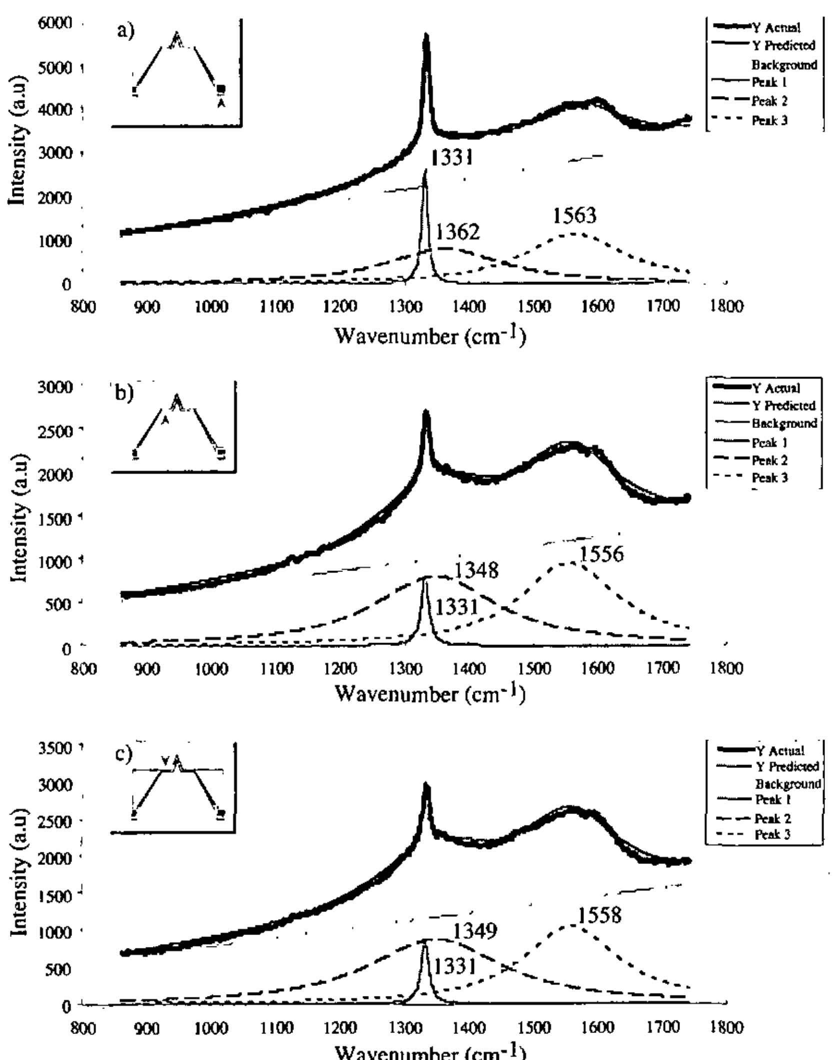

FIG. 5.9: Raman measurements realized at different locations on sample B.

In comparison to the Raman spectra of Fig. 5.8, it is observed that the proportion of diamond compared to that of graphitic defects is higher in sample B than in sample A. This could be due either to an improvement in the quality of the diamond layer or to the HNO_3 etching of the superficial graphitic compounds. Moreover, an improvement of diamond layer quality could be due either to the cyclic pressure variations during deposition or to the absence of boron in the diamond layer. Indeed, heavy boron doping is known to favor the formation of sp^2 carbon in HF-CVD diamond layers. In any case, the Raman spectra of Fig. 5.9 highlight sharp diamond peaks at $1331cm^{-1}$. For this undoped sample, the diamond peaks have almost not shifted from the expected value.
In Fig. 5.9a), the Raman peaks of disordered graphite ($1362cm^{-1}$) and of monocrystalline graphite ($1563cm^{-1}$) are attenuated compared to the diamond peak, demonstrating that only a few ppm of graphitic defects are present in the diamond layer. In Fig. 5.9b) and 5.9c), the Raman peaks of disordered graphite ($1348cm^{-1}$ and $1349cm^{-1}$, respectively) as well as the peaks of monocrystalline graphite ($1356cm^{-1}$ and $1358cm^{-1}$) are more pronounced, but still indicate a very low amount of sp^2 carbon in the diamond layer. In all these measurements, the location of the monocrystalline graphite peaks is shifted towards lower wavenumbers. This could be due to the heterogeneous structure of the layer (composed of sp^2 carbon and of sp^3 diamond), inducing vibrationnal frequencies which differ from, but are nevertheless close to, the ones of the different phases contained in the layer.
The Raman spectra of Fig. 5.9b) and Fig. 5.9c) are very similar, as can be expected for two measurements of the same layer. However, this was not the case for the figures 5.8b) and 5.8c), where the amounts of various forms of graphite were more significant in the measurement realized on the top-side of the wafer. This could simply be due to a more pronounced formation of graphitic compounds between the diamond grains in the earlier stage of the diamond deposition, compounds which, in the case of sample B, have been removed in HNO_3.
To conclude, the Raman spectra of sample B more closely resemble those of a good polycrystalline diamond layer than the ones of sample A. It is necessary, however, to keep in mind that the superficial graphitic

compounds of sample B could have been etched away in HNO_3 unlike those of sample A. Moreover, the reason for this improvement is not clearly defined. It could be due either to the fact that the diamond layer of sample B had not been doped with boron, or to the cyclic pressure variations during the diamond deposition. To clarify these points, it would be necessary, in the future, to perform another boron-doped diamond deposition with the same cyclic pressure variations and to make Raman investigations of this layer before and after etching in HNO_3 for sixteen hours.

TEM Observations

To determine the material composing the tip apex, or at least its crystal structure, it was necessary to turn to TEM analysis. The TEM observations of sample A were carried out at the EPFL (Ecole Polytechnique Fédérale de Lausanne), while the TEM investigations of sample B were performed at the IMS (Institut de Métallurgie Structurale) of the University of Neuchâtel.
On the dark-field image of the apex of one of the tips extracted from sample A (Fig. 5.10), the contrast which can be observed under the dashed line highlights a reduced total thickness of the material at this location, compared to that of the edges of the tip where no contrast can be observed. Considering the conical shape of the sample, this reduced thickness demonstrates that the tip apex is hollow and that the thickness of the diamond layer is thinner than 300nm at this location, when 2μm are expected. On the other hand, little white areas can be observed, corresponding to small crystals oriented in a specific direction and by which the incident electrons are scattered.
The diffraction pattern of this tip apex is presented in Fig. 5.11. The simultaneous presence of small bright spots and of blurred circles indicates that the tip apex is composed of many nanocrystals oriented in various directions, which are embedded in an amorphous matrix.
Finally, an image of the tip apex at a very high magnification was made (Fig. 5.12). The small "filament-like" atomic planes are characteristic of crystalline graphite. From this, it can be concluded that this tip apex is essentially composed of nanocrystals of graphite embedded in an amorphous material.

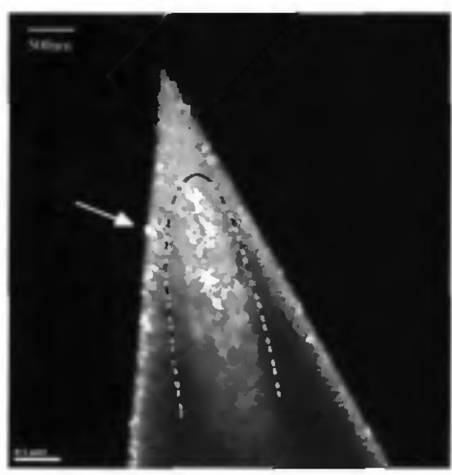

FIG. 5.10: Dark field image of the apex of a tip extracted from sample A. The white line outlines an area of reduced thickness in which it can be seen that the tip is hollow. The arrow points at one of the scattering crystals.

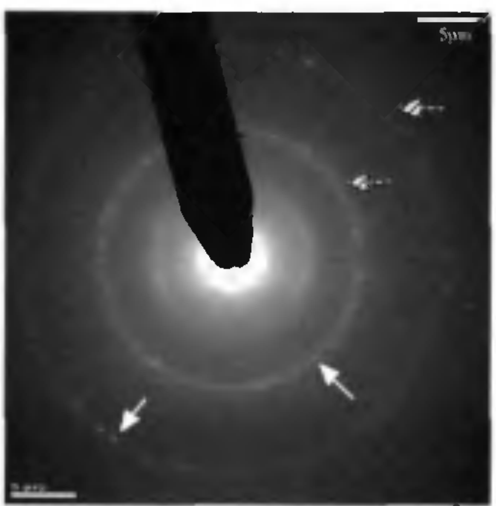

FIG. 5.11: Diffraction pattern of the tip apex of sample A. The blurred circles indicate the presence of amorphous material (dashed arrows) while the small bright spots (white arrows) are diffraction patterns of small crystals orientated in different directions.

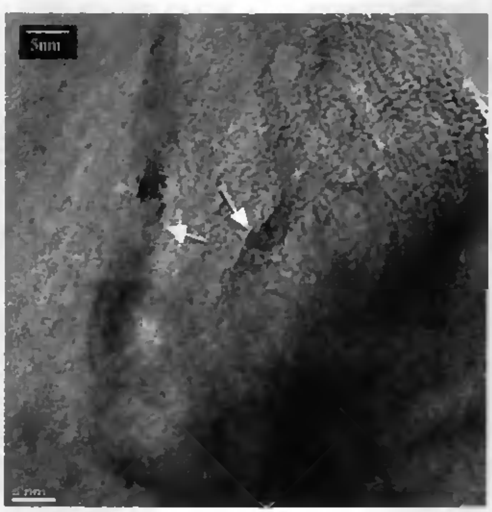

FIG. 5.12: TEM taken at high magnification (340'000x) highlighting atomic planes characteristic for crystalline graphite (indicated by the arrows).

TEM analysis of the apex of some tips extracted from sample B were also performed. A dark-field image of a tip apex is presented in Fig. 5.13a). Once more, the bright areas correspond to electron scattering nanocrystals oriented in a specific direction. Figure 5.13b) represents the same area after a slight rotation of the tip. It can been observed that the electrons are scattered by other nanocrystals oriented in a slightly different direction than those visible in Fig. 5.13a). From these pictures and others not presented here, it can be concluded that the majority of the material located at the right of the micrographs is nanocrystalline. On the other hand, the absence of scattering crystals at the very end of the tip apex (left parts of Fig. 5.13a) and b)) indicates that this area is amorphous.
The diffraction pattern of the small area enclosed by a circle in Fig. 5.13a) is presented in Fig. 5.14. There, the small bright spots correspond to nanocrystals and as no blurred circle can be observed, it can be concluded that this area does not contain amorphous material. To determine the composition of these nanocrystals, the diffraction pattern of Fig. 5.14 was compared with the diffraction pattern of a small area of the tip base (Fig. 5.15) which, according to SEM observations (see Fig. 5.4), is composed of

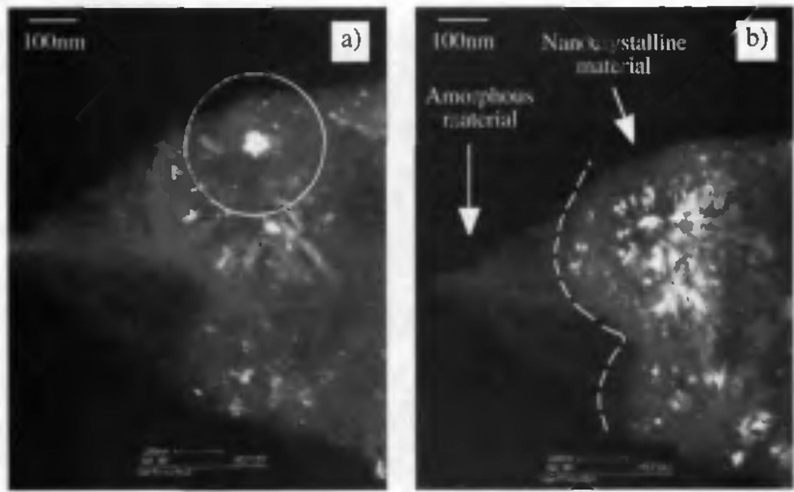

FIG. 5.13: Dark field images of a tip apex in sample B. a) The bright features correspond to the electrons scattered by small crystals oriented in a specific direction. The drawn white circle corresponds to the area defined by the diaphragm during the formation of the diffraction pattern. b) Same area after a slight rotation of the tip apex, highlighting other small crystals oriented in a slightly different direction than the ones in a).

polycrystalline diamond. The radii between the central transmitted spot and the nearest nanocrystal diffraction spots have been measured in both figures 5.14 and 5.15 and found to be identical at this resolution. From this value, the distance between the planes belonging to this particular family of scattering planes could be calculated to be 2.181Å±0.120Å. This experimental interplanar distance was finally compared to the values of tables, in which the interplanar distances of the various families of scattering planes have been reported for diamond as well as for monocrystalline graphite. The best matching values are 2.059Å for {111} diamond planes and 2.131Å and 2.031Å for various graphite families of planes. As the theoretical values for diamond and graphite interplanar distances are very close to each other, it is difficult to determine if the experimental value corresponds to diamond or to graphite. Based on the SEM observations presented in Fig. 5.4, and on the fact that graphitic compounds are etched away in a long fuming nitric acid etch, it has been concluded that the diffraction patterns correspond to diamond nanocrystals. Nevertheless, the presence of small amounts of graphite cannot be excluded.

Even if the tip is essentially composed of polycrystalline diamond, the presence of amorphous material at the extremity of the tip apex clearly indicates that the diamond deposition used for the realization of sample B is still not optimal at the deep end of the molds. To determine the atomic composition of these tips, Energy Dispersive Spectroscopy (EDS) [14] investigations of the tip apex as well as of the tip base were carried out. These qualitative analyses showed that the bases of the tips are essentially composed of carbon atoms, with a small amount of oxygen, while silicon was detected in addition to carbon and oxygen in the apices. Based on this, it is possible that the apices of the tips are composed of a very thin layer of oxycarbide of silicon.

FIG. 5.14: Diffraction pattern of a small area (ϕ 300nm) of the tip apex of sample B.

Such a thin tip apex will easily be broken once in contact with a sample during high resolution profilometry experiments, leaving in the best case, a nanocrystalline tip apex having a radius of curvature in the order of 200nm. Such a radius of curvature can also be obtained by simply coating a silicon tip with a CVD diamond layer. So, some more work will be necessary to investigate other modified diamond deposition processes to fill the silicon nitride mold with a 2μm thick polycrystalline diamond layer right up to the tip apex.

FIG. 5.15: Diffraction pattern of a small area (ø 300nm) of the polycrystalline tip base of sample B.

5.3 Mounting of the Diamond Tips

5.3.1 Mounting on Stubs for Profilometry Applications

For high resolution profilometry, the diamond tips must be mounted on aluminum stubs. To achieve this, two procedures have been followed: 1) the direct gluing method, which can be used only if the diamond membranes are big enough (about $1mm^2$) and 2) a second gluing method, which is done only after the partial removal of the silicon frame. In both cases, tips are glued on stubs in a serial fashion.

Direct Gluing

The direct gluing of a diamond tip on a stub can be done immediately after the removal of the second mold (Fig. 5.1f). The stub, on which glue has been applied, is positioned under the diamond membrane and brought into contact by means of a xyz table. After polymerization of the glue, the diamond membrane is manually broken and the stub withdrawn (Fig. 5.16).

FIG. 5.16: SEM of a diamond tip and membrane glued on an aluminum stub by means of the direct gluing method. The dimensions of the flat surface of the stub being very small, it is difficult not to apply the glue on its inclined sidewalls.

Later, if necessary, the overhanging rim of the diamond membrane can be removed by breaking the membrane around the tip with a tiny instrument. This step is quite dangerous, as the tip can be broken if touched.
This method can only be used if the dimensions of the membrane are big enough. Indeed, it is very difficult to apply the glue on the flat surface of the stub only. If glue is applied on the inclined sidewalls of the stub and the dimensions of the membrane are too small, the stub can also be glued to the {111} diamond coated silicon planes around the membrane, preventing withdrawal of the stub from the wafer.

Gluing after Partial Removal of the Silicon Frame

A safer alternative to the direct gluing method, which allows diamond membranes as small as $100x100\mu m^2$ to be glued on aluminum stubs, relies on a partial removal of the silicon frame in which the diamond membranes are embedded (Fig. 5.17g). For this technique, the inclined sidewalls of the stub were reshaped into vertical sidewalls, reducing problems resulting from glue application on the sidewalls of the stub. The following steps are identical to the one described in the direct gluing method (Fig. 5.17h). Figure 5.18 shows a diamond membrane and tip glued on a modified aluminum stub using the above-described gluing method. In this case, the membrane was broken on the <111>-oriented sidewalls, reducing the risk of breaking the tip.

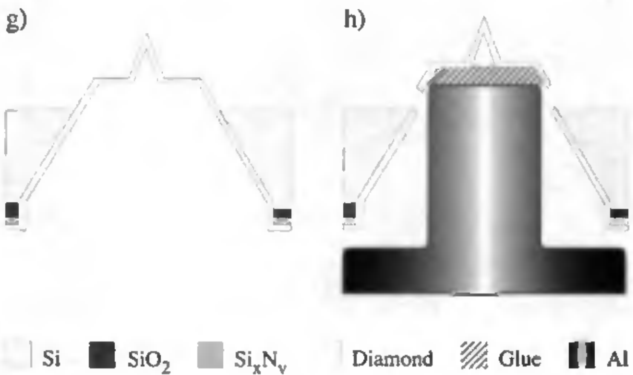

FIG. 5.17: (g) Partial removal of the silicon frame. (h) Gluing of the stub under the membrane and separation from the wafer.

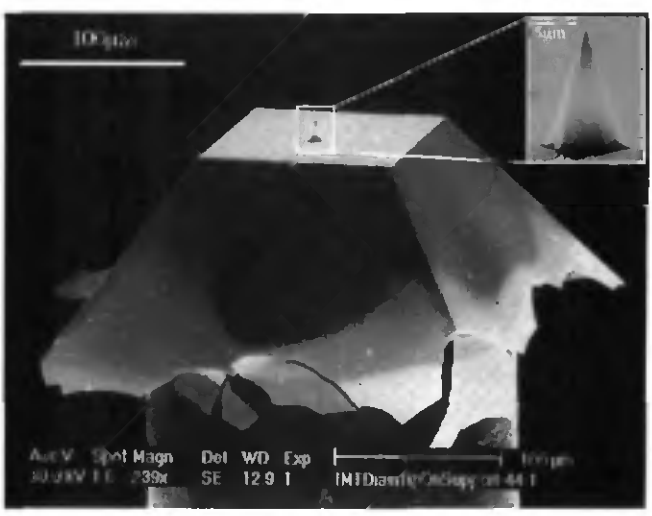

FIG. 5.18: SEM of a diamond membrane and tip glued on a stub using the second gluing method, preceded by a partial removal of the silicon frame.

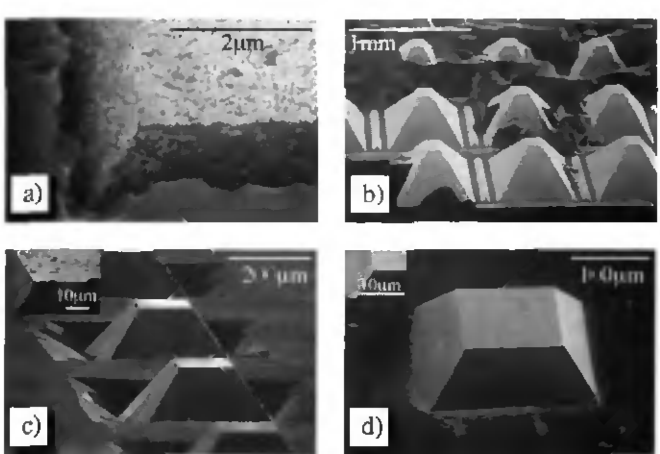

FIG. 5.19: (a) Underetching of the silicon at the interface with the diamond membrane. (b) Non-uniform etching of silicon in KOH. (c) Pronounced underetching of silicon in TMAH, leaving residues on the diamond membranes. (d) Clean uniform etching in HNA.

The partial removal of the silicon frame was more challenging than expected. Indeed, the silicon located next to the diamond layer was severely underetched during the removal of the silicon nitride second mold in the $HF:H_2O_2:H_2O$ solution (Fig. 5.19a). Attempts to anisotropically etch about 150μm of the silicon frame in KOH resulted in a strong non-uniformity in the etch depth on the wafer (Fig. 5.19b). By using TMAH instead of KOH, the underetching was reduced, but was still difficult to control. Moreover, residues were observed on the membranes (Fig.5.19c). An isotropic etch in HNA solution overcame the problem of underetching and left clean membranes (Fig. 5.19d). In this case, the transport dependent etch rate of the solution led to an overetching of one of the silicon frame borders, but not in a significant way for this technology.

5.3.2 Mounting on Cantilevers for AFM Applications

AFM requires the tip to be glued on a spring or cantilever. Since the above mentioned techniques are no more applicable, a transfer technology originally developed by Akyiama et al. [15] has been adapted for the transfer of diamond membranes and tips. The sequence of this modified transfer technology is depicted in Fig. 5.20.

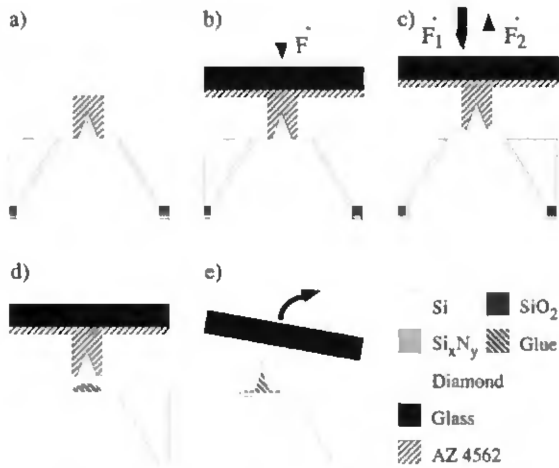

FIG 5.20: Sequence of the transfer technology used to transfer a diamond membrane and tip on a cantilever.

The first step of this process consists of protecting the diamond tips with a 40μm thick photoresist (AZ 4562) structured photolithographically [16, 17, 18]. For this step, the first photolithographic mask of the double molding process can be used (Fig. 5.20a). A 7μm thick AZ 4562 layer is spun at 4000rpm for 40 seconds on a glass wafer and softly cured in a convection oven at 85°C for 10 min. The glass wafer is then placed upside-down on the thick photoresist structures embedding the diamond tips. A weight is applied on this two-wafer system, and the whole is heated at 80°C for one hour, until the surface of the thick structured photoresist sticks to the thin photoresist layer and to the glass wafer (Fig. 5.20b). The diamond membranes are then mechanically broken and separated from the silicon frame (Fig. 5.20c). In the next step, a cantilever on which epoxy has been applied is accurately aligned under a diamond tip by means of a xyz table. Cantilever and tip are brought into contact and gently pressed, this for several hours, until total polymerization of the glue (Fig. 5.20d). Finally, the protective thick photoresist is removed and the glass wafer withdrawn (Fig. 5.20e), leaving the diamond tip and membrane glued to the cantilever as can be seen in Fig. 5.21.

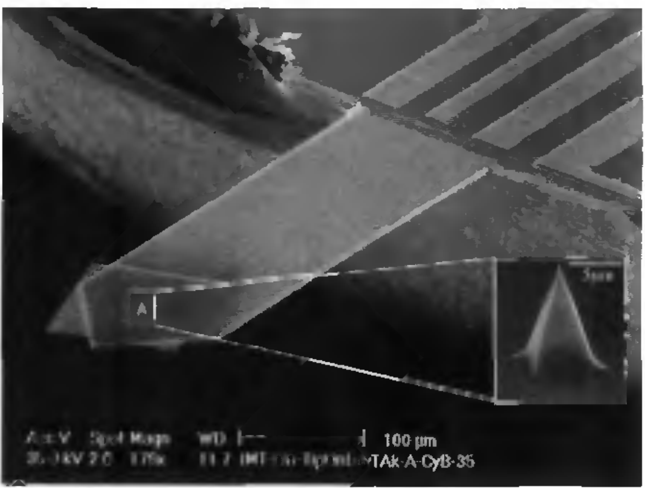

FIG. 5.21: Diamond tip and membrane transferred to a cantilever for AFM applications.

5.4 Conclusions

A modified double molding technology was presented, allowing the fabrication of HF-CVD diamond tips having a high aspect ratio and radii of curvature as small as 20nm. Such diamond tips proved to perfectly reproduce the geometry of the anisotropically etched silicon tips which served as a first mold.

These conical diamond tips can be glued on stubs for high resolution profilometry applications. Moreover, a transfer technology was successfully adapted to mount diamond tips and membranes on cantilevers for atomic force microscopy.

Raman analysis showed that the diamond membranes contain only a small amount of graphitic compounds. However, TEM analysis performed at the apex of such double molded tips indicated a reduced thickness of the material at this location. Highly magnified images also showed wavy structures, typical for graphite, on the surface of the tip apex. Finally, diffraction patterns of the tip apex indicated that the apex was composed of small nanocrystals embedded in an amorphous matrix. This may be evidence for inefficient diamond deposition in the very end of narrow holes, due probably to a reduced mass transfer of reactive gases in such confined geometries.

In order to improve gas exchange in the molds, cyclic pressure variations were applied during the last diamond deposition performed in this work. Diffraction patterns indicated that the tip apex was made out of essentially polycrystalline diamond, except for the last 300nm of the tip, where dark field TEM images revealed that it was composed of an amorphous material. The simultaneous presence of silicon, carbon and oxygen atoms at the tip apex, as found by EDS, suggested that it consists of a thin layer of oxycarbide of silicon. More work will be necessary to improve the diamond deposition efficiency far into the deepest extremity of the silicon nitride mold.

References

1 R. Kaneko and S. Oguchi, "Ion-Implanted Diamond Tip for a Scanning Tunneling Microscope", Japanese Journal of Applied Physics 29 (1990) 1854-1855.

2 Ph. Niedermann, W. Hänni, N. Blanc, R. Christoph and J. Burger, "Chemical Vapor Deposition Diamond for Tips in Nanoprobe Experiments", Journal of Vacuum Science and Technology A 14 (1996) 1233-1236.

3 K. Okano, K. Hoshina, M. Iida, S. Koizumi and T. Inuzuka, "Fabrication of Diamond Field Emitter Array", Applied Physics Letters 64 (1994) 2742-2744.

4 H.E. Hintermann and A.K. Chattopadhyay, "Low Pressure Synthesis of Diamond Coatings", Annals of the CIRP 42 (1993) 769-783.

5 O. Marti, B. Drake and P.K. Hansma, "Atomic Force Microscopy of Liquid-Covered Surfaces: Atomic Resolution Images", Applied Physics Letters 51 (1987) 484-486.

6 N. Liu, Z. Ma, X. Chu, T. Hu, Z. Xue, X. Jiang and S. Pang, "Fabrication of Diamond Tips by the Microwave Plasma Chemical Vapor Deposition Technique", Journal of Vacuum Science Technology B 12 (1994) 1712-1715.

7 T. R. Albrecht, S. Akamine, T.E. Carver and C.F. Quate, "Microfabrication of Cantilever Styli for the Atomic Force Microscope", Journal of Vacuum Science Technology A 8 (1990) 3386-3396.

8 C. Müller, W. Hänni, M. Binggeli and H.E. Hintermann, "Uniform Diamond Coatings on 4 In Si Wafers", Diamond and Related Materials 2 (1993) 1211-1214.

9 D.S. Knight and W.B. White, "Characterization of Diamond Films by Raman Spectroscopy", Journal of Material Research 4 (1989) 385-393.

10 P.V. Huong, "Structural Studies of Diamond Films and Ultrahard Materials by Raman and Micro-Raman Spectroscopies", Diamond and Related Materials 1 (1991) 33-41.

11 T. Lopez-Rios, E. Sandré, S. Leclercq and E. Sauvain, "Polyacetylene in Diamond Films Evidenced by Surface Enhanced Raman Scattering", Physical Review Letters 76 (1996) 4935-4938.

12 Y. Namba, E. Heidarpour and M. Nakayama, "Size Effects Appearing in the Raman Spectra of Polycrystalline Diamonds", Journal of Applied Physics 72 (1992) 1748-1751.

13 S.-A. Stuart, S. Prawer and P.S. Weiser, " Variation of the Raman Diamond Line Shape with Crystallographic Orientation of Isolated Chemical-Vapour-Deposited Diamond Crystals", Diamond and Related Materials 2 (1993) 753-757.

14 J.I. Goldstein, D.E. Newbury, P. Echlin, P.C. Joy, Ch. Fiori and E. Lifshin, "Scanning Electron Microscopy and X-Ray Microanalysis", edited by J.J. Hren, J.I Goldstein and P.C. Joy, Plenum Publishing Corporation, ISBN 0-306-40768-X, 222ff.

15 T. Akyiama, U. Staufer and N.F. de Rooij, "Wafer- and Piece-wise Si Tip Transfer Technologies for Applications in Scanning Probe Microscopy", accepted for publication in the Journal of Micro-Electro-Mechanical Systems.

16 L. Dellmann, S. Roth, C. Beuret, L. Paratte, G.-A. Racine, H. Lorenz, M. Despont, P. Renaud, P. Vettiger and N.F. de Rooij, "Two Steps Micromoulding and Photopolymer High-Aspect Ratio Structuring for Applications in Piezoelectric Motor Components", Microsystem Technologies 4 (1998) 147-150.

17 S. Roth, L. Dellmann, G.-A. Racine and N.F. de Rooij, "High Aspect Ratio UV Photolithography for Electroplated Structures", Proceedings of Micromechanics and Microsystems Europe, MME'98, Ulvik, Norway (1998) 55-58.

18 P.-F. Indermühle, L. Dellmann, S. Roth and N.F. de Rooij, "Patterned Thick Photoresist Layers for Protection of Protruding Structures During Wet and Dry Etching Processes", Journal of Micromechanics and Microengineering 8 (1998) 74-76.

Diamond Tips: Probes for High Resolution Profilometry

The high resolution profiler is an instrument which combines the high scan rate, the large scan size and the ease-of-use of a standard profilometer with the microanalysis and three-dimensional imaging capability of an atomic force microscope.
The aim of this work is to mount a double-molded diamond tip as a probe in a high resolution profiler and to study the achievable topographic images of specific samples in comparison with images obtained with other diamond probes currently used with this instrument.

6.1 Introduction

A standard surface profilometer generally provides profile scans of the sample topography with a vertical resolution on the order of nm, a high scan rate (up to 250μm/sec) and scan lengths between 50μm and 10mm. The principle of measurement is quite simple. A stylus (radius of curvature: 6.25μm) is quickly brought into contact with the sample and scanned over the surface. Its deflection is electronically recorded and converted by software to provide an image of the measured topography. Protruding features having heights of about 10nm can be measured with a vertical resolution of about 1nm. However, the measured depth of narrow pits, as well as the lateral resolution, strongly depend on the probe radius of curvature (Fig. 6.1). The heavy load (10-100μN) applied on the standard profilometer probe, however, does not allow the use of a stylus with submicrometer-sized radius of curvature.
On the other hand, the AFM [1] is able to image the surface of a sample with vertical as well as lateral atomic resolution, as long as the probe radius of curvature is small enough. The principle of this instrument is described in

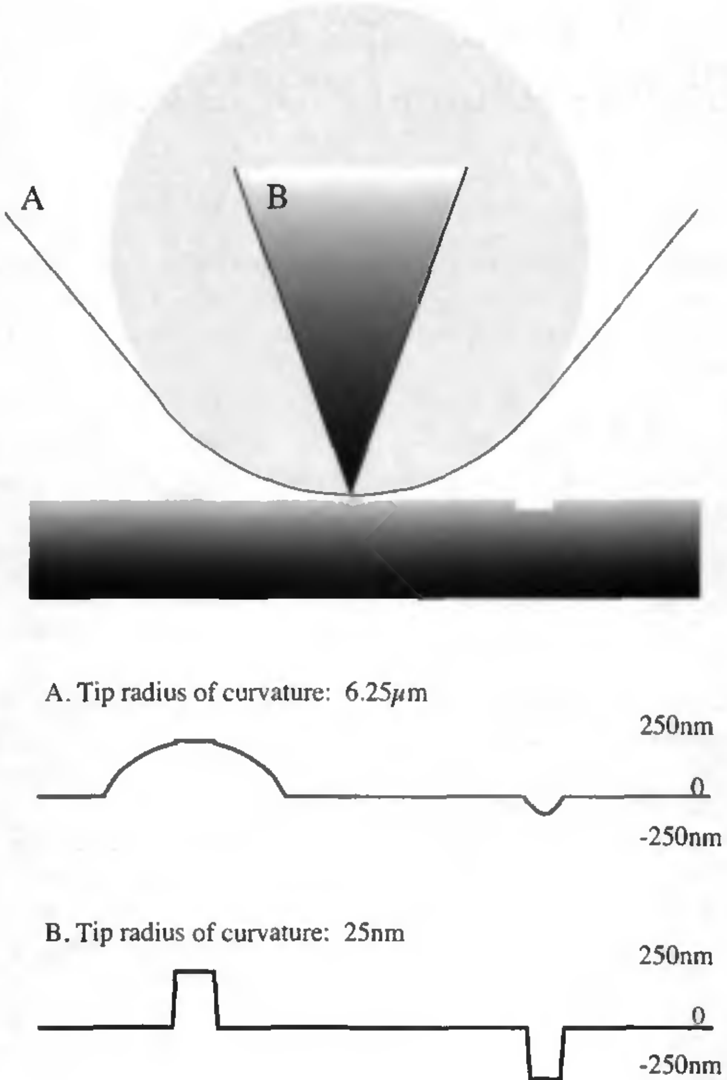

FIG. 6.1: Illustration of the influence of the radius of curvature of the probe while scanning a sample composed of a 1μm wide, 250nm thick protruding feature and a 1μm wide pit having a depth of 250nm. The scale is preserved in the schematics but, for the sake of clarity, the vertical axis of the resulting profiles has been extended by a factor 5.

section 1.1.1. As measurements are performed with only small forces between the probe and the sample, tips with radius of curvature even smaller than 25nm can be used. Atomic force microscopy, however, is a time consuming topographical analysis. The size of the scanned sample area is usually very small, and it is therefore quite difficult to localize the measurement very accurately.
As a bridge between the standard profilometer and the atomic force microscope, a high resolution profiler has been developed by Tencor [2]. This dual-stage instrument is able to combine the ease-of-use, the large scan length and high scan speed of a standard profilometer with accurate positioning and measurements of nearly atomic resolution. The principle and characteristics of the HRP-100 are detailed in the next section.

6.2 The HRP-100: A High Resolution Profiler

In January 1997, Tencor Instruments (nowadays KLA-Tencor) introduced a breakthrough metrology system: the Tencor HRP-100 (Fig. 6.2). This instrument is the first surface profiling system capable of measuring the surface topography of a wafer on both the macroscopic and microscopic scale. The HRP-100 combines long scans up to 200mm with fine-area analysis of submicrometer features, as well as the measurement repeatability and ease-of-use of a standard stylus profilometer with the high resolution analysis and imaging capabilities of an AFM.
To achieve these requirements, the HRP-100 is composed of two scanning stages: 1) the macroscopic sample stage, similar to a standard profilometer's

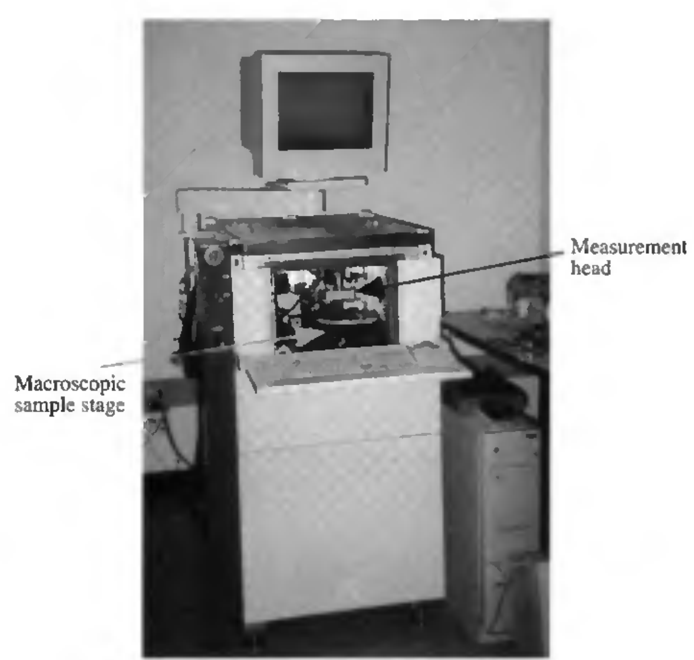

FIG. 6.2: Photograph of the high resolution profiler HRP 100 © KLA-Tencor.

xyz-stage, to perform long scans (90µm to 200mm) and to locate patterns needing more accurate investigations, and 2) the microscopic sensor stage used for local area analysis (<= 90x90μm^2) with nearly atomic resolution. To avoid crushing the tip or damage to the sample during the approach of tip to sample, an acoustic sensor is integrated into the sensor stage. This acoustic sensor uses reflected sound to detect the distance from the stylus to the sample, allowing in this way the use of styli with very small radii of curvature. The measurement head, fixed on the sensor stage, is composed of two sets of optics for pattern recognition, a cantilever-shaped stylus holder, a capacitive detection system, and a magnetic set-up to maintain a constant stylus force as low as 0.5µN or 0.1µN in the case of the modified HRP-100 used in this work (Fig. 6.3).

It is possible to perform single-line profile scans as well as area scans. The software allows the acquisition of 2-D and 3-D images of the topography of the sample and advanced data analysis (fitting, leveling, filtering,...). Typical characteristics of the HRP-100 styli are given in the next section.

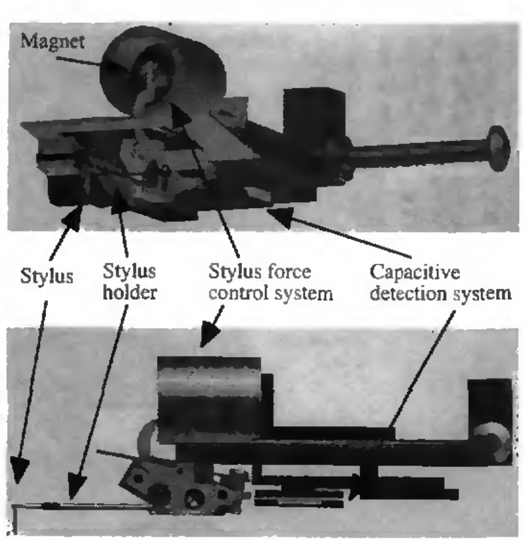

FIG. 6.3: Schematic of the crucial part of the measurement head of the HRP-100.

6.3 Measurements

Comparative measurements were realized at KLA-Tencor (Milpitas, CA, USA) on a selection of samples with four different types of diamond probes mounted in the HRP-100. The aim of this work was to determine if the double-molded conical diamond tips could be used as probes in the HRP-100, and to compare the measurements obtained with these recently developed tips and tips already used in the HRP-100.

6.3.1 HRP Diamond Probes

Diamond probes are either formed at the end of a mechanically-shaped shank or glued on stub. In every case, the shank or stub is mounted on an aluminum arm acting as a cantilever. This arm can be manipulated with tweezers and clamped in the sensing element of the measurement head.

Standard Probe

The standard probe consists of a mechanically-shaped stainless steel shank, having a length of about 4mm. The diameter of this shank is about 1mm and its diamond measuring tip has been milled to obtain a conical shape with a total aperture angle of typically 60° and a radius of curvature of 2±0.5μm at the tip apex (Fig. 6.4).
This kind of tip is very stable and has a long lifetime. It is generally used for long scans across the wafer or repetitive scans on samples where a high resolution is not crucial, or for samples having low aspect ratio structures.

Durasharp Probe

The Durasharp tips are provided by KLA-Tencor for high resolution measurements with the HRP-100. These tips are formed from the standard probes described above by sharpening the diamond apex with a focused ion beam. This sharpening yields 0.3-1μm high diamond supertips having a cone angle of 40±5° and a radius of curvature ranging from 30 to 50nm (Fig. 6.5).
The efficiency of the Durasharp tips in high resolution profilometry has been demonstrated. Unfortunately, they are produced with a serial process

and are therefore quite expensive. Their geometry is not regular, giving rise to pronounced tip effects while scanning samples with significant height differences. Moreover, they have a high risk of breaking while scanning deep holes with sharp edges having a depth similar to the height of the supertip.

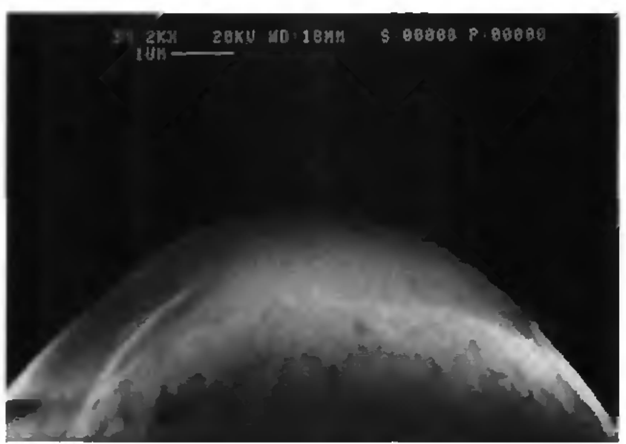

FIG. 6.4: SEM of the apex of a diamond standard probe, having a radius of curvature of about 2μm.

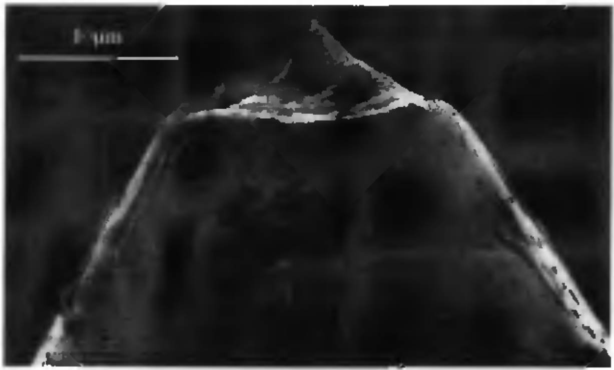

FIG. 6.5: SEM of an unused Durasharp tip showing two stages of sharpening. A first step removes materials in order to keep a general angle of aperture of about 60° on the first 5μm of the tip. The second step defines the 0.3μm high supertip.

Pyramidal Probe

Pyramidal diamond tips were produced by Ph. Niedermann (CSEM, Neuchâtel, Switzerland) by means of a simple molding technique, that is, by HF-CVD of diamond in pyramidal holes anisotropically etched in a {100} silicon wafer [3]. After patterning of the diamond layer, the diamond-coated side of the silicon wafer was bonded to an already structured glass wafer. The silicon wafer was then completely etched away and the glass wafer diced. Glass chips, on which a pyramidal diamond tip was bonded, were finally glued on aluminum stubs (Fig. 6.6).
These batch-processed probes are very stable and their shape is regular. They have a height of about 30μm and a radius of curvature as small as 20nm. Nevertheless, their aperture angle (70°) prevents them from reaching the bottom of high aspect ratio structures.

Conical Probe

The conical diamond tips were developed as an alternative to the expensive and irregular Durasharp tips, as well as to the pyramidal tips whose angle of aperture is too wide for representative imaging of high aspect ratio structures. These tips, realized by the double molding process presented in chapter 5, have a height of about 13μm, a total cone angle of 34-41° and a radius of curvature as small as 15nm (Fig. 6.7). To act as a probe in the HRP-100, these tips were glued on an aluminum stub following the process described in section 5.3.1.
These batch-processed tips have a regular shape, an aperture angle similar to the Durasharp tips and a radius of curvature similar to the pyramidal tips. Moreover, their height is more than sufficient for the usual applications of the HRP-100. Like the pyramidal tips, these conical tips are hollow, being fabricated by a molding process. The purpose of the following measurements will be to determine if these tips are suitable as HRP probes, with emphasis on their geometry, their resistance to wear and breaking, and the resolution they can achieve.

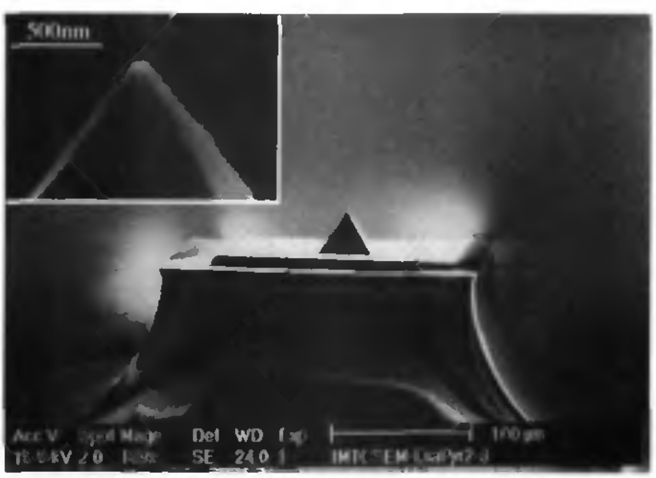

FIG. 6.6: SEM of a pyramidal diamond tip bonded on a structured glass chip.

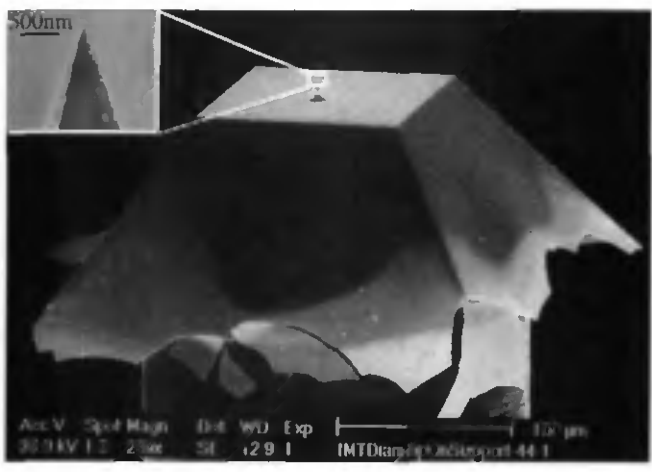

FIG. 6.7: SEM of a diamond double-molded conical tip glued on an aluminum stub.

6.3.2 Comparison on Different Samples

Each kind of diamond probe was used to image different samples following the same sequence. An image obtained with the HRP always being a convolution of the sample and probe apex shapes, an image of each diamond probe apex was first obtained by scanning a special sample provided with very sharp features, called a tip characterizer. An image of the diamond tip apices can be obtained without requiring SEM observations before starting the measurements on other specific samples. At the end of the measurement sequence, the tip apexes were once more imaged using this tip characterizer and finally were observed with a SEM.
The apices of double-molded conical diamond tips exhibited a high tendency to break or to be worn as will be discussed later. It was therefore necessary to use a new conical probe for each of the measurements in a series presented here, whereas only one specimen of each other kind of tip was used for an entire series of measurements.

Tip Characterizer I (New Probes)

The tip characterizer is a commercially available $2x2mm^2$ silicon tip array (TGT01 © NT-MDT Co., Moscow, Russia). The tips have a height of 0.7μm, an angle of aperture of 22° and are guaranteed to have a radius of curvature smaller than 10nm. The pitch of the array is 3μm (Fig. 6.8). The characteristics of this sample makes it possible to image essentially the apex of the probe used to scan these grating.
All the measurements on this sample were realized with the parameters given in Table 6.1. The distance between two scanned lines in the y-direction is 50nm, which does not allow a very precise measurement of the diamond probe radius of curvature in this direction.
The measurements are presented in Fig. 6.9. Note the similarity between the apices of the Durasharp tip and the conical tip, and the characteristic shape of the pyramidal tip.

TABLE 6.1: Main parameters used for scanning the tip characterizer sample.

Scan length x direction	*5μm*	*Point interval (x dir.)*	*5nm*
Scan size y direction	*5μm*	*Lines spacing (y dir.)*	*50nm*
Scan speed	*0.5μm/s*	*Stylus force*	*0.1μN*

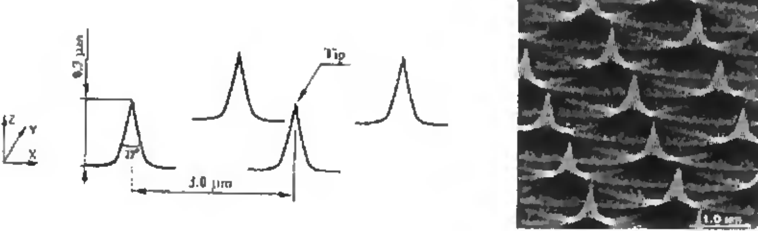

FIG. 6.8: Schematic and SEM of the tip characterizer sample.

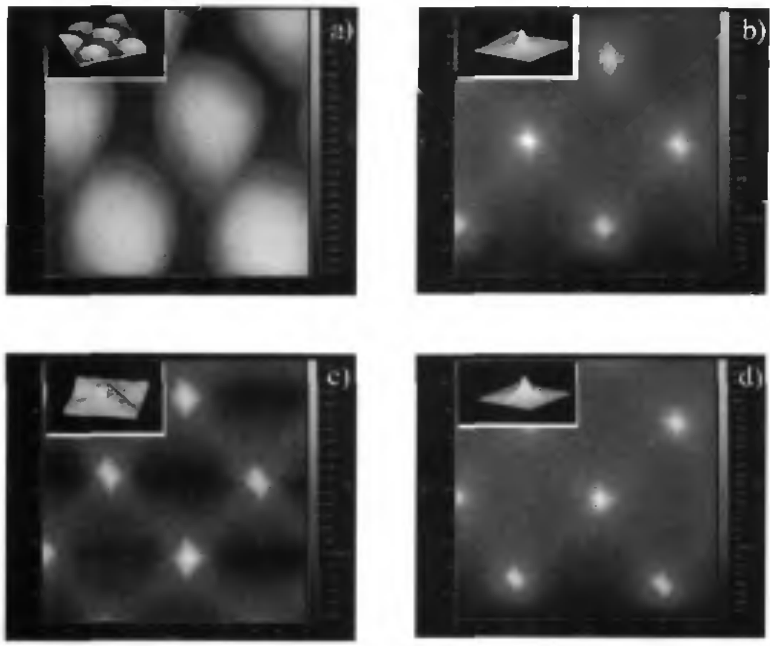

FIG. 6.9: Measurements realized with the HRP-100 on the tip characterizer sample with four new probes. a) Standard probe: the radius of curvature of this probe is too hig compared to the geometry of the sample to allow an estimation of the radius of curvature. b) Durasharp tip: the radius of curvature is estimated to be 35nm in the x-direction and 65nm in the y-direction (probably due to the reduced resolution in this direction). c) Pyramidal tip: the radius of curvature is estimated to be ~80nm. d) Conical tip: the radius of curvature is estimated to be ~70nm.

Hemispherically Grained Silicon

The hemispherically grained silicon (HSG) sample is composed of small hemispheres (ø 50-200nm) of silicon located at the surface of a silicon wafer. Their proximity makes their imaging quite challenging and does generally not allow the probe to reach the silicon wafer surface. The quality of the topographical image obtained therefore strongly depends on the tip angle of aperture and radius of curvature.

The parameters used for the measurements are presented in Table 6.2. They are identical for all the probes except for the conical tip, where the adopted parameters are indicated in bold characters. There, the line spacing parameter was increased in the hope of reducing tip wear or probability of breaking.

The measurements presented in Fig. 6.10 clearly show that the standard probe is inappropriate for imaging this kind of sample, while the pyramidal probe, probably due to its wide angle of aperture, does not produce a very reliable image of the sample. Both the Durasharp tip and the conical tip give quite a reliable image of the sample, the Durasharp one being a little smoother. An interesting parameter to determine is the maximum depth reached by the probe, giving a good estimation of the efficiency of each probe to image this sample. Here also, note the similarity between the Durasharp tip and the conical tip.

Shallow Trenches for Isolation

The shallow trenches isolation (STI) sample is composed of small, nearly rectangular islands (~200nm x 1.5µm) surrounded by narrow (~300nm) ditches having a depth of ~350nm, which can be filled, in a later step, with an insulating material. The high aspect ratio features of this sample are particularly difficult to image for tips having a wide angle of aperture. Moreover, the steepness of the edges of the islands can easily break thin, sharp tips, or the tip can get stuck in the cavity and drag the sample.

The parameters used for the measurements are presented in Table 6.3. They are identical for all the probes except for the conical tip, where the adopted parameters are indicated in bold characters. The scan length and the scan size parameters were decreased in the hope of reducing the tip wear or damage.

TABLE 6.2: Main parameters used for scanning the HSG sample.

Scan length x direction	*0.5µm*	*Point interval (x dir.)*	*1nm / 5nm*
Scan size y direction	*0.5µm*	*Lines spacing (y dir.)*	*2nm / 5nm*
Scan speed	*0.25µm/s*	*Stylus force*	*0.1µN*

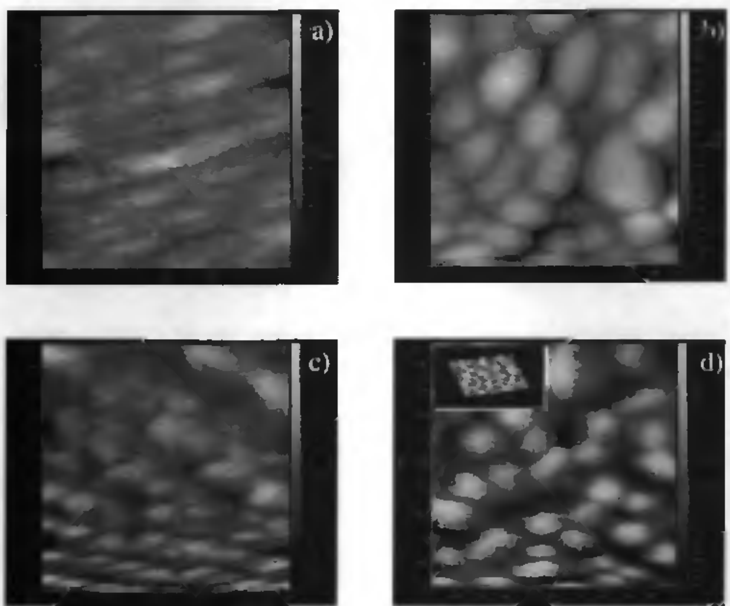

FIG. 6.10: Measurements realized on the HSG sample. a) Standard probe: maximum depth reached: 12nm. b) Durasharp tip: maximum depth: 28nm. c) Pyramidal tip: maximum depth: 20nm. d) Conical tip: maximum depth: 28nm.

The images obtained are presented in Fig 6.11. The shifts observed with the Durasharp tip indicate that the steep edges of the islands probably hooked the probe. Once more, the observation of the maximum depth reached by the probe gives a good indication about the measuring efficiency of the various diamond tips. In spite of the shifts, the Durasharp tip is the most efficient from this point of view. The pyramidal tip is less efficient in the narrow interstices than the conical tip, but can go deeper in wider holes. Finally, the

TABLE 6.3: Main parameters used for scanning the STI sample.

Scan length x direction	*2μm / 1μm*	*Point interval (x dir.)*	*1nm / 3nm*
Scan size y direction	*2μm / 1μm*	*Lines spacing (y dir.)*	*10nm*
Scan speed	*0.25μm/s*	*Stylus force*	*0.1μN*

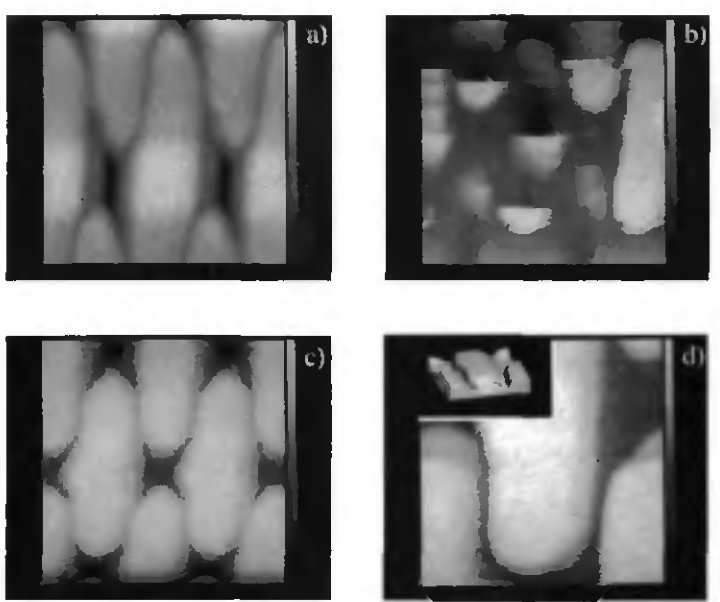

FIG. 6.11: Measurements realized on the STI sample. a) Standard probe: maximum depth reached: 28nm in the larger holes / 6nm in the narrower interstices. b) Durasharp tip: maximum depth: 310nm in the larger holes / 150nm in the narrower interstices. c) Pyramidal tip: maximum depth: 240nm in the larger holes / 76nm in the narrower interstices. d) Conical tip: maximum depth: 219nm in the larger holes / 95nm in the narrower interstices.

depth penetration of the standard probe showed once more that this tip is unsuited to these kinds of measurements. The results indicate that there is a high probability that the conical tip was broken very early during this measurement. Note the asymmetry of the measurement in the ascending and descending slopes, which is characteristic of an asymmetrically broken tip.

Silicon Nitride Lines and Spaces

The last typical sample for HRP-100 measurements is a grating of 14 lines and spaces, etched to a depth of ~325nm in a silicon nitride layer. The increasing width of the trenches made it possible to precisely establish when the probe reaches the bottom of the holes. The measurements were strongly dependent on the aspect ratio of the tip, and the steep edges of the structures were once more dangerous for sharp and thin tips. Only profile line measurements were realized on this sample, the area profiling bringing no additional information. The parameters used for these measurements are given in Table 6.4.
The measurements are given in Fig. 6.12. Once more, the standard probe is inadequate, the probe not being able to reach the bottom of the trenches even in the widest case. Both the pyramidal and the conical probes could reach the bottom of the 12th of the 14 trenches in the array, whereas the Durasharp tip could only reach the bottom of the 13th. Note the asymmetry of the inverted peaks corresponding to the trenches measured with the Durasharp and the conical tips. From this, it may be concluded that both of these tips are broken. Nevertheless, they exhibit a resolution similar to that of the pyramidal tip in this measurement.

Tip Characterizer II (Used Probes)

Finally, after measurements of the silicon nitride lines and spaces, the probes were used to scan the tip characterizer sample once more in order to evaluate their wear after this measurement sequence. These results, presented in Fig. 6.13, will be compared to the SEM observations presented below. At this point, the standard tip, as well as the pyramidal tip, do not appear to have suffered from these measurements. On the other hand, the increase of the flat area surface at the tip apex leaves no doubt that the Durasharp tip is worn or broken. Finally, the measurement realized with the conical probe clearly shows the hollow structure of the probe, indicating that the tip is broken or worn. The thickness of the tip walls are estimated to be smaller than 250nm, which indicates that the thickness of the diamond layer is reduced at the tip apex compared to that of the membrane (2μm).

TABLE 6.4: Main parameters used for scanning the silicon nitride line and space sample.

Scan length x direction	*25µm*	*Point interval (x dir.)*	*1nm*
Scan speed	*0.25µm/s*	*Stylus force*	*0.1µN*

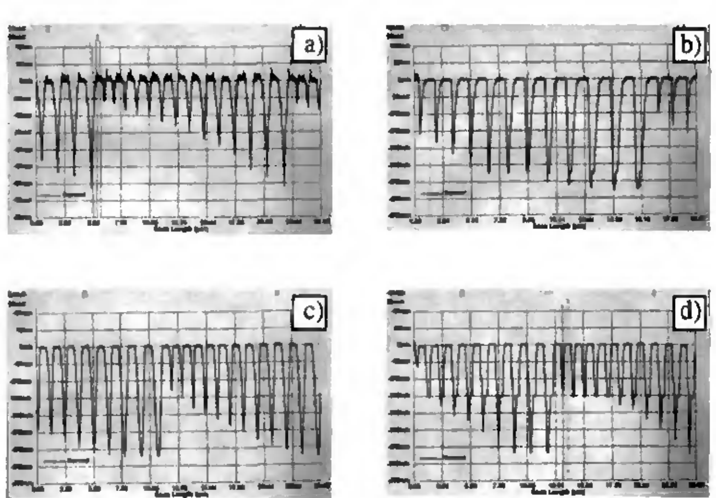

FIG. 6.12: Measurements realized on the silicon nitride line and space sample. a) Standard probe: maximum depth reached: 69nm in the 14th hole. b) Durasharp tip: maximum depth reached in the 13th hole: 328nm. c) Pyramidal tip: maximum depth reached in the 12th hole (width: 945nm). The probe scanned the bottom of the hole over a distance of 58nm. d) Conical tip: maximum depth reached in the 12th hole (width: 943nm). The probe scanned the bottom of the hole over a distance of 38nm.

SEM Observations

To get a better estimation of the wear of the tips used for these measurement sequences, SEM observations were made (Fig. 6.14). The standard probe still has a radius of curvature of 2±0.5µm and it is very difficult to see if this tip has been worn or not. The Durasharp tip is effectively broken at the base of the supertip, underlining the difficulty to image samples like STI or silicon nitride lines and spaces. The radius of curvature of the pyramidal tip is at this step ~125nm, but it is difficult to say exactly to what extent it has been worn, because it was not possible to make SEM observations of this tip before the measurements.

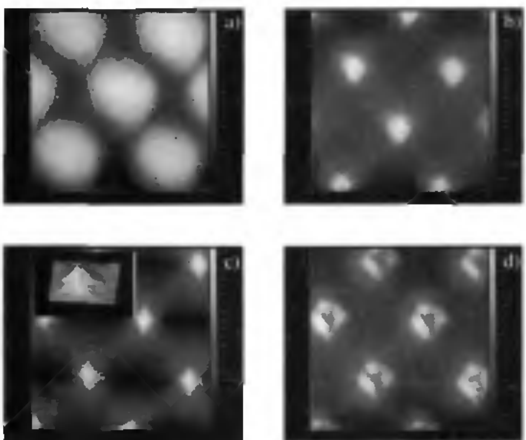

FIG. 6.13: Measurements realized with the tip characterizer at the end of the measurement sequence. a) Standard probe: no major change. b) Durasharp tip: the tip is clearly broken or worn. c) Pyramidal tip: no major change. d) Conical tip: a hollow structure can be seen in the center of each image, indicating that the tip is broken or worn.

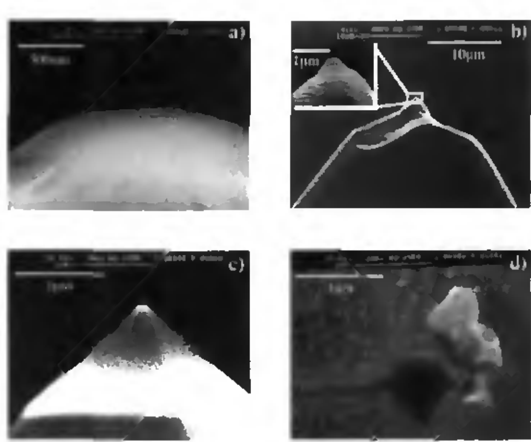

FIG. 6.14: SEMs of the apex of the different diamond tips after the final measurement on the tip characterizer sample. a) Standard probe: worn or not worn, that's the question... b) Durasharp tip: the tip is clearly broken at the base of the supertip. c) Pyramidal tip: this tip is probably slightly worn. d) Conical tip: this tip is also broken or worn, and the hollow shape of this probe can clearly be distinguished.

Finally, the SEM image of the conical probe also clearly shows its hollow structure, confirming the breaking or wear of this tip. From this micrograph, the thickness of the conical tip walls can be estimated to be ~185nm. This highlights two problems: 1) the diamond layer at the tip apex is more than ten times thinner than the thickness of the diamond membrane and so insufficient and 2) the quality of the material composing the tip apex is subject to discussion. TEM observations were later performed on other diamond tips originating from the same wafer, and their diffraction patterns revealed that the tip apex was composed of a significant amount of amorphous material (see section 5.2.3).

6.4 Conclusions

The first double-molded conical diamond tips were mounted on the HRP-100. Measurements on various challenging samples, such as HSG, STI or silicon nitride lines and spaces were made. It was observed that the resolution of the conical tip is superior to the one of the standard tip, and comparable with the resolution obtained with the Durasharp and pyramidal tips.

Unfortunately, the measurements made so far have shown that it is highly probable that the present conical tips are broken during the measurements. This is due to problems which were not identified prior to these experiments. With these measurements, it was possible to see for the first time that the thickness of the diamond layer is drastically reduced at the very end of the tip apex (<165nm in the apex compared to 2μm for the membrane), which could explain the breaking of the conical tip while scanning samples having high aspect ratio features. Moreover, TEM analysis performed later on other conical tips extracted from the same wafer revealed a significant amount of amorphous material in the tip apex.

The exact composition of the probe apex is still unknown, but it is proposed that the narrow geometry of the conical second mold affects the diamond deposition at the very bottom of the mold. This is probably due to inefficient gas exchange in such narrow structures, and more diamond deposition experiments have to be made to overcome this problem.

References

1 G. Binnig and C. F. Quates, "Atomic Force Microscope", Physical Review Letters 56 (1986) 930-933.

2 HRP-100, KLA-Tencor, Milpitas, CA, USA.

3 Ph. Niedermann, W. Hänni, N. Blanc, R. Christoph and J. Burger, "Chemical Vapor Deposition Diamond for Tips in Nanoprobe Experiments", Journal of Vacuum Science Technology A 14 (1996) 1233-1236.

Diamond Tips: Probes for Atomic Force Microscopy 7

The mounting of double-molded diamond tips on cantilevers was demonstrated in chapter 5. The aim of this work was to investigate the use of these conical tips as probes for atomic force microscopy topography analysis.

7.1 Introduction

It was demonstrated in chapter 3 that, if mounted on sufficiently rigid cantilevers, the hardness of diamond-coated probes makes them well suited for use as indenters for nanoindentation and surface scratching, and secondly, directly as probes for AFM investigations of the modifications they have induced [1]. The present chapter will elaborate on the use of double-molded diamond tips in AFM topography imaging. A tip transfer process developed by Akiyama et al. [2] was modified to demonstrate that conical double-molded diamond tips can be individually transferred onto a cantilever (see section 5.3.2). In this way, such diamond tips could also be mounted on cantilevers equipped with integrated actuation and detection, even if the technologies used to realized the levers and the diamond tips are not compatible. Moreover, tips made of different materials (silicon, silicon nitride, nickel, tungsten, diamond,...) and of different shapes could be transferred onto the same chip provided with a series of cantilevers. Finally, in the case of sophisticated and expensive cantilevers, a broken tip could be replaced by dissolving the glue underneath it and adding a new one afterwards.

7.2 Measurements

For the AFM measurements, a cantilever provided with a double-molded conical diamond tip was mounted in a commercial AFM (Nanoscope III, Digital Instrument). The approach was quite challenging because it was difficult to ensure that the end of the cantilever did not touch the sample before the tip. This is due to the fact that the dimensions of the diamond membrane did not allow the tip to be glued on the end of the cantilever (Fig. 5.21). This problem could be solved by adapting the design of the membrane in a next generation.

To make the approach easier, it was decided to image the sidewall of a silicon piece which had been diced with a diamond circular saw. In this way, the chip could be mounted on one of its sidewalls to get a sample which was sufficiently narrow. The imaging was performed in dynamic mode. The resonance frequency of the cantilever was measured to be 38kHz, demonstrating that gluing the low mass diamond membrane on the cantilever did not drastically affect its resonance frequency.

Figure 7.1 shows an image of one of the sidewalls of the diced silicon piece. The traces of the dicing blade can clearly be seen. The imaging of smaller features (<50nm) is sharp, proving that the resolution of the conical diamond tip is satisfactory.

After a few AFM investigations, SEM observations of the diamond tip apex were made. Fig. 7.2 clearly shows that the tip apex has been broken, probably during the approach attempts. On the left upper part of the figure, a zoom-in of the tip apex is presented. From this picture, the thickness of the layer which forms the tip apex can be estimated to be smaller than 25nm.

This SEM investigation raised a doubt concerning the material from which the tip apex is formed. The lack of crystallized grains in the interior part of the tip indicates that the material is probably not diamond and seems rather to be amorphous, as later confirmed by means of TEM observations (section 5.2.3). Nevertheless, these experiments demonstrated that it is possible to perform AFM investigations with a double-molded diamond tip glued on a preprocessed cantilever. In the future, once the diamond deposition into the deepest recesses of the silicon nitride molds has been optimized, some more AFM imaging will have to be performed with such double-molded diamond probes.

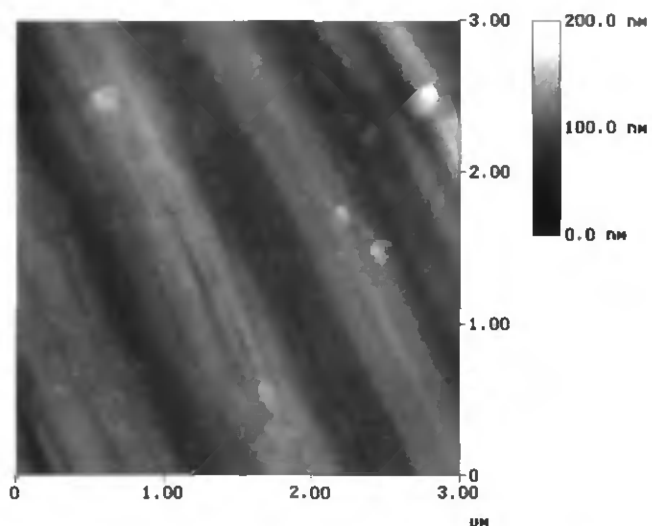

FIG. 7.1: AFM investigation of the sidewall surface of a piece of silicon diced with a diamond circular saw. The image was made in tapping mode (© Nanoscope, DI) with a double-molded diamond tip transferred onta a cantilever.

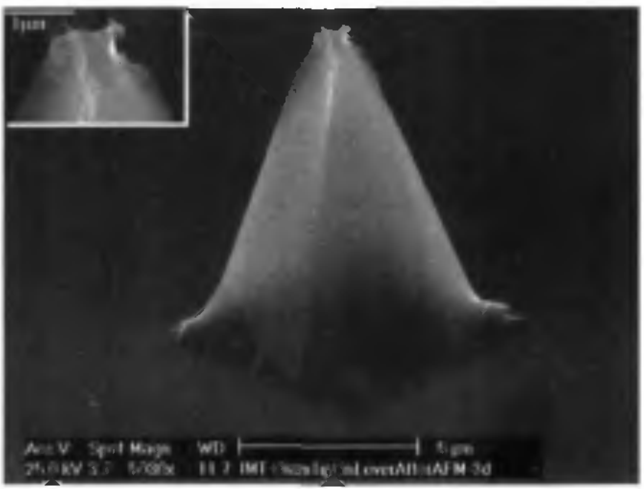

FIG. 7.2: SEM of the double-molded probe glued on a cantilever after being used as a probe for a few AFM investigations.

7.3 Conclusions

Double-molded diamond tips glued on cantilevers have been used as probes in a commercial AFM. The resolution of the AFM investigations was satisfactory.

Nevertheless, some difficulties were encountered during the approach step, due to the position of the tip onto the cantilever. Indeed, due to the dimensions of the transferred diamond membrane, the tip had to be glued away from the end of the cantilever, making it difficult to ensure that during the approach, the tip and not the end of the cantilever touches the sample first. This inconvenience can be overcome by changing the size of the diamond membrane in a next generation. For this investigation, it was decided to use a narrower sample, in this particular case one of the sidewalls of a silicon piece diced with a diamond circular saw. AFM imaging produced a sharp picture even of small features (<50nm), proving that the resolution obtained with these tips is fully satisfactory.

SEM observations of the tip apex were made once the tip had performed a few AFM investigations. They revealed that the tip apex had been broken, probably during an approach step, and particularly that the material forming the tip apex was thinner than 25nm. Moreover, the lack of the typical crystallized grains in the interior side of the tip indicates that the tip apex material is probably not diamond, but an unknown amorphous material. This was confirmed by the TEM investigations realized later.

Diamond deposition seems to be delicate in such narrow holes. It has been proposed that this phenomenon is due to reduced gas exchange in these holes. Substantial effort will be made in future to overcome this inconvenience.

References

1 N. X. Randall, "Development and Application of a Multifunctional Nanotribological Tool", PhD Dissertation, University of Neuchâtel, Switzerland, 1997.

2 T. Akiyama, U. Staufer and N.F. de Rooij, "Wafer- and Piece-wise Si Tip Transfer Technologies for Applications in Scanning Probe Microscopy", accepted for publication in the Journal of Micro-Electro-Mechanical Systems.

Conclusions

This thesis dealt with the development of a new microfabrication technique for the realization of diamond tips. With this technology, based on two successive molding steps, high aspect ratio diamond microtips having very small radii of curvature and regular sidewalls could be fabricated. Integrated onto cantilevers or tiny stubs, such probes could be mounted in an atomic force microscope or in a high resolution profiler, respectively, to perform topographical analysis of samples at the nanometer scale.

In a first approach, the fabrication of silicon microtips by anisotropic wet etching was studied. Their shape and sharpness were also analyzed in order to determine if such tips could be used as a first mold in the double molding technique.

In a second step, a fabrication process was developed for the realization of sharp silicon tips integrated onto thin cantilevers having highly reproducible geometries. This technique was also applied to the realization of AFM probes provided with thicker cantilevers having high spring constants. These latter devices were coated with a thin HF-CVD diamond layer and were mounted in a modified AFM. They were then successfully used to perform sequences of nanoscratching experiments on hard disk materials, and subsequent high-resolution AFM imaging of the induced nanomodifications.

Next, the double molding technique was developed and tested with platinum as the final tip material. The removal of silicon from the second mold, the subsequent filling of this mold, and, finally, removal of the mold itself, were evaluated in this development. With this process, 47μm high Pt tips were realized and shown to perfectly reproduce the shape and radius of curvature of the KOH-etched tips used as first mold.

Finally, the double molding process was adapted to the realization of HF-CVD diamond tips. With this process, it was possible to form diamond tips having a high aspect ratio, regular sidewalls, a small total angle of aperture,

and a very sharp apex. Raman spectroscopy analysis as well as TEM and EDS investigations of the diamond membranes and tips were performed. From these experiments, it was concluded that the membranes and tips were made out of high quality polycrystalline diamond with only a small number of graphitic defects, except at the very end of the tip apex. Indeed, the last 300nm of the tip apex were found to be composed of a very thin layer of an amorphous material. Attempts were made to improve the diamond deposition deep into the very point of the second mold. However, further investigations of diamond deposition will have to be performed in the future.
Such diamond tips were successfully mounted on small stubs for high resolution profilometry applications. Moreover, a transfer technology was modified in order to glue such tips at the ends of preprocessed cantilevers, to be used as probes for AFM imaging.
During a visit to KLA-Tencor (Milpitas, USA), the diamond tips mounted on stubs were used as probes on a high resolution profiler and compared to other diamond probes currently utilized with this instrument. The achievable resolution of these double-molded diamond tips was comparable to the best of the commercially available tips, which are fabricated with a serial process and are therefore quite expensive. Moreover, the tips realized during this work proved to have ideal shape characteristics for these kinds of applications. Unfortunately, it was found that the high loads applied on the probe during the measurements tended to break the amorphous apex of the double-molded diamond tips.
Finally, a tip transferred onto a cantilever was mounted in an AFM and used to produce sharp pictures of small features, this despite the fact that SEM observations made after several AFM imaging revealed that the tip apex had been damaged.

In the future, the following steps of the double-molding process have to be improved:

- During the realization of the silicon tips acting as a first mold, the formation of "flat knife" tip apices has to be avoided. Therefore, two strategies can be taken into account. The most expensive would be the use of electron-beam direct writing for the patterning of the silicon dioxide masks. This technique could ensure the realization of perfectly square

masks, which could limit the occurrence of etching asymmetries during the tip formation. The second strategy would be to change the silicon dioxide mask design, in order to get tip apices defined by the intersection of three planes only. Nevertheless, the general shape of such tips is not symmetrical and could induce irregular tip artifacts in profilometry applications when scanning samples having high aspect ratio features.

- Concerning the realization of the second mold, the number of tip-shaped silicon nitride molds which were broken during the back-side silicon underetching has to be reduced. This phenomenon seems to be due to an accumulation of stress at the base of these molds. It is therefore suggested to incorporate a stress barrier, which would be located outside the limits of the final silicon nitride membrane acting as a second mold. This stress barrier could be, for example, a silicon tip array realized during the formation of the tip acting as a first mold.
- The diamond deposition into the deepest recesses of the silicon nitride mold has to be improved. Therefore, the seeding step has to be adapted in order to ensure that diamond particles can reach these areas of the mold. Then, during the diamond deposition, the exchange of gases into the molds could be improved by periodically varying the pressure in the CVD reactor. Pressure variations have already been applied during the last diamond deposition and this first trial was unsuccessful to fill the mold's deepest point with polycrystalline diamond. So, the pressure and switching time parameters still need to be optimized.
- Finally, to allow gluing of the diamond tip and membrane as close as possible to the end of the preprocessed cantilever, the dimensions of the diamond membrane have to be reduced. The design of the back-side mask defining the membrane must therefore be adjusted.

Acknowledgments

This thesis is the result of the work, advice, assistance and support of many people, in particular the collaborators of the Sensors, Actuators and Microsystems Laboratory (SAMLAB) of the Institute of Microtechnology (IMT) in Neuchâtel. To them I would like to express my deepest appreciation and gratitude.

First of all, I would like to thank Prof. Nico F. de Rooij for giving me the opportunity to work in his enthusiastic team, for creating a research environment of the highest quality, for giving me the chance to spend one month at KLA-Tencor in Milpitas CA, as well as for his support and encouragement.

I would particularly like to express my gratitude to Dr. Urs Staufer, supervisor of the group "Tools for Nanoscience" to which I belong, for his guidance, his comments, his patience and all his suggestions. Thank you also, Urs, for accepting to be one of the co-examiners of my work, and for correcting the first version of this thesis. I would like also to thank Dr. Pierre-François Indermühle for introducing me to the world of AFM probe fabrication, Dr. Terunobu Akiyama for helping me to adapt the silicon tip transfer technology he developed to diamond tips, and Dr. Camille Stebler for lending me precious instruments for tip-to-cantilever alignment.

Special thanks also to Prof. Milena Koudelka-Hep for accepting to be co-examiner of this thesis, for explaining some of the mechanisms of chemistry to me, and for her very enjoyable company during the coffee breaks!

This work has been realized in collaboration with the Swiss Center for Electronics and Microtechnology (CSEM). I would like to particularly thank Dr. Philippe Niedermann for all our discussions, for gluing the diamond tips on stubs, for many SEM observations and for being one of the co-examiners of this thesis. I gratefully acknowledge Dr. Werner Hänni for the diamond depositions and for several hours of discussions and

explanations about the diamond deposition process. For the Raman spectroscopy investigations and analysis, I thank very much Claudine Julia Schmutz, as well as Nick Randall for the nanomechanical modifications. I would like to acknowledge Dr. André Perret and Dr. Frédéric Sollberger for discussions about wet etchants and Louis Klatz for preparing these "appetizing" solutions. Finally, I thank Claude Ketterer for some of the SEMs presented in this dissertation.

At the end of this work, I spent one month at KLA-Tencor, Milpitas, California. I would like to thank all the surface metrology division team and in particular Dr. Tom McWaid for letting me use a HRP 100 and for his help and explanations. I would also like to thank Dr. Marco Tortonese for very interesting discussions, and integrating me into the Palo Alto social life.

The TEM investigations have been performed by Prof. Philippe-André Buffat (EPFL), Dr. Evelyne Sauvain-Vallat (IMT) and Dr. Massoud Dadras (IMS), who also realized the EDS analysis. Thank you very much as well as for your comments and explanations.

Further I thank Dr. Olaf Ohlsson (Nanosensors GmbH) for having kindly agreed to be co-examiner for this thesis.

The realization of this work would not have been possible without the competence of our excellent technicians, Sylvain Jeanneret, Pierre-André Clerc, Sabina Jenny, Sylviane Pochon, Gianni Mondin, Bastien Droz and José Vaquera. I thank them very much for the way they run the microfabrication laboratory, as well as for their advice and their flexibility when I asked them to perform some "crazy" operations! Many thanks also to Mathias Schulze and Christophe Kottelat, who often helped me in this patience-consuming world of computer users!

My gratitude goes also to Dr. Sabeth Verpoorte who spent many hours on this manuscript to correct my "French-flavoured" English, to Dr. G.-A. Racine for introducing me in the microfabrication laboratory and for answering my questions concerning technology as well as computers, to Pierre Thiébaud for his friendship and for our enriching discussions during lunch and coffee breaks, to Margrit Rüegg, our secretary for letting my hands free of administrative tasks, to Dr. Marc-Alexis Grétillat for very

helpful discussions and comments, and to Dr. Philippe Luginbuhl who often animated our office with his incredible stories and exclamations that came from the heart!

I also wish to thank all my colleagues and ex-colleagues for the stimulating and attractive atmosphere they generate, or generated, in this research group. In particular I acknowledge Dr. Nicolas Blanc, Marc Boillat, Danick Briand (his first weeks in the lab were a poem!), Dr. Jürgen Brugger, Bas de Heij, Philippe Dubois, Dr. Volker Gass, Benedikt Guldimann, Dr. Christian Linder, Dr. Cornel Marxer, David Strike (who also corrected much of my English prose!), Dr. Bart van der Schoot, Dr. Peter van der Wal (another beer?) and my office-mates, Vincent Pasquier and Lutz Haase. Special thanks to the sketch-team, always ready for animating every event: Dr. Philippe Arquint, Dr. Lionel Paratte, Dr. Jean-Charles Fiaccabrino, Dr. Florence Grétillat, Dr. Wilfried Noell, Marco Meijerink, Olivier Guenat, and of course, The (with a capital T!) KTS Corporation: Laurent Dellmann, Sylvain Roth and Grégor Schürmann, who, moreover, showed a lot of imagination for the microfabrication lab decoration!

Now, I would like to thank my parents, Alain and Alexandra, for so many things, but in particular for their support in all circumstances and for their love. Many thanks also to all my relatives and friends for their interest in the completion of this work, but above all for giving me always new reasons to enjoy life! It is not possible to dress a complete list but I would like to address special thanks to Stéphanie, not only for our common gastronomic taste, as well as to Renate and Uwe.

Finally, I thank you, Matthias, for all these small things which color life and render it delightful!

List of Publications

Refereed Articles

C. Beuret, Ph. Niedermann, U. Staufer and N.F. de Rooij, "Fabrication of Metallic Probes by a New Technology Based on Double Molding", Microelectronic Engineering 41/42 (1998) 543-546.

L. Dellmann, S. Roth, C. Beuret, G.-A. Racine, H. Lorenz, M. Despont, Ph. Renaud, P. Vettiger and N.F. de Rooij, "Fabrication Process of High Aspect Ratio Elastic and SU-8 Structures for Piezoelectric Motor Applications", Sensors and Actuators A 70 (1998) 42-47.

L. Dellmann, S. Roth, C. Beuret, L. Paratte, G.-A. Racine, H. Lorenz, M. Despont, Ph. Renaud, P. Vettiger and N.F. de Rooij, "Two Steps Micromoulding and Photopolymer High-Aspect Ratio Structuring for Applications in Piezoelectric Motor Components", Microsystem Technologies 4 (1998) 147-150.

P. Thiébaud, C. Beuret, M. Koudelka-Hep, M. Bove, S. Martinoia, M. Grattarola, H. Jahnsen, R. Rebaudo, M. Balestrino, J. Zimmer and Y. Dupont, "An Array of Pt-Tip Microelectrodes for Extracellular Monitoring of Activity of Brain Slices", Biosensors & Bioelectronics 14 (1999) 61-65.

Conference & Workshop Papers

C. Beuret, G.-A. Racine, J. Gobet, R. Luthier and N.F. de Rooij, "Microfabrication of 3D Multidirectional Inclined Structures by UV Lithography and Electroplating", Proceedings IEEE Micro Electro Mechanical Systems, Oiso, Japan (1994) 81-85.

G.-A. Racine, C. Beuret, R. Luthier and N.F. de Rooij, "Speed Control of Elastic Force Motors by Means of Integrated Piezoelectric Sensors", Proceedings IEEE Micro Electro Mechanical Systems, Oiso, Japan (1994) 124-129.

P.H. s'Heeren, C. Beuret, O. Larsson, A. Bertholds and D. Reynaerts, "Microstructuring of Silicon by Electro-Discharge Machining (EDM) - part II: Applications", Proceedings of Eurosensors X, the 10th European Conference on Solid-State Transducers, Leuven, Belgium (1996) 255-258.

C. Beuret, Ph. Niedermann, W. Hänni, P.-F. Indermühle, U. Staufer and N.F. de Rooij, "Silicon/Diamond Tips for Atomic Force Microscopy", Poster presented at Nano Hasliberg 2, 2nd Hasliberg Workshop on Nanoscience (1996) P68.

L. Dellmann, S. Roth, C. Beuret, G.-A. Racine, H. Lorenz, M. Despont, Ph. Renaud, P. Vettiger and N.F. de Rooij, "Fabrication Process of High Aspect Ratio Elastic Structures for Piezoelectric Motor Applications", Digest of Technical Papers of the 9th International Conference on Solid-State Sensors & Actuators, TRANSDUCERS'97, Chicago, USA (1997) 641-644.

C. Beuret, Ph. Niedermann, U. Staufer and N.F. de Rooij, "Fabrication of Metallic Probes by a New Technology Based on Double Molding", Micro- and Nano-Engineering'97, Athens, Greece (1997) NFIII-3.

E. Ammann, C. Beuret, P.-F. Indermühle, N.F. de Rooij and H. Siegenthaler, "Local Nanoscale Probing with an Electrolytic Thin-Layer STM Probe", Poster presented at Nano Hasliberg 3, 3rd Hasliberg Workshop on Nanoscience (1998) P5.

Patent

Ph. Niedermann, C. Beuret and S. Jeanneret, "Procédé de fabrication d'un organe palpeur pour capteur micromécanique, notamment pour microscope à force atomique", European Patent Application EP 0 882 944 A1 (December 9, 1998).

Biography

Cynthia Beuret was born on August 14, 1970, in Neuchâtel, Switzerland. In 1988, she started her study in physical electronics at the University of Neuchâtel. In 1991, during her study, she worked for four months at the Centre Suisse d'Electronique et de Microtechnique (CSEM) in the Lithomask department (nowadays Photronics) on various projects using e-beam lithography. She received her MSc degree in physical electronics from the University of Neuchâtel in August 1993. In September of that year she joined the Institute of Microtechnology (IMT) of the University of Neuchâtel as a research and teaching assistant. From September 1993 to February 1996, her principal research interest was the development of thick photoresist molds for electroplated multidirectional inclined structures. In 1994 and 1995, she spent four months as a visiting scientist at AGIE, Losone, Switzerland in order to develop a technology for the Micro-Electro-Discharge Machining (μ-EDM) of silicon. In March 1996, she started her PhD work on the development of microfabrication technologies for the realization of components for scanning probe microscopy. This work allowed her to spend one month in 1998 at KLA-Tencor, Milpitas, CA, USA in order to evaluate double-molded diamond tips as probes for high resolution profilometry.